ADVANCED FLIP CHIP AND WAFER LEVEL PACKAGES FOR
2.5D AND 3D IC PACKAGE TECHNOLOGY

ADVANCED FLIP CHIP AND WAFER LEVEL PACKAGES FOR 2.5D AND 3D IC PACKAGE TECHNOLOGY

XU CHENG

XU CHENG

SCHOOL OF MECHANICAL AND AEROSPACE ENGINEERING

2018

2018

ADVANCED FLIP CHIP AND WAFER LEVEL PACKAGES FOR 2.5D AND 3D IC PACKAGE TECHNOLOGY

XU CHENG

School of Mechanical and Aerospace Engineering

A thesis submitted to the Nanyang Technological University in partial fulfilment of the requirement for the degree of Doctor of Philosophy

2018

ABSTRACT

The demand of electronic product explodes in recent years, and the trend of electronic product is portable, multifunctional and budget currently. The fan-out wafer level packaging technology is a kind of wafer level packaging technology, and it becomes more and more attractive and popular because of its flexibility to integrate diverse devices in a very small form factor. The fan-out wafer level packaging technology has the advantages of high density of input/output, minimal package size and low cost. The fan-out wafer level package (FOWLP) is usually used to volume sensitive devices such as mobile phones and wearables. However, the strength of ultrathin FOWLP is low, and the low package strength often leads to crack issues. Therefore, the study of strength behavior of FOWLP is essential. FOWLP is made up of various materials and thus the proper structure design and material selection are important to meet the reliability requirement. The FOWLP strength is evaluated by the experimental method and numerical method. We confirm three significant characteristics of FOWLP strength from the experimental work. The wafer grinding process, FOWLP dimension and thermal factor affect the FOWLP strength significantly. The numerical work proves that the flexure strength of over-molded structure FOWLP is higher than the flexure strength of other structure FOWLPs with the same package thickness. Two theoretical models of FOWLP strength are proposed. These two models are based on the location of FOWLP initial fracture point. The comparison of FOWLP strength model with experiment results and simulation results shows that they are identical. A new theoretical model of FOWLP fatigue crack growth is proposed. This model additionally considers the effect of thermal factor on the FOWLP fatigue crack growth.

ACKNOWLEDGMENT

The author would like to express his gratitude to the people who have given their hands throughout the author's Ph.D. study journey. The author's thanks and appreciations also extend to:

Associate Professor Zhong Zhaowei, the author's supervisor. He shows his generosity, encouragement and patience in guiding the author in various aspects during the Ph.D. study. He is also always trying to motivate and encourage the author to reach his goal.

Dr. Choi Won Kyoung, the author's co-supervisor. She shows her attention, suggestion and guidance to the author. She also shares a lot of her knowledge and experience on the aspect of advanced packaging with the author. She is also always explaining the author's doubts throughout the project.

Ms. Heng Chee Hoon, NTU biological laboratory assistant manager, Mr. Leong Kwok Phui, NTU materials laboratory manager and Ms. Yeong Peng Neo, NTU materials laboratory Executive. They show their generosity and patience in guiding and teaching the author to use the laboratory machines. They also provide the technical support to the author's experiment from hardware to software. Ms. Lee Koon Fong, mechatronics laboratory manager. She kindly and tremendously helps the author to purchase necessary experiment accessories.

All the author's colleagues from STATS ChipPAC Pte. Ltd. especially the technology division team. The author wants to thank them for sharing their knowledge and experience with him.

Last but not least, the author wants to appreciate Singapore Economic Development Board to establish this Industrial Postgraduate Programme. It provides an opportunity to let the author train in such a marvelous company during his Ph.D. studying journey.

PUBLICATION LIST

[1] C. Xu, Z. W. Zhong, and W.K. Choi, "Evaluation of Fan-out Wafer Level Package Strength by Three-Point Bending Testing," in IEEE 23rd International Symposium on the Physical and Failure Analysis of Integrated Circuits, Singapore, 2016, pp. 297-300.

[2] C. Xu, Z. W. Zhong, and W.K. Choi, "Thermal Effect on Fan-out Wafer Level Package Strength," in IEEE 18th Electronics Packaging Technology Conference, Singapore, 2016, pp. 700-703.

[3] C. Xu, Z. W. Zhong, and W.K. Choi, "Effect of High Temperature Storage on Fan-out Wafer Level Package Strength," in China Semiconductor Technology International Conference (CSTIC) 2017, Shanghai China, 2017, pp. 1-3.

[4] C. Xu, Z. W. Zhong, and W.K. Choi, "Epoxy Molding Compound Effect on Fan-out Wafer Level Package Strength during Post-Mold Thermal Process," in 16th IEEE ITHERM Conference, Orlando USA, 2017, pp. 1388-1392.

[5] C. Xu, Z. W. Zhong, and W.K. Choi, "Numerical and Experimental Study of Fan-out Wafer Level Package Strength," in 2017 IEEE 67th Electronic Components and Technology Conference, Orlando USA, 2017, pp. 2187-2192.

[6] C. Xu, Z. W. Zhong, and W.K. Choi, "Thermal test Effect on Fan-out Wafer Level Package Strength," in 12th International Microsystems, Packaging, Assembly and Circuits Technology, Taiwan, 2017, pp. 271-274.

[7] C. Xu, Z. W. Zhong, and W.K. Choi, "Evaluation of Fan-out Wafer Level Package Strength," *Microelectronics International*, under review.

TABLE OF CONTENTS

ABSTRACT i

ACKNOWLEDGMENT ii

PUBLICATION LIST iii

LIST OF FIGURES viii

LIST OF TABLES..xiv

LIST OF ACRONYMS xvi

LIST OF SYMBOLS xviii

CHAPTER 1 INTRODUCTION..21

1.1 Research background 21

1.2 Research motivation...26

1.3 Research objectives..30

1.4 Research scope...30

1.5 Organization of the thesis 31

CHAPTER 2 LITERATURE REVIEW..32

2.1 Methodology of strength evaluation 32

2.2 Evaluation of silicon die strength by 3PB test method 37

2.2.1 Effect factors on silicon die strength 37

2.2.2 Fracture analysis of silicon die 43

2.2.3 Strength data analysis of 3PB test 48

2.3 Methodology of reliability test..53

2.3.1 Temperature cycling test..53

2.3.2 High temperature storage test..56

2.3.3 Unbiased highly accelerated stress test..58

CHAPTER 3 RESEARCH METHODOLOGY..60

3.1 Evaluation of IC chip strength..60

3.2 Proposed research..64

3.3 Proposed research methodology..67

CHAPTER 4 EVALUATION OF FOWLP STRENGTH BY 3PB TEST METHOD..70

4.1 Experiment of 3PB test..70

4.2 Evaluation of FOWLP strength..75

4.2.1 Structure effect on FOWLP strength..75

4.2.2 PSV effect on FOWLP strength..80

4.2.3 Temperature cycling test effect on FOWLP strength..85

4.2.4 High temperature storage test effect on FOWLP strength..89

4.3 Evaluation of EMC strength..92

4.3.1 Experiment configuration..93

4.3.2 Thermal related assembly process effect on EMC strength..97

4.3.3 Thermal related reliability test effect on EMC strength..102

4.4 Optimized design of FOWLP structure 105

4.4.1 FOWLP dimension 105

4.4.2 PCB bar placement 110

4.4.3 Grinder wheel selection 113

4.5 Summary 116

CHAPTER 5 NUMERICAL STUDY OF FOWLP STRENGTH 120

5.1 Simulation of 3PB test 120

5.2 Evaluation of FOWLP strength by numerical method 125

5.2.1 Simulation conditions 126

5.2.2 Simulation result and discussion 132

5.2.3 Study the effect of mesh element size 135

5.3 Evaluation of proposed FOWLP strength by numerical method 137

5.3.1 Design of proposed FOWLP 138

5.3.2 Simulation conditions 144

5.3.3 Simulation result and discussion 145

5.4 Summary 148

CHAPTER 6 DEVELOPMENT OF THEORETICAL MODEL OF FOWLP STRENGTH 150

6.1 Theoretical model of FOWLP strength 150

6.1.1 Weibull distribution 150

6.1.2 Analytical model formulation 154

6.1.3 Derivation of governing equation 156

6.1.4 Experimental and numerical result and discussion 163

6.2 Theoretical model of FOWLP fatigue crack growth 170

6.2.1 FOWLP fracture mechanics 170

6.2.2 Proposed theoretical model of FOWLP fatigue crack growth 173

6.3 Summary 176

CHAPTER 7 CONCLUSIONS AND FUTURE WORK 178

7.1 Conclusions 178

7.1.1 Conclusions of evaluation of FOWLP strength by 3PB test method 179

7.1.2 Conclusions of numerical study of FOWLP strength 183

7.1.3 Conclusions of development of theoretical model of FOWLP strength 184

7.2 Major Contributions 186

7.3 Future work 187

REFERENCES 190

LIST OF FIGURES

Figure 1-1 Illustration of wafer level chip scale package (left) and fan-out wafer level package (right) [9]. 22

Figure 1-2 Thermal performance of plastic ball grid array (top) and fan-out wafer level package (bottom) [24]. 23

Figure 1-3 The applications of wafer level package in a smartphone [25]. 24

Figure 1-4 The revenue forecast of FOWLP activity [25]. 25

Figure 1-5 FOWLP assembly process flow. 26

Figure 1-6 Trend prediction of WLP carrier size [25]. 27

Figure 1-7 A high warpage wafer is broken during the assembly process. 29

Figure 2-1 Ball-on-ring test apparatus [84]. 32

Figure 2-2 Ball breaker test apparatus [86]. 33

Figure 2-3 The apparatus of point load test and line load test [88, 89]. 34

Figure 2-4 The fixture of bending test [93]. 35

Figure 2-5 The loading mechanism of three-point bending test [93]. 36

Figure 2-6 The loading mechanism of four-point bending test [93]. 36

Figure 2-7 Surface AFM images of grinding only, grinding followed by polishing and grinding followed by chemical wet etching (from left to right) [106]. 38

Figure 2-8 Flexure strength of Yeung BBT and the RMS value of specimen surface roughness [109]. 39

Figure 2-9 Chippings appear on the die kerf after the wafer sawing process [119]. ...40

Figure 2-10 Illustration of step cut method [120]. 41

Figure 2-11 Illustration of laser grooving process [121]. 42

Figure 2-12 Illustration of DbT method [125]. 43

Figure 2-13 Illustration of grinding patterns [94]. 44

Figure 2-14 Two possible directions of loading force and grinding patterns [126]. ..44

Figure 2-15 Four kinds of grinding patterns of silicon die on a wafer [128, 129]. 45

Figure 2-16 Classification of fracture patterns [130]. 46

Figure 2-17 Initial fracture point appears on the silicon die surface [116]. 47

Figure 2-18 Comparison of sidewall conditions of silicon die after the mechanical sawing process (top) and laser sawing process (bottom) [116]. 48

Figure 2-19 Comparison of two-parameter Weibull distribution and three-parameter Weibull distribution in the lower region of failure probability [140]........................49

Figure 2-20 Example of temperature profile of temperature cycling test [153]. 55

Figure 2-21 Bump cracks appear on the flip chip package after the HTS test [162]. 57

Figure 2-22 Crack development and propagation during the UHAST at 110℃, 120℃ and 130℃ / 100% RH [177]. 59

Figure 3-1 Proposed research flow chart. 65

Figure 4-1 Instron universal tester 5566. 70

Figure 4-2 Customized 3PB fixture. 71

Figure 4-3 Example of load versus extension curves of 3PB test. 72

Figure 4-4 FOWLP specimen layout. 73

Figure 4-5 FOWLP specimen assembly process flow: debonding, lithographing PSV, backside grinding and laminating BSP tape. 74

Figure 4-6 Wafer region code. 74

Figure 4-7 Assembly process flow of group A specimens: debonding, backside grinding and laminating BSP tape. 75

Figure 4-8 Comparison of flexure strength among specimen A-1, specimen A-2 and specimen A-3. 76

Figure 4-9 The initial fracture point appears on the silicon die edge of specimen A-1. 79
Figure 4-10 The initial fracture point appears on the silicon die surface of specimen A-1. 79
Figure 4-11 The initial fracture point appears on the silicon die surface of specimen A-2. 79
Figure 4-12 The initial fracture point appears on the silicon die edge of specimen A-3. 80
Figure 4-13 Comparison of flexure strength between specimen A-1 and specimen B-1. 81
Figure 4-14 Comparison of flexure strength between specimen A-2 and specimen B-2. 82
Figure 4-15 Comparison of flexure strength between specimen A-3 and specimen B-3. 83
Figure 4-16 The initial fracture point appears on the silicon die edge of specimen B-1. 84
Figure 4-17 The initial fracture point appears on the silicon die surface of specimen B-2. 85
Figure 4-18 The initial fracture point appears on the silicon die surface of specimen B-3. 85
Figure 4-19 Flexure strength of group B specimen after the TC test. 87
Figure 4-20 Average flexure strength of group B specimen after the TC test. 87
Figure 4-21 Flexure strength of group B specimen after the HTS test.......................90
Figure 4-22 Average flexure strength of group B specimen after the HTS test. 91
Figure 4-23 FUTURE-TECH microhardness tester FM-300e. 94

Figure 4-24 Proposed indentation locations of Vickers hardness test in a specimen and the definition of resulting indentation diagonal D1 and D2. 94

Figure 4-25 An EMC specimen wafer before debonding...95

Figure 4-26 Comparison of average Vickers pyramid number among EMC specimens..98

Figure 4-27 Comparison of average flexure strength among EMC specimens. 99

Figure 4-28 3PB test curves (load versus extension) of EMC (top) and FOWLP (bottom) specimens..101

Figure 4-29 Comparison of flexure strength between EMC specimens and FOWLP specimens...102

Figure 4-30 Comparison of average flexure strength among EMC specimens after the HTS test. 103

Figure 4-31 Side view of EMC-4 specimen after the 1000 hours HTS test. 104

Figure 4-32 Comparison of flexure strength among group C specimens. 107

Figure 4-33 Comparison of flexure strength among group D specimens.................109

Figure 4-34 Group E specimen layout (Green columns are PCB bar). 111

Figure 4-35 Comparison of specimen E-1 flexure strength.....................................112

Figure 4-36 Comparison of specimen E-2 flexure strength.....................................113

Figure 4-37 Comparison of flexure strength among group F specimens. 115

Figure 5-1 ANSYS simulation software. 120

Figure 5-2 The experiment of 3PB test for a FOWLP specimen. 121

Figure 5-3 The simulation model of 3PB test for a FOWLP specimen...................122

Figure 5-4 Meshed 3PB fixture rollers. 123

Figure 5-5 Meshed FOWLP specimen. 123

Figure 5-6 The upper roller is instructed a downward displacement. 124

Figure 5-7 The displacement step control graph with an effective range from 0.15 mm to 0.25 mm. 125

Figure 5-8 The FOWLP specimen status after each assembly process. 126

Figure 5-9 Specimen A-1 simulation model. 127

Figure 5-10 Specimen B-1 simulation model. 127

Figure 5-11 Specimen B-2 simulation model. 128

Figure 5-12 Specimen B-3 simulation model. 129

Figure 5-13 Comparison of two-parameter Weibull distribution between experiment results and simulation results. 133

Figure 5-14 Comparison of two-parameter Weibull distribution among simulation models with different element sizes. 136

Figure 5-15 The assembly process flow of proposed new FOWLP specimen. 140

Figure 5-16 Transformed section of proposed new specimen, specimen B-2 and specimen B-3. 141

Figure 5-17 Stress distribution of proposed new specimen, specimen B-2 and specimen B-3. 143

Figure 5-18 The simulation model of proposed new FOWLP. 144

Figure 5-19 Comparison of two-parameter Weibull distribution among specimen B-2, specimen B-3 and the proposed new specimen. 146

Figure 6-1 Illustration of contact area (dark area) in the 3PB test. 160

Figure 6-2 Comparison of specimen B-1 strength model with experiment results and simulation results. 167

Figure 6-3 Comparison of specimen B-2 strength model with experiment results and simulation results. 168

Figure 6-4 Comparison of specimen B-3 strength model with experiment results and simulation results. 168

LIST OF TABLES

Table 2-1 Temperature cycling test conditions [153]. 54

Table 2-2 High temperature storage test conditions [160]. 56

Table 2-3 Unbiased highly accelerated stress test conditions [176]. 58

Table 3-1 The effect level of wafer sawing process and wafer grinding process on various strength test methods. 61

Table 4-1 FOWLP specimens and 3PB test specifications (structure effect). 76

Table 4-2 FOWLP specimens and 3PB test specifications (PSV effect). 80

Table 4-3 The material properties of pure EMC specimens. 95

Table 4-4 Observation points in the thermal related assembly processes. 96

Table 4-5 EMC specimens and Vickers hardness test specifications. 97

Table 4-6 EMC specimens and 3PB test specifications. 98

Table 4-7 EMC specimens and 3PB test specifications (HTS test effect). 103

Table 4-8 Group C specimen specifications. 106

Table 4-9 Group D specimen specifications. 108

Table 4-10 Group E specimen specifications. 110

Table 4-11 Group F specimen specifications. 114

Table 4-12 Wafer surface roughness of Group F specimen. 116

Table 5-1 The material properties of simulation models. 121

Table 5-2 The flexure strength and extension of specimen A-1 and specimen B-1 after the experiment of 3PB test. 130

Table 5-3 The flexure strength and extension of specimen B-2 and specimen B-3 after the experiment of 3PB test. 131

Table 5-4 Summary of scale parameters and shape parameters of specimens. 132

Table 5-5 Summary of node number, element number and elapsed time of simulation models. 136

Table 5-6 Calculation process of neutral surface of proposed new specimen. 141

Table 5-7 Distances between the FOWLP specimen neutral surface and the lower surface of silicon die. 142

Table 6-1 3PB test flexure strength and corresponding failure probability of specimen B-1, specimen B-2 and specimen B-3. 164

Table 6-2 3PB test average fracture load, extension and Young's modulus of specimen B-1, specimens B-2 and specimens B-3. 165

Table 6-3 The contact length and volume ratio or area ratio of specimen. 165

Table 6-4 The shape parameters and scale parameters of FOWLP strength models. 165

Table 6-5 Simulation model flexure strength and corresponding failure probability of specimen B-1, specimen B-2 and specimen B-3. 166

LIST OF ACRONYMS

3D	3-dimensional
3PB	Three-Point Bending
4PB	Four-Point Bending
ASTM	American Society for Testing and Materials
BBT	Ball Breaker Test
BLR	Board Level Reliability
BoR	Ball-on-Ring
BSP	Backside Protection
CAGR	Compound Annual Growth Rate
CTE	Coefficient of Thermal Expansion
DbT	Dicing-by-Thinning
EMC	Epoxy Molding Compound
FEM	Finite Element Method
FOWLP	Fan-Out Wafer Level Package
IC	Integrated Circuit
IMC	Intermetallic Compound
I/O	Input/Output
ISO	International Organization for Standardization
JEDEC	Joint Electron Device Engineering Council
HTS	High Temperature Storage
LLT	Line Load Test
LSA	Laser Ablation

LSE	Least Square Estimation
MLE	Maximum Likelihood Estimation
PBGA	Plastic Ball Grid Array
PCB	Printed Circuit Board
PEFT	Plate-on-Elastic-Foundation Test
PLT	Point Load Test
PMC	Post-Mold Curing
PnP	Pick and Place
PSV	Passivation
RDL	Redistribution Layer
RH	Relative Humidity
RMS	Root Mean Square
SAC	Tin/Silver/Copper, Sn-Ag-Cu
SEM	Scanning Electron Microscope
TC	Temperature Cycling
TSV	Through Silicon Via
SiP	System in Package
UHAST	Unbiased Highly Accelerated Stress Test
WLP	Wafer Level Package
WLCSP	Wafer Level Chip Scale Package

LIST OF SYMBOLS

a	Ball test parameter
A	Surface area under loading
A_0	Surface area
b	Ball test parameter
B	Width
c	Radius of distributed load
C	Fatigue material constant
d	Length of indentation diagonal
D	Fatigue material constant
E	Young’s modulus
F	Fracture load
G	Strain energy release rate
G_c	Critical train energy release rate
i	ith item
J	J-integral
k	Elastic foundation modulus
k	Boltzmann constant
K	Stress intensity factor
K_c	Critical stress intensity factor
ΔK	Range of stress intensity
l	Contact length
L	Fixture span

L_h	Half of fixture span
m	Shape parameter
n	Sample size
P	Failure probability
P_S	Failure probability (surface model)
P_U	Failure probability (universal model)
P_V	Failure probability (volume model)
Q	Activation energy
r	Radius of load force
R	Disk radius
s	Stress density
t	Disk thickness
T	Absolute temperature
U	Strain energy
U_s	Surface energy
v	Poisson's ratio
V	Volume under loading force
V_0	Volume
w	Deflection
W	Thickness
z	Contact radius
Γ	Thermal factor
δ	Deflection
Δ	FOWLP strength parameter
σ	Flexure strength

σ_0	Scale parameter
σ_u	Threshold strength
σ_{min}	Smallest strength

CHAPTER 1 INTRODUCTION

1.1 RESEARCH BACKGROUND

Nowadays, there are various electronic products among people life especially the smart electronic products. The smart electronic products become more and more popular with the development of high-speed internet. For example, people watch news through their smartphone anywhere; teachers use tablets to teach in an interactive way; beyond the traditional fixed channel, people can watch internet channel or video website through smart televisions. The trend of electronic products is smaller, more functional and cheaper. The requirements of growing and diversifying system drive the development of new packaging technologies [1-4]. The wafer level packaging technology is proposed at the beginning of this century, and it becomes ripe and important after 15 years development.

The wafer level packaging technology is used to package integrated circuit on wafers. The initial wafer level packaging technology is known as the wafer level chip scale packaging technology [5, 6]. It is because the size of wafer level chip scale package (WLCSP) is as the same as the size of functional die. The advantages of WLCSP are the small package size, superior electrical performance and low packaging cost. The WLCSP is one of the smallest packages in the semiconductor market. However, the limitations of WLCSP are the low number of input/output (I/O) and unrealizable 3-dimensional (3D) routing. The WLCSP also shows poor performance of thermal-mechanical [7, 8] when it works on the printed circuit board (PCB).

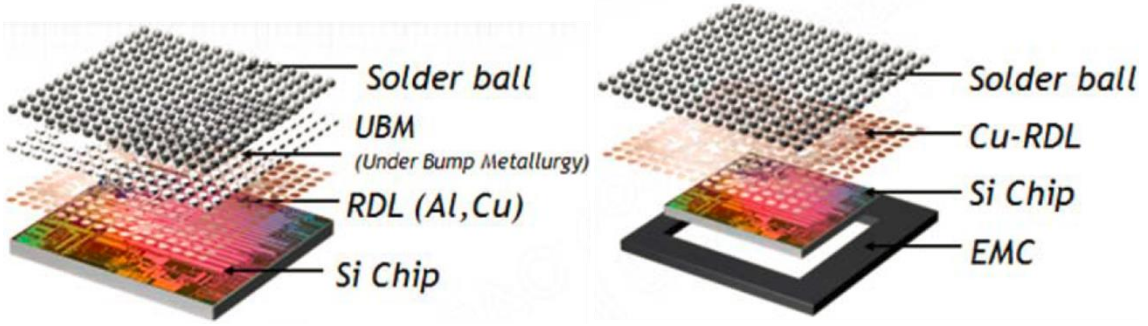

Figure 1-1 Illustration of wafer level chip scale package (left) and fan-out wafer level package (right) [9].

The fan-out wafer level packaging technology [10, 11] is developed to compensate the issues of wafer level chip scale packaging technology. The fan-out wafer level packaging technology is a further development of the wafer level chip scale packaging technology, and its most significant aspect is the fan-out area [9, 12-14]. Figure 1-1 shows the illustration of wafer level chip scale package and fan-out wafer level package. The number of I/O of fan-out wafer level package (FOWLP) is much higher than the number of I/O of WLCSP. The FOWLP can be further developed for the 2.5D/3D [15] FOWLP [16-20] or FO-PoP (package on package) [21-23] through laser ablation (LSA) or through silicon via (TSV) technology. For the aspect of thermal-mechanical reliability, the FOWLP also shows better performance than other packages (as shown in Figure 1-2) such as plastic ball grid array (PBGA) [24]. Therefore, the advantages of fan-out wafer level packaging technology can be summarized into six aspects:

- Dimension: small package size and thin package thickness.
- I/O density: fine pitch and large number of I/O.
- Integration: 2.5D/3D and system in package (SiP).

- Electrical performance: short interconnections and even minimal interconnections.
- Thermal performance: low power consumption.
- Cost: low packaging cost and test cost.

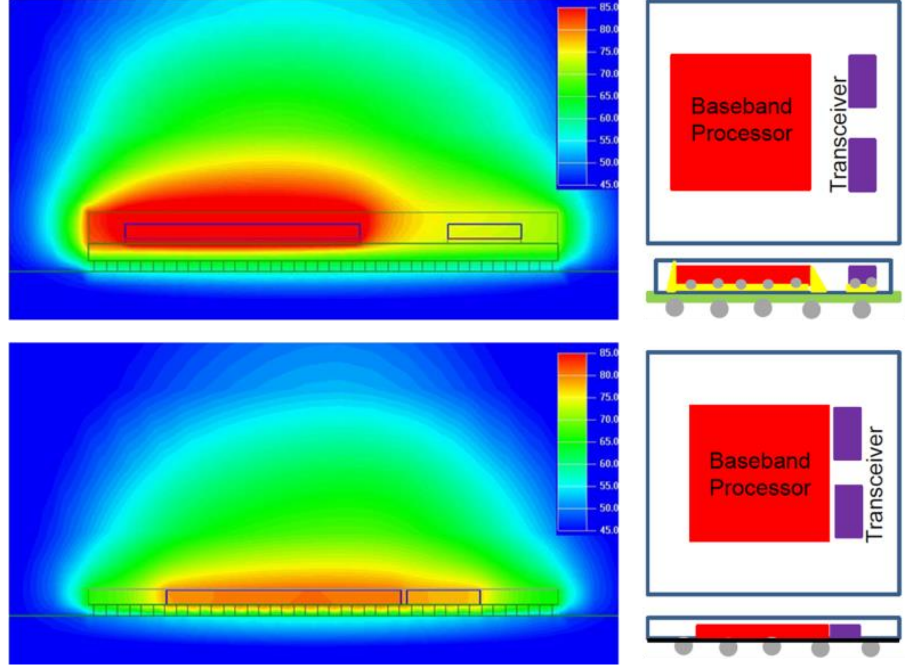

Figure 1-2 Thermal performance of plastic ball grid array (top) and fan-out wafer level package (bottom) [24].

In the early year 2009, Infineon becomes the first company to commercialize the wafer level package (WLP). The chip from Infineon is a wireless baseband with multiple functions such as GPS, FM radio and Bluetooth in the LG mobile phones. The WLPs are used to the volume sensitive electronic products. Therefore, the major application of FOWLP is consumer electronic products such as mobile phones, laptops, digital cameras and portable media players. The FOWLP is used to the mobile phone (as shown in Figure 1-3) as the baseband modem, power management units, drives, transceivers and processors. For example, there are 16 out of 48 and 12

out of 44 WLPs in iPhone 6S plus and Huawei Mate 7 respectively. There are average five to seven WLPs in a mobile phone now, and this number is still increasing. In recent years, the application of FOWLP extends to the field of automotive (sensors, GPS and drivers) and medical (drivers, processors and power units).

Figure 1-3 The applications of wafer level package in a smartphone [25].

According to the Yole Developpement report [25], there are two dominated players in the FOWLP market. STATS ChipPAC and NANIUM take up 59% and 25% share of the total $174 million market revenue respectively in the year 2014. Other companies such as Infineon, Freescale, ASE and STMicroelectronics share the remaining 16% share of market revenue. Researchers forecast the market revenue of FOWLP could achieve a 30% CAGR (compound annual growth rate) until the year 2020 and reach $676 million (as shown in Figure 1-4).

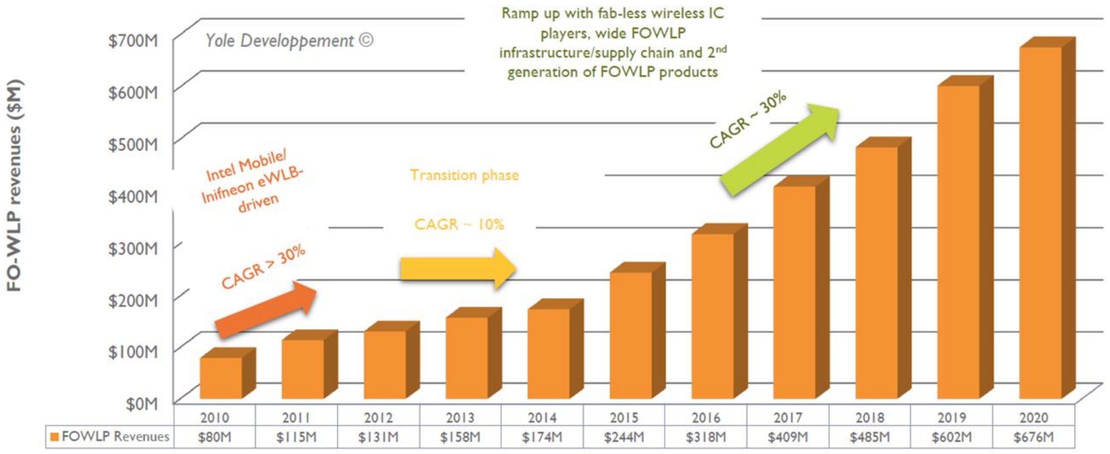

Figure 1-4 The revenue forecast of FOWLP activity [25].

There are three major assembly processes in the fan-out wafer level packaging technology: reconstitution process, redistribution process and backend of line process (as shown in Figure 1-5). The reconstituted process is used to rearrange the processed functional dies to an artificial wafer and encapsulated this artificial wafer by the epoxy molding compound (EMC). The reconstituted process consists of four minor processes. The wafer grinding process and wafer sawing process aim to process the functional wafer into certain thickness and dimension. The pick and place process builds the artificial wafer by picking the processed dies and placing them onto a metal carrier. The molding process uses EMC to encapsulate the artificial wafer. The redistribution process is used to lithograph passivation (PSV) layers and redistribution layers (RDLs) alternately. There are two RDLs and three PSV layers typically. The FOWLP also may have one RDL and two PSV layers as a version of low-cost FOWLP. The last backend of line process operates the wafer grinding process again to finalize the package thickness. The backside protection (BSP) tape lamination process applies the backside protection tape to the package to protect the

package. The laser marking process and solder ball drop process is essential before singulating the package wafer.

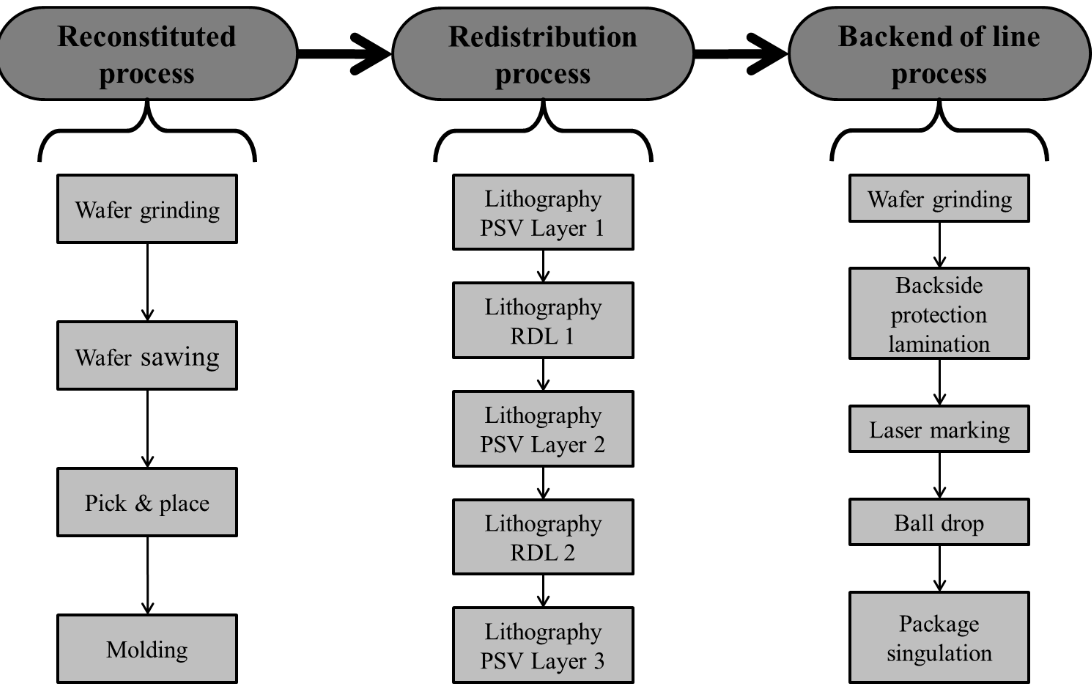

Figure 1-5 FOWLP assembly process flow.

1.2 RESEARCH MOTIVATION

There are three critical criterions to judge the packaging technology – performance, form factor and cost. The wafer level packaging technology shows a good trade-off among these three criterions. Although the fan-out wafer level packaging technology has its superiority, it also faces some challenges such as packaging cost, die shift, wafer warpage and reliability.

The packaging cost is a hot topic in the semiconductor packaging industry. There are three aspects proposed to reduce the packaging cost. The first aspect is to simplify the process. There are two RDLs and three PSV layers lithographed during the redistribution process typically. There is a low-cost solution, and the FOWLP only has one RDL and two PSV layers. This change reduces the process time and workforce without yield loss. The second aspect is the expansion of carrier scale. The first generation WLP is implemented on the 8-inch carrier. The mainstream WLP can be implemented stably on the 12-inch carrier. The next generation WLP turns to the panel carrier [26-28] (as shown in Figure 1-6) and thus the yield will increase exponentially and the cost will reduce significantly. The third aspect is new materials. The new and era material could simplify the process, reduce cost and provide better reliability. For example, SiO_2 is a new dielectric material, and it has the feature of low temperature curable [29]. SiO_2 can be fully cured at 200℃ instead of 350℃. The low curable temperature could reduce the energy consumption and risk of failure.

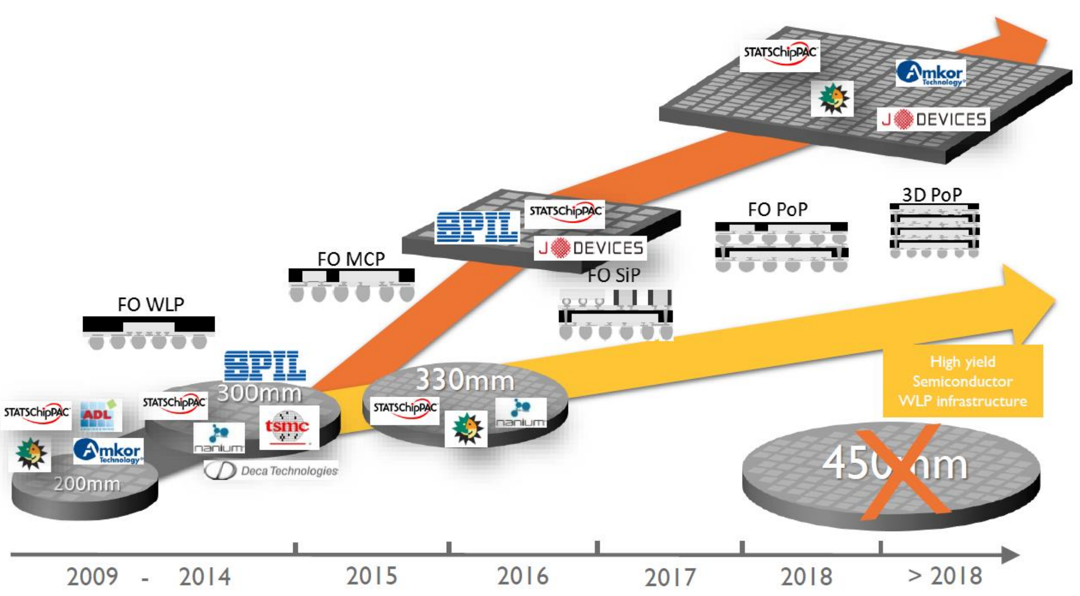

Figure 1-6 Trend prediction of WLP carrier size [25].

The most important process in the whole wafer level packaging process is the reconstituted process. The quality of reconstituted wafer is very critical. The most frequent issues are the die shift and high warpage. The die shift issue is caused by the pick and place (PnP) process and molding process. The PnP process is used to build artificial wafers by picking the dies from wafer rings and placing them onto a metal carrier. Nowadays, the PnP machine can achieve very high accuracy (the die shift range is less than 10 μm). Therefore, the PnP process has a minor effect on the die shift. However, the molding process [30, 31] usually causes the die shift issue. The molding process uses the epoxy molding compound [32-35] to encapsulate the artificial wafer after the PnP process. The coefficient of thermal expansion (CTE) of mold plate and chemical shrinkage is the main contributor to die shift [36]. The drag force of die shift can be reduced by optimizing the diameter of molding wafer, increasing the thickness of molding wafer and reducing the filling speed [37]. The epoxy molding compound with low CTE and low cure shrinkage are preferred [38-40].

The high warpage issue is very serious [41-47]. The 12-inch wafer level packaging technology shows a good trade-off between the yield and reliability currently. The high warpage wafer often causes machine handling issues. The machine sometimes cannot handle the wafer or fail to handle the wafer. The former only causes the process delay or abort. However, the latter causes the wafer damage (as shown in Figure 1-7) and machine breakdown.

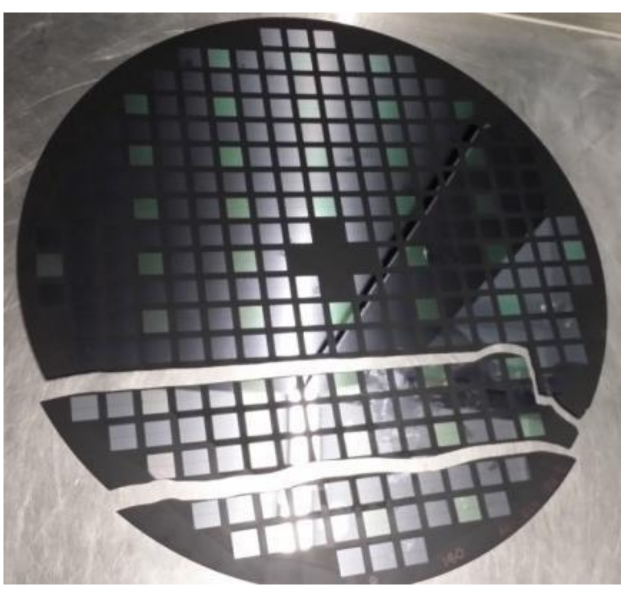

Figure 1-7 A high warpage wafer is broken during the assembly process.

The different kinds of packaging technology have common mutual reliability issues, and they also have their own reliability issues. The package structure and manufacturing process decide the type of reliability. For example, the reliability of solder joint [48-62] is critical to flip chip packages [63-70]. The reliability of solder joint is not critical to FOWLPs because the FOWLP does not have solder joints. However, the size of FOWLP is thin and small and thus the FOWLP is usually used to volume sensitive devices. The strength of ultrathin FOWLP is low, and the low package strength often leads to crack issues. There is much research about the silicon strength and silicon die strength [71-74]. However, the research about the package level strength is little [75-83], and there is not any research about the FOWLP strength. The FOWLP is made up of silicon dies, passivation layers, redistribution layers, backside protection tapes and solder balls. The effect of individual component and external environment on the FOWLP strength is uncertain. Therefore, the study of strength behavior of FOWLP is significant.

1.3 RESEARCH OBJECTIVES

The main objectives of this research consist of:

- Studying the strength behavior of various FOWLP structure.
- Understanding the effect of material and assembly process on the FOWLP strength.
- Investigating the effect of thermal on the FOWLP strength.
- Developing theoretical models of FOWLP strength and FOWLP fatigue crack growth.

1.4 RESEARCH SCOPE

The scope of this research is limited to:

- Evaluating the effect of structure and PSV layer on the FOWLP strength.
- Investigating the effect of temperature cycling test and high temperature storage test on the FOWLP strength.
- Studying the effect of thermal related assembly process and thermal related reliability test on the EMC strength and hardness. The thermal related assembly process contains the post-mold curing process, PSV layer curing process and reflow process. The thermal related reliability test contains the temperature cycling test and high temperature storage test.
- Investigating the effects of various factors (FOWLP dimension, PCB bar and grinding method) on the FOWLP strength.
- Studying the FOWLP strength by the numerical method.
- Establishing simulation models of FOWLP strength test.

- Developing theoretical models of FOWLP strength and FOWLP fatigue crack growth.

1.5 ORGANIZATION OF THE THESIS

This thesis is organized into the following chapters:

Chapter 2 shows a comprehensive literature review of the existing studies of silicon strength and functions of various reliability tests.

Chapter 3 explains the methodology of this research and the proposed research plan.

Chapter 4 introduces the experimental study of FOWLP strength by the 3PB test method.

Chapter 5 introduces the numerical study of FOWLP strength by the finite element method.

Chapter 6 proposes the theoretical model of FOWLP strength and FOWLP fatigue crack growth.

Chapter 7 concludes the whole research work and proposes the suggestions of future work.

CHAPTER 2 LITERATURE REVIEW

2.1 METHODOLOGY OF STRENGTH EVALUATION

There are several methods used to evaluate the silicon strength such as the three-point bending test, four-point bending test, ball-on-ring test, ball breaker test and plate-on-elastic-foundation test. The ball-on-ring test, ball breaker test and plate-on-elastic-foundation test are usually used to evaluate the effect of silicon surface on the silicon strength. It is because these methods can isolate the effect of silicon edge defects. However, the three-point bending test and four-point bending test method are the most popular evaluation method of silicon strength. It is because the three-point bending test and four-point bending test cover the silicon surface and silicon edge at the same time.

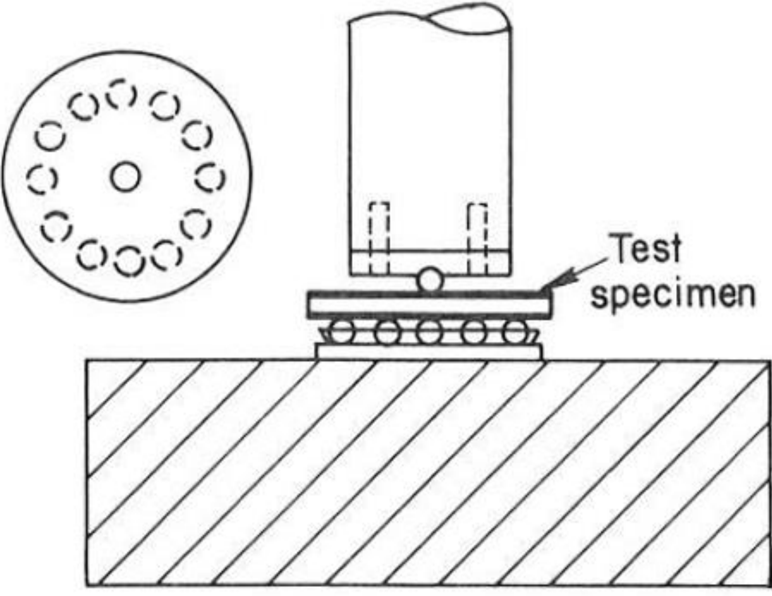

Figure 2-1 Ball-on-ring test apparatus [84].

The ball-on-ring (BOR) test (as shown in Figure 2-1) is considered as the best biaxial strength test method. The BOR test is used to evaluate the strength of brittle specimen, and it is a popular strength test method for ceramics [84, 85]. However, the specimen shape of BOR test is disk. The shape of IC chip is rectangular or square. Therefore, some errors are added to the specimen strength when we assume the shape of IC chip is disk.

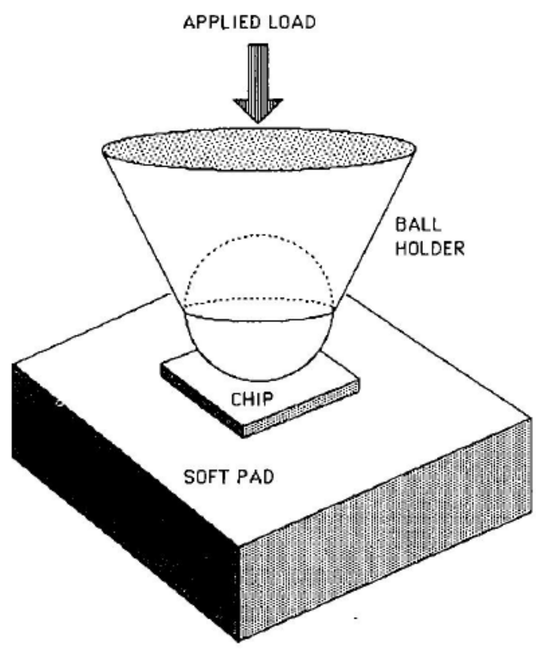

Figure 2-2 Ball breaker test apparatus [86].

The ball breaker test (BBT) and plate-on-elastic-foundation test (PEFT) are similar. They are only sensitive to the specimen surface defects. Therefore, they have the advantage of isolating specimen edge defects. The apparatus of ball breaker test (BBT) includes a loading rod, a Teflon ball and a soft flat pad platform (as shown in Figure 2-2). The plate-on-elastic-foundation test (PEFT) was introduced by Tsai et al., and it was specially designed for chip scale specimens [87]. Figure 2-3 shows two kinds of PEFT – point load test (PLT) and line load test (LLT). The PLT uses a

pointer with the radius of 0.25 mm while LLT uses a plate carbon steel tool with the thickness of 0.3 mm.

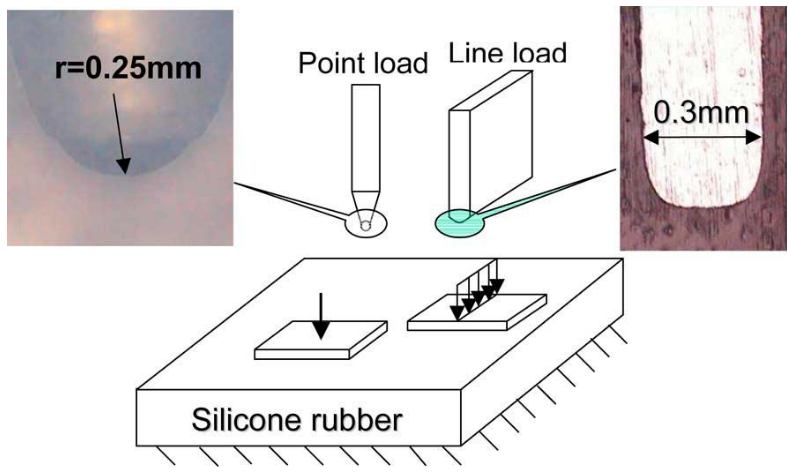

Figure 2-3 The apparatus of point load test and line load test [88, 89].

The three-point bending (3PB) test and four-point bending (4PB) test are the most common and widely used method of strength test. Both tests can evaluate the specimen flexure strength, flexure strain and modulus. The ISO (International Organization for Standardization) standard 'Plastics – Determination of flexural properties (ISO 178)' [90] and the ASTM (American Society for Testing and Materials) standard 'Test Methods for Flexural Properties of Unreinforced and Reinforced Plastics and Electrical Insulating Materials (D790)' [91] are formulated for the 3PB test. The ASTM standard 'Standard Test Method for Flexural Properties of Unreinforced and Reinforced Plastics and Electrical Insulating Materials by Four-Point Bending (D6272)' [92] is formulated for the 4PB test.

The 3PB test and 4PB test can be implemented easily by any universal testing machine. However, the key point is the fixture (as shown in Figure 2-4). The 3PB fixture has two rollers on the lower side to provide the support for the specimen. The

span of two rollers should be adjustable to fit the specimen size. The last point of 3PB fixture is the upper loading head. The loading head forces on the specimen centerline. The force scale is controlled by the digital load cell. The 4PB fixture is similar to the 3PB fixture especially the lower sides of fixture. The 4PB fixture upper loading head has two rollers instead of one. These two rollers separate at the same distance from the fixture centerline.

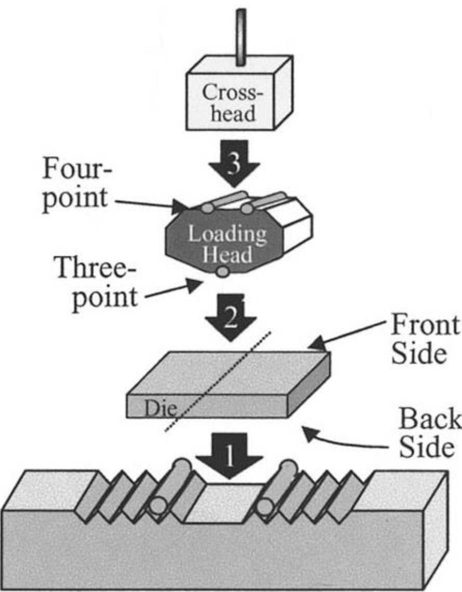

Figure 2-4 The fixture of bending test [93].

Figure 2-5 shows the loading mechanism of 3PB test. The highest bending moment of 3PB test always appear along the specimen centerline, and the centerline area suffers the highest stress during the 3PB test. Therefore, the 3PB test result is highly sensitive to the specimen surface and edge defects especially the portion along the centerline. The flexure strength of 3PB test can be obtained by [93]

$$\sigma_{3PB} = \frac{3LF}{2BW^2} \tag{2.1}$$

where the fracture load F is obtained from the 3PB test, B is the width of specimen, W is the thickness of specimen and L is the fixture span [93].

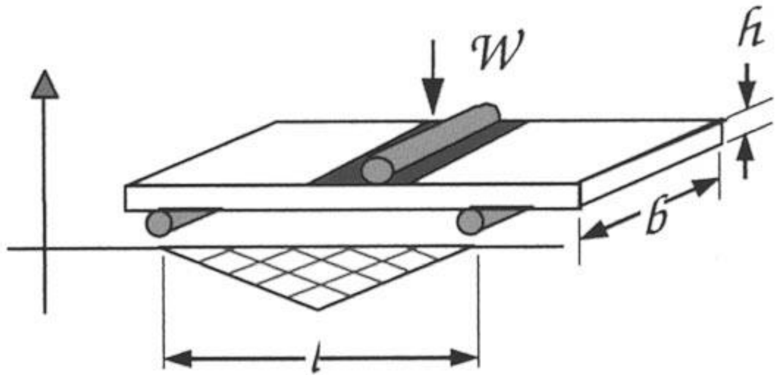

Figure 2-5 The loading mechanism of three-point bending test [93].

Figure 2-6 shows the loading mechanism of 4PB test. The highest bending moment appears in between the upper rollers. The 4PB test flexure strength can be obtained by [93]

$$\sigma_{4PB} = \frac{3L_hF}{BW^2} \tag{2.2}$$

where the new parameter a is the shortest distance between an upper loading roller and a lower supporting roller [93].

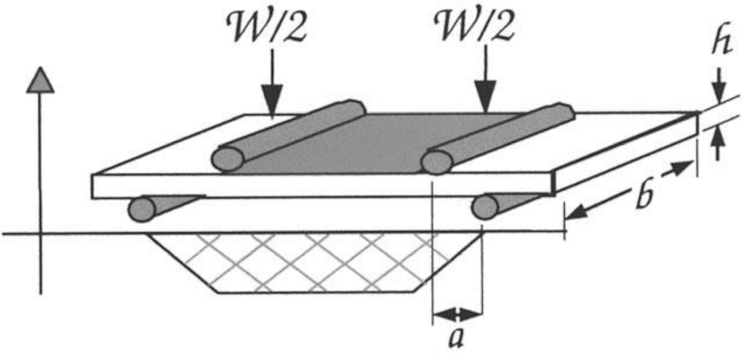

Figure 2-6 The loading mechanism of four-point bending test [93].

2.2 EVALUATION OF SILICON DIE STRENGTH BY 3PB TEST METHOD

2.2.1 EFFECT FACTORS ON SILICON DIE STRENGTH

The effect factors on the silicon strength can be classified into two groups. The first group of effect factor is related to the silicon own profile such as the silicon shape, size and thickness. Some research has shown that the silicon own profile factors do not affect the silicon strength obviously and directly [94, 95]. The second group of effect factor is related to the assembly process such as the wafer grinding process and wafer sawing process. The wafer grinding process and wafer sawing process create defects on the silicon surface and silicon edge respectively. However, there are three widely accepted effect factors on the silicon strength – silicon surface defects, silicon edge defects and weak planes of silicon crystal lattice [87].

The wafer grinding process is the very first process in the whole fan-out wafer level packaging assembly process. The aim of wafer grinding process is to grind the incoming wafer to the required thickness for further processes [96-104]. The wafer grinding process has three grinding steps. The first grinding step is the normal grinding by fine grit wheels. The second grinding step is the fine grinding by super-fine grit wheels. The third grinding step is the polishing by ultrafine grit wheels. The roughness of grinding side is fine enough after the second grinding step and thus the third grinding step is less used. Beyond the mechanical grinding method, the chemical wet etching and plasma etching methods also can replace the polishing step to gain an ultrafine wafer surface (as shown in Figure 2-7). In comparison, the

plasma etched wafer surface is smoother than the chemical etched wafer surface [105].

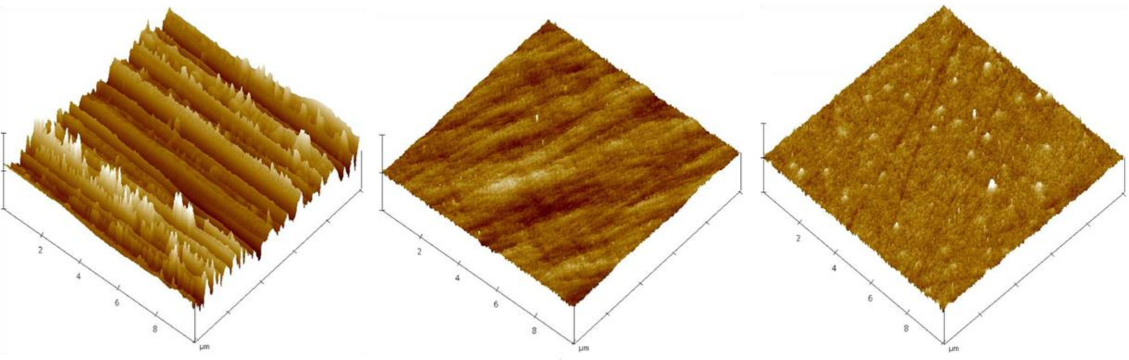

Figure 2-7 Surface AFM images of grinding only, grinding followed by polishing and grinding followed by chemical wet etching (from left to right) [106].

The silicon surface condition after the wafer grinding process is one of the most critical factors, which affects the silicon die strength [107]. The silicon dies with smooth surface always show higher strength than those silicon dies with rough surfaces [104, 108]. Yeung et al. ground her wafers by three methods [109]. Method 1 was the normal grinding process. Method 2 was the conventional chemical wet etching process. Method 3 was the wet etching process by the HF-based acid solution. She used the ball breaker test instead of the 3PB test. The ball breaker test only works on the silicon die surface, while the 3PB test works on the silicon die surface and edge. Therefore, the ball breaker test is much better than the 3PB test when we want to evaluate the effect of surface condition on the silicon die strength. The obtained flexure strength in the 3PB test should be lower than the obtained flexure strength in the ball breaker test [106]. The reason is the effect of silicon die edge defects.

Figure 2-8 shows the flexure strength of Yeung BBT. We can find that the chemical wet etching process improves the silicon die strength significantly. The HF-based acid solution is more efficient than normal chemical wet etching solutions. The RMS (root mean square) value of wafer surface roughness shows that the RMS value of Method 3 wafer is far lower than the RMS value of Method 2 wafer. Therefore, Method 3 has the highest average strength and the tightest strength distribution.

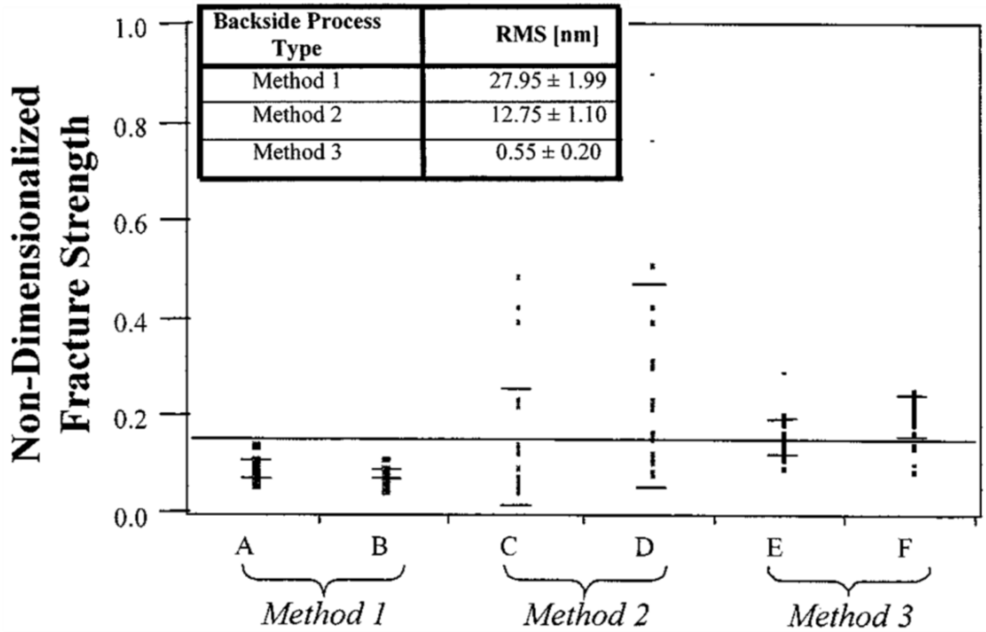

Figure 2-8 Flexure strength of Yeung BBT and the RMS value of specimen surface roughness [109].

The wafer sawing process is conducted after the wafer grinding process. The aim of wafer sawing process is to saw the incoming wafer to the required size for further processes [110]. There are two wafer sawing methods – mechanical sawing method [111, 112] and laser sawing method [113-115]. The mechanical sawing method uses diamond blades to saw the wafers. Most wafer sawing tasks could be achieved perfectly by the proper blade selection. The diamond blade collection is broad, and there are different thickness and grit size diamond blades. The laser

sawing method is also known as the stealth dicing method [116-118]. It is because the saw straight of laser sawing is extremely tiny. The saw straight of laser sawing cannot be observed by naked eyes, and it only becomes visible under the high magnification microscope. Therefore, the laser sawing method can offer an extreme low kerf loss.

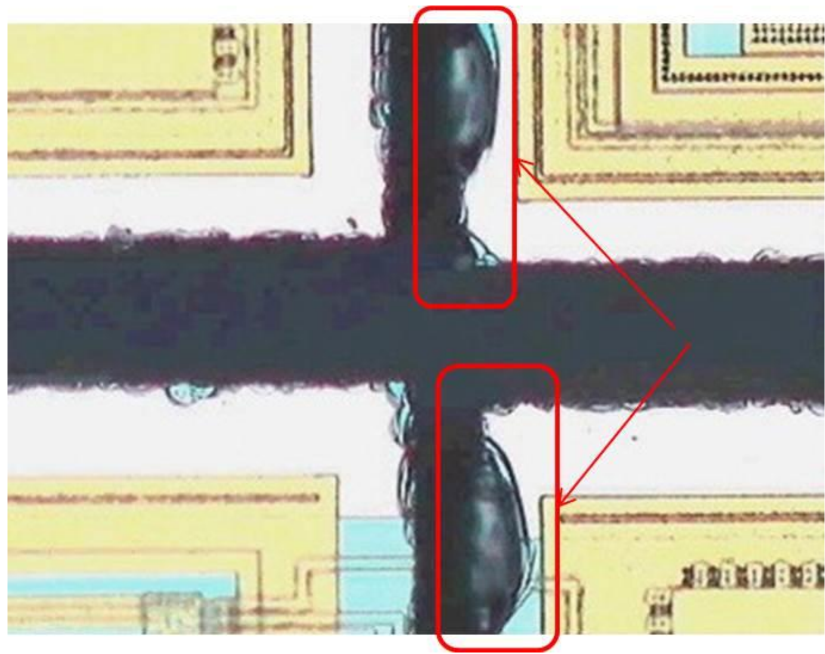

Figure 2-9 Chippings appear on the die kerf after the wafer sawing process [119].

The silicon edge condition after the wafer sawing process is one of the most critical factors, which affects the silicon die strength. The silicon dies with neat edge always show high strength. The silicon die edge defects are known as chippings. Figure 2-9 shows the chippings appear on the die kerf after the wafer sawing process. The quality measurement criteria of wafer sawing process are the chipping wide and the number of occurrences.

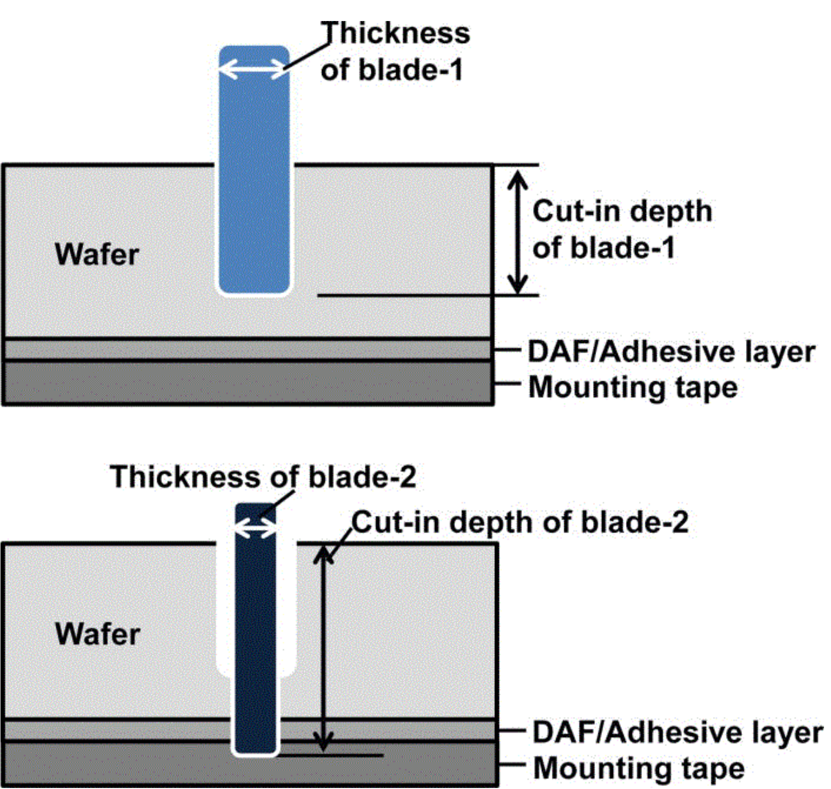

Figure 2-10 Illustration of step cut method [120].

Figure 2-10 shows one of mechanical sawing methods – step cut, and this method can reduce and avoid chippings effectively. The step cut method uses two different thickness diamond blades. The thickness of blade-1 should be thicker than the thickness of blade-2. The cutting depth of blade-1 is only 10-20% of the total wafer thickness. However, blade-2 is used to cut through the wafer.

The saw straight of functional wafer is coated. The laser grooving process (as shown in Figure 2-11) is used to minimize the coating effect on chippings. The laser grooving process is used to remove the coating layer before performing the mechanical sawing [121, 122]. The laser grooving process is similar to the step cut method, and it also can help to reduce chippings.

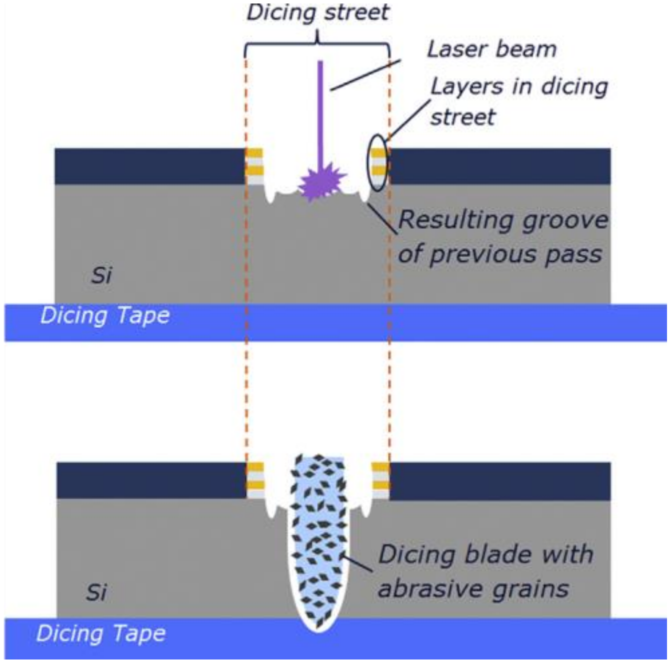

Figure 2-11 Illustration of laser grooving process [121].

The mechanical sawing method has the limitation of sawing thin wafers [123]. The machine vibration and cooling water may damage the thin wafers. By contrast, the laser sawing method is quite suitable for the thin wafer sawing. However, the parameters of laser beam such as repetition rate and pulse width should be carefully reviewed [124]. The Dicing-by-Thinning (DbT) method [125] can avoid the sidewall defects and edge defects of thin die effectively. Figure 2-12 shows the process flow of DbT method. The DbT method saws the wafer before the wafer grinding process. However, the DbT method does not cut through the wafer. The pre-cut wafer is bonded to a substrate before the grinding process. Finally, the pre-cut wafer is ground till the dies raise and separate. There are two pre-cut methods. One is the mechanical sawing method, while the other one is the dry etching method. Although both pre-cut methods improve the thin die strength, the dry etching method is superior to the mechanical sawing method.

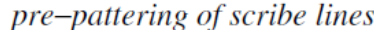

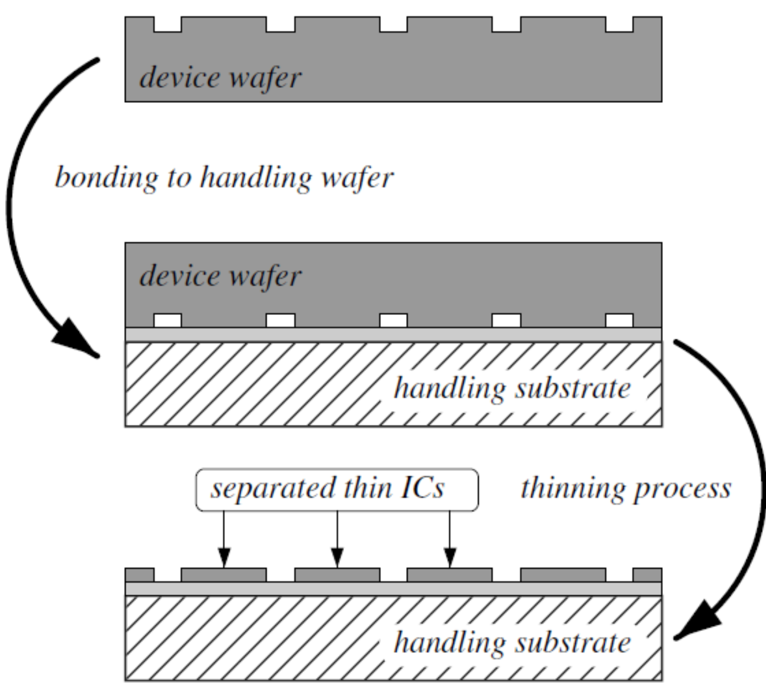

Figure 2-12 Illustration of DbT method [125].

2.2.2 FRACTURE ANALYSIS OF SILICON DIE

The fracture analysis of silicon die includes the fracture pattern analysis and the initial fracture point analysis. The fracture pattern and initial fracture point have the close relationship with the assembly process and the strength evaluation method. The wafer grinding process and wafer sawing process create surface defects and edge defects on the silicon die. The surface defect and edge defect decide the initial fracture point, and the surface defect affects the fracture pattern. However, not all the strength evaluation methods cover both kinds of defect. For example, the BBT only works on the specimen surface and thus the fracture of silicon die is only due to the silicon die surface defects. The 3PB test works on the specimen centerline and thus it

covers both silicon die surface defects and edge defects. Therefore, we only discuss the fracture pattern and initial fracture point caused by the 3PB test in this section.

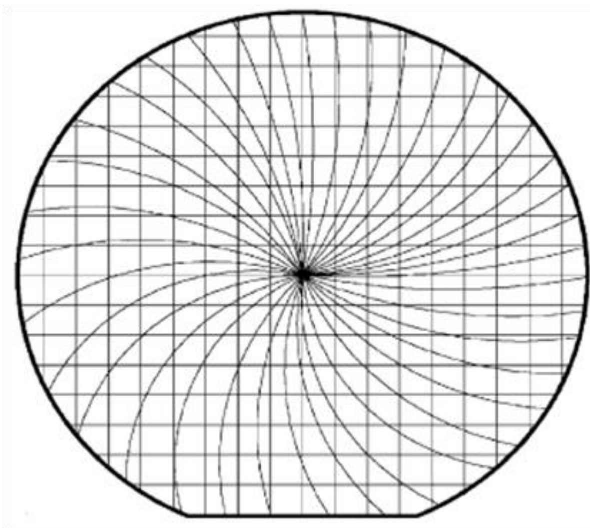

Figure 2-13 Illustration of grinding patterns [94].

The wafer grinding surface is not perfectly flat. It is because of the limitation of grinding machine or grinding process. We can find the grinding patterns easily on the ground surface after the wafer grinding process. Figure 2-13 shows the grinding patterns, and they look like ship propellers. Figure 2-14 shows two possible directions of loading force and grinding pattern. The actual grinding patterns look like grooves by the surface analysis machine, and it is similar to the specimen bottom surface in Figure 2-14, although the illustration is drawn exaggeratedly.

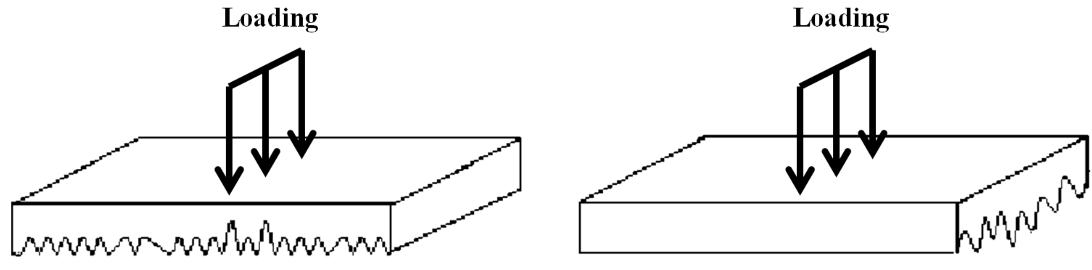

Figure 2-14 Two possible directions of loading force and grinding patterns [126].

The grinding patterns must have some angles with the silicon die edge. The angle is varied by the location of silicon die on the wafer. Therefore, there is an angle between the bending force and grinding patterns. Figure 2-15 shows four kinds of grinding patterns of silicon die on a wafer. The grinding patterns have the significant effect on the fracture load. The fracture load may drop significantly when the bending force is parallel to the grinding patterns. It is because the appearance of grinding patterns can accelerate the fracture. Vice versa, the fracture load may increase significantly when the bending force is perpendicular to the grinding patterns. The silicon die strength depends on the location of silicon die on a wafer [127]. In order to minimize the grinding patterns effect, the polishing process or etching process should be added to the wafer grinding process.

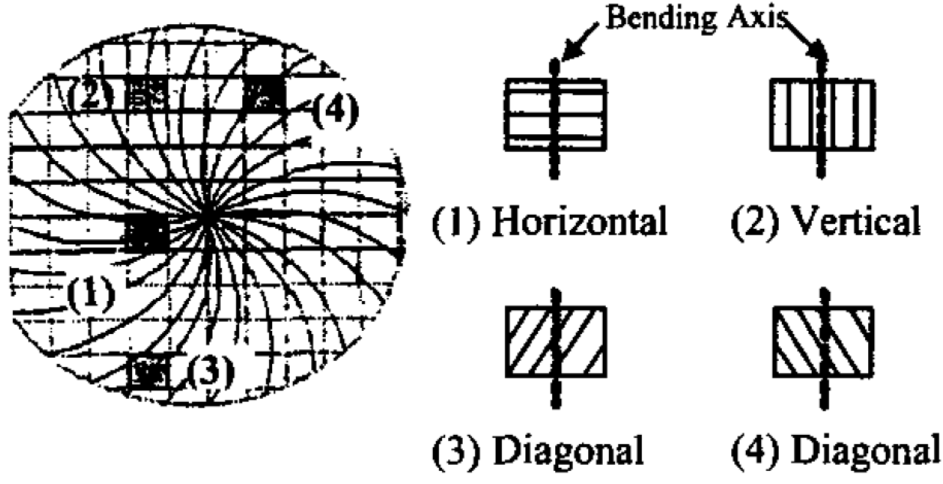

Figure 2-15 Four kinds of grinding patterns of silicon die on a wafer [128, 129].

Figure 2-16 shows the classification of fracture patterns, and it was summarized by Chen et al. [130]. There are four kinds of fracture pattern for silicon dies after the 3PB test. For type A, the fracture plane of silicon die is sharp and flat, and the silicon die only breaks into two pieces. The bending force must be parallel

with the grinding patterns in type A case, and the flexure strength of type A specimen must be the lowest. For type D, the silicon die breaks into many small pieces. The bending force must be perpendicular to the grinding patterns in type D case, and the flexure strength of type D specimen must be the highest. The silicon die breaks into countable pieces with irregular fracture planes in type B and type C cases. The bending force must be neither parallel nor perpendicular to the grinding patterns, and the flexure strength of type B and type C specimens must be in between the flexure strength of type A and type D specimens. This phenomenon is named as the directional behavior of silicon die strength

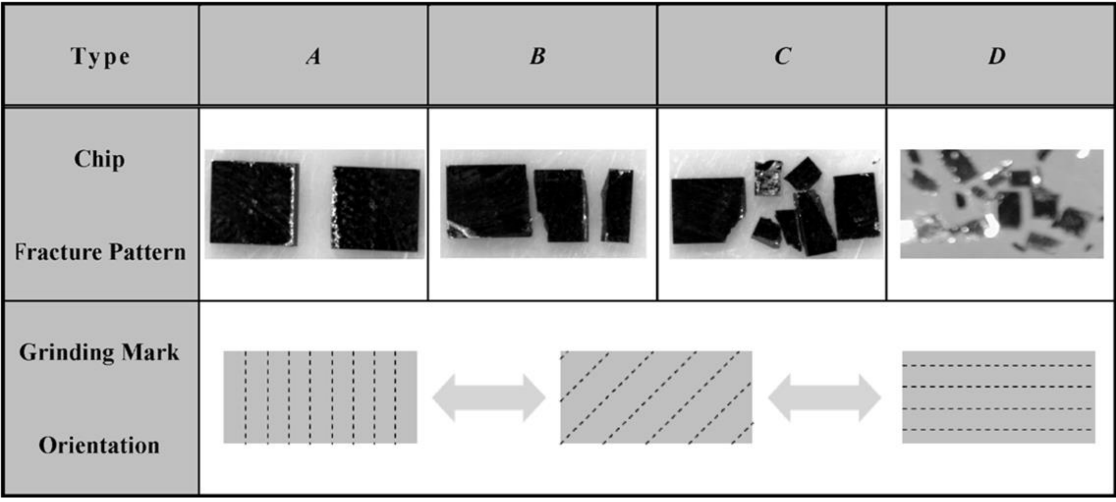

Figure 2-16 Classification of fracture patterns [130].

The initial fracture point may appear on the silicon die surface and edge. The emergent frequency of initial fracture point on the silicon die surface is higher than that on the silicon die edge after the 3PB test. Figure 2-17 shows an example of initial fracture point appears on the silicon die surface. The 3PB test applies a line load along the specimen centerline. Therefore, the surface area under the bending force is larger than the edge area under the bending force and thus the probability of

fracture appears on the silicon die surface is greater than that appears on the silicon die edge.

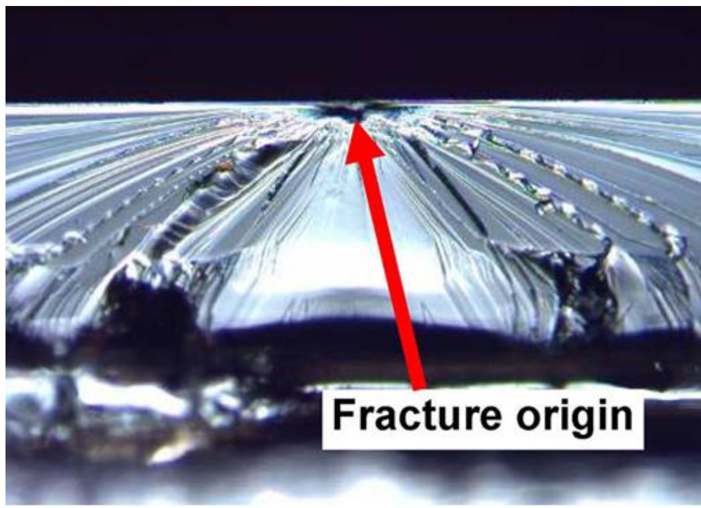

Figure 2-17 Initial fracture point appears on the silicon die surface [116].

The initial fracture point sometimes appears on the silicon die sidewall. The reason is the wafer sawing method. The laser sawing method must be applied. Figure 2-18 shows the comparison of sidewall conditions of silicon die after the mechanical sawing process and laser sawing process. The silicon die sidewall is smooth and clean after the mechanical sawing process. By contrast, the silicon die sidewall is rough after the laser sawing process.

A neutral surface must exist in a bending object. The neutral surface should parallel to the upper and lower surfaces of specimen. The bending stress varies linearly with the distance from the neutral surface. Therefore, the maximum stress must appear on the upper and lower surfaces of specimen. The upper surface (loading surface) of specimen suffers the compression stress, while the lower surface of specimen suffers the tension stress in the bending test. Silicon is sensitive and brittle material, and its fracture is due to the tension stress rather the compression stress.

Therefore, the initial fracture point always appears on the opposite side of loading force.

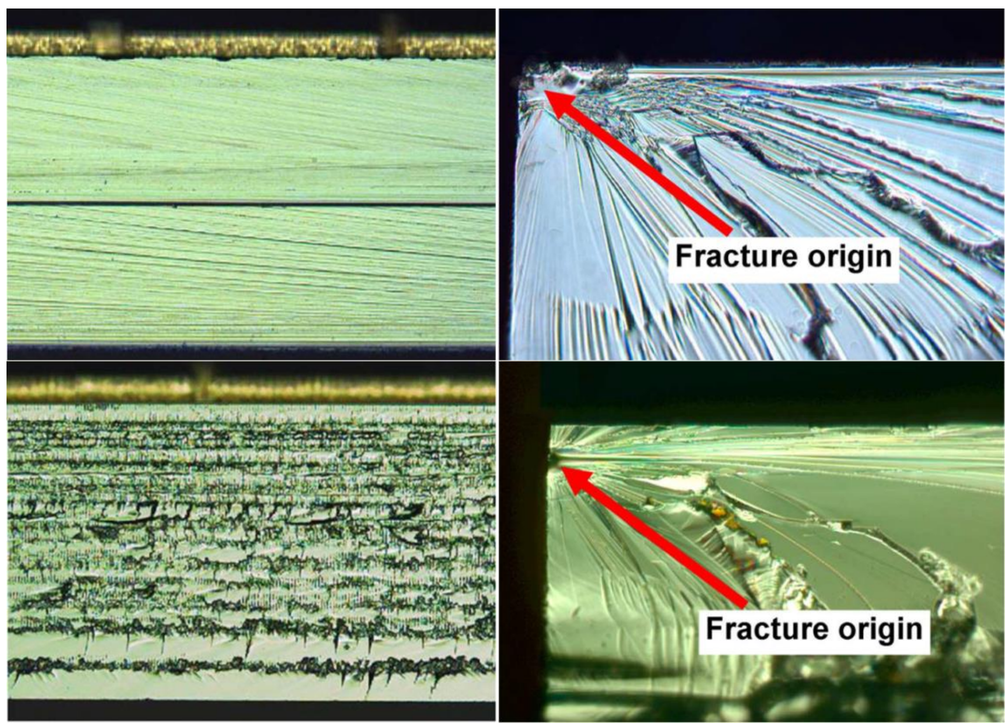

Figure 2-18 Comparison of sidewall conditions of silicon die after the mechanical sawing process (top) and laser sawing process (bottom) [116].

2.2.3 STRENGTH DATA ANALYSIS OF 3PB TEST

The average value method can judge the quality of a set of data. However, it is not suited to judge the quality of silicon die strength data. The statistical methods are considered as the best method to describe the silicon die strength data [131]. The normal distribution is the most basic statistical method, and it provides the distribution of failure probability for a set of data. The normal distribution is often used in the natural and social sciences. However, Weibull distribution is the most popular method to analyze the silicon die strength data.

Weibull distribution [132, 133] was described and named by Swedish mathematician Waloddi Weibull in 1951 [134]. He used this method to describe the material strength. Nowadays, Weibull distribution is widely used to describe the strength of brittle material [135-137] such as ceramics and silicon [138, 139]. There are two kinds of Weibull distribution – two-parameter Weibull distribution and three-parameter Weibull distribution, and they can be expressed as [134]

$$P = 1 - exp[-\varphi(\sigma)] \tag{2.3}$$

$$\varphi(\sigma) = \begin{cases} \left(\dfrac{\sigma}{\sigma_0}\right)^m & \sigma_u = 0, two\ parameter\ Weibull\ distribution \\ \left(\dfrac{\sigma - \sigma_u}{\sigma_0}\right)^m & \sigma_u \neq 0, three\ parameter\ Weibull\ distribution \end{cases}$$

where σ is the flexure strength, σ_0 is the scale parameter, m is the shape parameter or Weibull modulus and σ_u is the threshold strength.

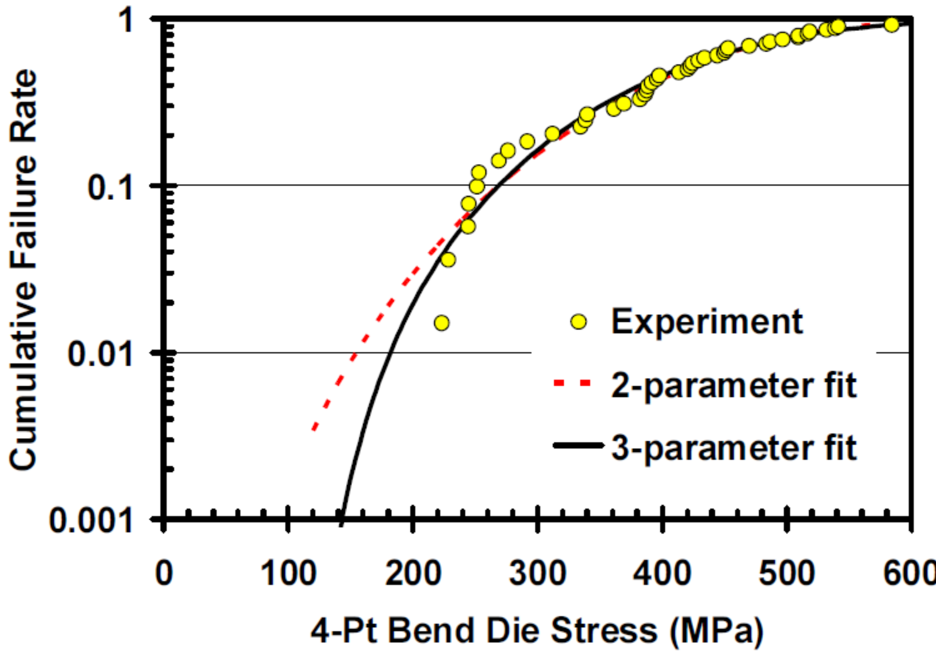

Figure 2-19 Comparison of two-parameter Weibull distribution and three-parameter Weibull distribution in the lower region of failure probability [140].

The three-parameter Weibull distribution can provide a better data fitting (as shown in Figure 2-19) than the two-parameter Weibull distribution especially in the lower region of failure probability [141, 142]. However, the two-parameter Weibull distribution is good enough to describe the data, and it is simple to use.

We should establish the failure probability (P_i) list before solving the scale parameter and shape parameter of two-parameter Weibull distribution. The failure probability list can be estimated by the probability estimation equations. The first step is to rearrange the silicon die strength data in the ascending order and substitute the silicon die strength data to the probability estimation equations one by one. There are four kinds of probability estimation equations [143]

$$P_i = \frac{i - 0.5}{n} \tag{2.4}$$

$$P_i = \frac{i}{n + 1} \tag{2.5}$$

$$P_i = \frac{i - 0.3}{n + 0.4} \tag{2.6}$$

$$P_i = \frac{i - 0.375}{n + 0.25} \tag{2.7}$$

where i is the ith silicon die strength data and n is the total number of specimen. Equation (2.6) is considered as the best estimator regardless the sample size.

To take the logarithm on the two-parameter Weibull distribution equation twice [144], and we have

$$\ln\ln\left(\frac{1}{1-P}\right) = m\ln\sigma - m\ln\sigma_0 \quad (2.8)$$

according to the equation

$$Y = a + bX \quad (2.9)$$

we can define the

$$Y = \ln\ln\left(\frac{1}{1-P}\right) \quad (2.10)$$

$$X = \ln\sigma_0 \quad (2.11)$$

The scale parameter and shape parameter can be solved by two different estimation methods – least square estimation (LSE) method and maximum likelihood estimation (MLE) method. The solvers of least square estimation method are [144-147]

$$m = \frac{N\sum_{i=1}^{N} x_i y_i - \sum_{i=1}^{N} x_i \sum_{i=1}^{N} y_i}{N\sum_{i=1}^{N} x_i^2 - \sum_{i=1}^{N} x_i \sum_{i=1}^{N} x_i} \quad (2.12)$$

$$\ln\sigma_0 = -\frac{1}{m}\frac{\sum_{i=1}^{N} y_i \sum_{i=1}^{N} x_i^2 - \sum_{i=1}^{N} x_i \sum_{i=1}^{N} x_i y_i}{N\sum_{i=1}^{N} x_i^2 - \sum_{i=1}^{N} x_i \sum_{i=1}^{N} x_i} \quad (2.13)$$

where x_i and y_i is the ith value of $\ln\sigma_0$ and $\ln\ln\left(\frac{1}{1-P}\right)$ respectively.

The least square estimation method is simple, and it can be solved manually without computer assisting. However, the maximum likelihood estimation method is quite complex. Its solvers are [144-146]

$$\frac{N}{m} + \sum_{i=1}^{N} \ln \sigma_i - N \frac{\sum_{i=1}^{N} \sigma_i^m \ln \sigma_i}{\sum_{i=1}^{N} \sigma_i^m} = 0 \tag{2.14}$$

$$\sigma_0 = \left(\frac{1}{N} \sum_{i=1}^{N} \sigma_i^m \right)^{\frac{1}{m}} \tag{2.15}$$

where m needs the assistance of computer to be solved. However, σ_0 is quite easily to be solved once we have the value of m.

The MLE method is proved as the best estimation method in statistics [148-150]. The MLE method has a superior performance regardless the sample size. However, Wu et al. found that the maximum likelihood estimation method often led to overestimation and thus the maximum likelihood estimation method had a lower safety factor than the least square estimation method in the engineering point of view [143].

Paul et al. found that the log-normal distribution was better than Weibull distribution, and the sample size had the significant effect on the accuracy of log-normal distribution [151]. We can get the log-normal distribution [152] when we take logarithm on the normal distribution equation [151]

$$P_f(\sigma) = \frac{1}{\sqrt{2\pi} c\sigma} exp\left\{ -\frac{[\log(\sigma/b)]^2}{2c^2} \right\} \tag{2.16}$$

where b is the log-normal scale parameter and c is the shape parameter.

Paul et al. used four batches of specimen in his experiment. The sample sizes are 45, 18, 18 and 18. Paul et al. used the probability estimation equation (2.4) and

the maximum likelihood estimation method to calculate the scale parameter and shape parameter.

The accuracy of Weibull distribution can be improved by increasing the sample size. The recommended threshold of sample size is 53 for Weibull distribution. The least square estimation method has a superior performance when the sample size is below 53, and the maximum likelihood estimation method is superior when the sample size is above 53. Therefore, the statement from Paul et al. is not persuasive enough, and the comparison between log-normal distribution and Weibull distribution is uncertain.

2.3 METHODOLOGY OF RELIABILITY TEST

2.3.1 TEMPERATURE CYCLING TEST

The temperature cycling (TC) test is used to determine the effect of varied temperature on electronic devices. The testing specimens are stored in a chamber. The chamber temperature always rises and drops between the high temperature and the temperature below the ice point. The TC test is similar to using an electronic device in an extreme environment. For example, you are using a phone in an extremely cold area, and then you bring the phone to the warm area and return for a few times. Therefore, the main purpose of TC test is to evaluate the electronic devices lifespan under the extreme environment.

Table 2-1 Temperature cycling test conditions [153].

Condition	Min Temperature (℃)	Max Temperature (℃)	Cycles/hour	Soak mode
A	-55 (-10, +0)	+85 (-0, +10)	2-3	1, 2 & 3
B	-55 (-10, +0)	+125 (-0, +15)	2-3	1 & 2
C	-65 (-10, +0)	+150 (-0, +15)	2	1 & 2
G	-40 (-10, +0)	+125 (-0, +15)	<1-2	1, 2, 3 & 4
H	-55 (-10, +0)	+150 (-0, +15)	2	1 & 2
I	-40 (-10, +0)	+115 (-0, +15)	1-2	1, 2, 3 & 4
J	-0 (-10, +0)	+100 (-0, +15)	1-3	1, 2, 3 & 4
K	-0 (-10, +0)	+125 (-0, +15)	1-3	1, 2, 3 & 4
L	-55 (-10, +0)	+110 (-0, +15)	1-3	1, 2, 3 & 4
M	-40 (-10, +0)	+150 (-0, +15)	1-3	1, 2, 3 & 4
N	-40 (-10, +0)	+85 (-0, +10)	1-3	1, 2 & 3

The JEDEC standard JESD22-A104 – 'Temperature Cycling' regulates the apparatus and procedures of TC test. There are 11 kinds of TC test condition [153], and they are listed in Table 2-1. The temperature range is from -55℃ to 150℃. One temperature cycle (as shown in Figure 2-20) means that the temperature rises from the extreme low point to the extreme high point and returns. The typical TC test rate is one to three cycles per hour. The other regulation of TC test is the soak time. There are four soak modes, and their minimum soak time is 1, 5, 10 and 15 minutes respectively.

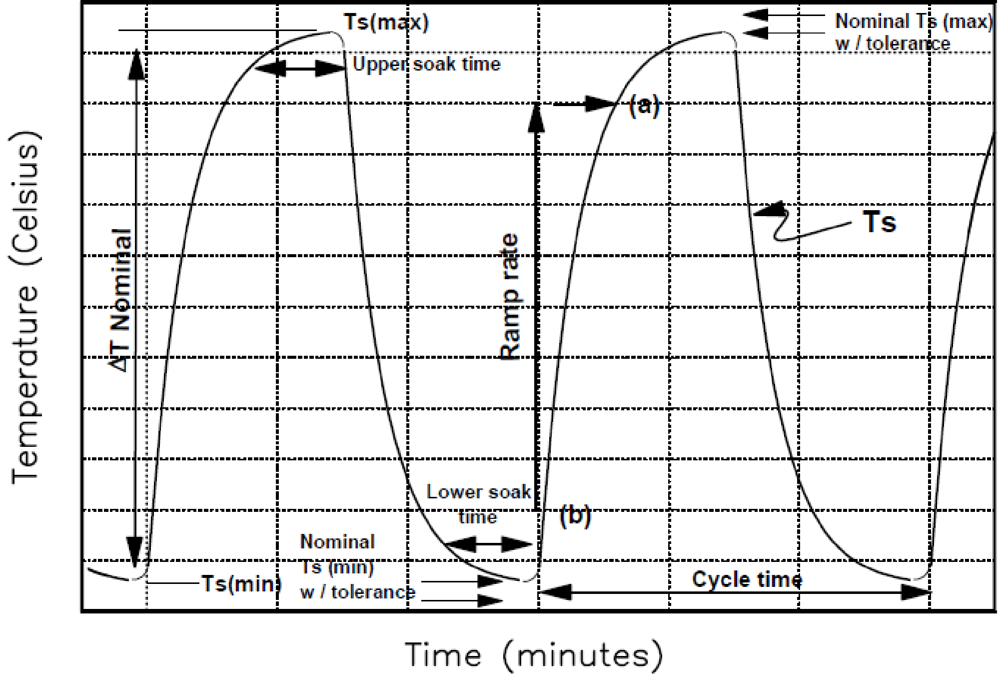

Figure 2-20 Example of temperature profile of temperature cycling test [153].

The main failure modes of IC chip are package crack and disconnection failure after the TC test [154]. The reason is the mismatched coefficient of thermal expansion (CTE). The packages are made up of various materials. Each material has its own physical and chemical properties. The CTE defines the size changes of material with respect to the temperature. The mismatched CTE causes complex internal force within a package. The internal force could provide the tension force or compression force to accelerate the package structure deformation [155-159]. The TC test temperature changes rapidly and the temperature range is large. Therefore, the package suffers strong deformations periodically during the TC test, and the TC test has the significant effect on the package structure and solder joint.

2.3.2 HIGH TEMPERATURE STORAGE TEST

The high temperature storage (HTS) test is used to determine the effect of time and temperature on electronic devices. The testing specimens are stored in a high temperature chamber. The high temperature vaporizes the moisture and isolates the humidity effect on electronic devices. The HTS test is similar to operating electronic devices for a long time. The difference is the HTS test heats the electronic devices by the external heat source while the operating electronic device is heated by itself. Therefore, the main purpose of HTS test is to evaluate the lifespan of electronic devices under the longtime operating condition.

Table 2-2 High temperature storage test conditions [160].

Condition	Temperature (°C)
A	125 (-0, +10)
B	150 (-0, +10)
C	175 (-0, +10)
D	200 (-0, +10)
E	250 (-0, +10)
F	300 (-0, +10)
G	85 (-0, +10)

The JEDEC standard JESD22-A103 – 'High Temperature Storage Life' regulates the apparatus and procedures of HTS test. There are seven kinds of HTS test condition [160], and they are listed in Table 2-2. The most frequently used conditions are condition B and condition C. Condition B HTS test is known as the normal HTS test, while condition C HTS test is known as the accelerated HTS test. The accelerated HTS test provides a challenging environment to the specimens, and it accelerates the specimen failure and shortens the testing time.

The main failure mode of IC chip is functional failure such as electrical failure or interconnection failure after the HTS test. The reason is the changes in material properties during the HTS test [161]. The electronic devices such as IC chips or packages are made up of various materials. The HTS test provides the high temperature and high energy environment to drive various materials to interact with each other. Therefore, some new materials are formed after the HTS test, and they may affect the package reliability.

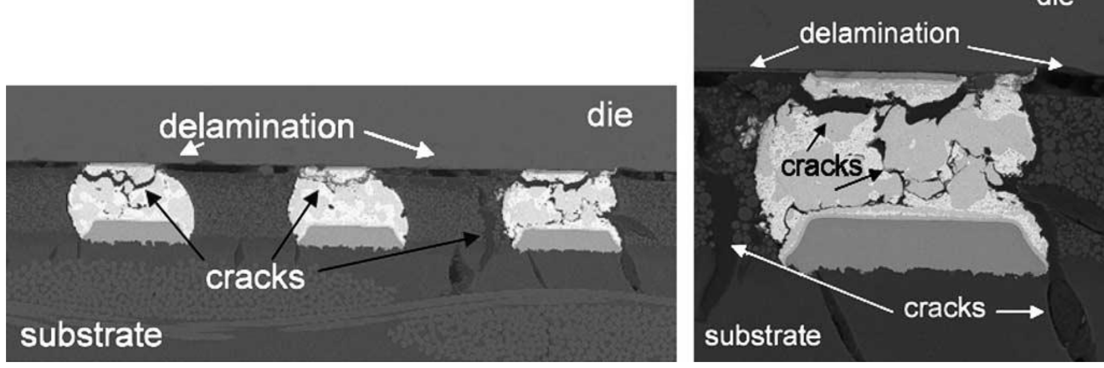

Figure 2-21 Bump cracks appear on the flip chip package after the HTS test [162].

The intermetallic compound (IMC) is formed after the HTS test. The IMC has the feature of brittle and easily crack under any thermal or mechanical loading. Once the crack appears on the IMC, the electrical interconnection of package is affected and the package function may fail. For the wire bonding packages [163-168], the IMC platelets can be found on the bond pad. The IMC platelets reduce the strength of wire pull or bond pull. For the flip chip packages [162, 169-171], the IMC platelets can be found in solder joints (as shown in Figure 2-21). The solder joints may easily crack once it is filled up with IMC platelets. However, the IMC effect on packages

with less material composition is minor such as pure silicon wafers [172], stacked chips [173] and wafer level packages [174, 175].

2.3.3 UNBIASED HIGHLY ACCELERATED STRESS TEST

The unbiased highly accelerated stress test (UHAST) is used to simulate extreme electronic device operating conditions. The testing specimens are baked in a chamber at the extreme temperature and humidity condition. The moisture is pressurized into the electronic devices at the extreme temperature condition. The function of electronic device is affected once the moisture reaches the device internal circuits. The UHAST is similar to using electronic devices in a moisture environment. Therefore, the main purpose of UHAST is to evaluate the insulation and integrity of electronic device.

Table 2-3 Unbiased highly accelerated stress test conditions [176].

Condition	Temperature (℃)	Relative humidity (%)	Duration (hour)
A	130 (-2, +2)	85 (-5, +5)	96 (-0, +2)
B	110 (-2, +2)	85 (-5, +5)	264 (-0, +2)

The JEDEC standard JESD22-A118 – ‘Accelerated Moisture Resistance’ regulates the apparatus and procedures of UHAST. There are only two kinds of UHAST condition [176], and they are listed in Table 2-3. Condition A temperature is 130℃ and humidity is 85%, while condition B temperature is 110℃ and humidity is 85%. The testing time is 96 hours and 264 hours respectively.

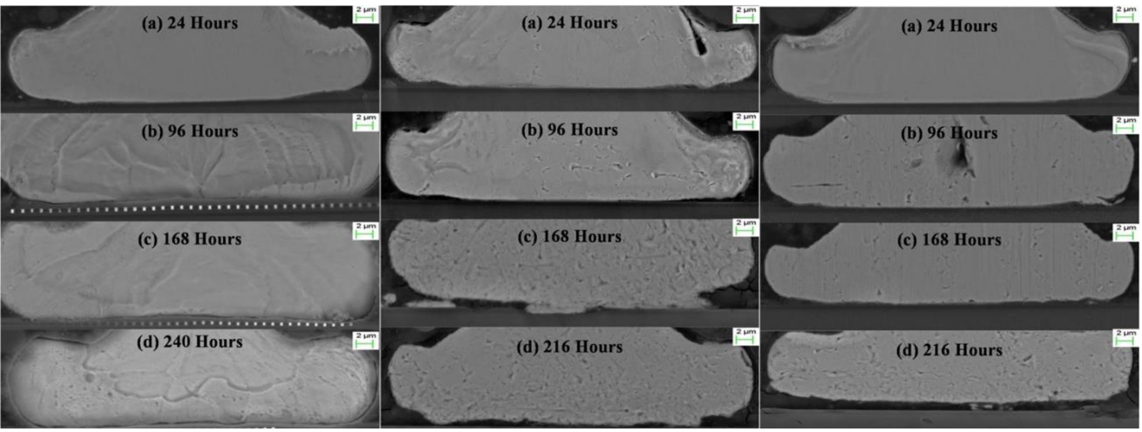

Figure 2-22 Crack development and propagation during the UHAST at 110℃, 120℃ and 130℃ / 100% RH [177].

The main failure modes of IC chip are the electrical failure and interconnection failure after the UHAST (as shown in Figure 2-22). The reason is the package leakage. The underfill and epoxy molding compound are isolation materials, and they are used to protect the IC chip interconnections and internal circuits. The UHAST uses high temperature to pressurize the moisture to enter the package. The moisture can cause short circuit issues. Therefore, the UHAST can evaluate the ability of IC chip to prevent leakage and the finishing quality of underfill or epoxy molding compound [177, 178].

CHAPTER 3 RESEARCH METHODOLOGY

3.1 EVALUATION OF IC CHIP STRENGTH

Silicon is a key component in the semiconductor packaging industry, and the core of IC chip is the silicon die. The silicon die takes up the major place in an IC chip especially the chip scale package. Therefore, there is much research related to the silicon die strength.

There are several methods used to evaluate the silicon die strength such as the three-point and four-point bending test, ball-on-ring test, ball breaker test and plate-on-elastic-foundation test. The 3PB test method is considered as the most popular evaluation method of silicon die strength. There are three widely recognized effect factors on the silicon strength, and they are silicon surface defects, silicon edge defects and weak planes of silicon crystal lattice. The silicon surface defects and silicon edge defects are created by the wafer grinding process and wafer sawing process respectively. All the strength test methods are affected by the wafer grinding process and wafer sawing process more or less. The effects of wafer sawing process and wafer grinding process on the strength test method using point loading force are small and moderate, while the effects of wafer sawing process and wafer grinding process on the strength test method using line loading force are moderate and big. Table 3-1 lists the effect level of wafer sawing process and wafer grinding process on various strength test methods.

Table 3-1 The effect level of wafer sawing process and wafer grinding process on various strength test methods.

Strength Test Method	Effect Level	
	Sawing	Grinding
Three-point bending test	Moderate	Big
Four-point bending test	Big	Big
Ball-on-ring test	Small	Moderate
Ball breaker test	Small	Moderate
Single point loading plate-on-elastic-foundation test	Small	Moderate
Line point loading plate-on-elastic-foundation test	Moderate	Big

The wafer grinding process is the very first process in the whole fan-out wafer level packaging assembly process. The aim of wafer grinding process is to grind the incoming wafer to the required thickness for further processes. The roughness of grinding side is fine enough after the second grinding step and thus the third grinding step is less used. Beyond the mechanical grinding method, the chemical wet etching and plasma etching methods also can replace the polishing step to gain an ultrafine wafer surface. In comparison, the plasma etched wafer surface is smoother than the chemical etched wafer surface.

The wafer sawing process is conducted after the wafer grinding process. The aim of wafer sawing process is to saw the incoming wafer to the required size for further processes. There are two wafer sawing methods – mechanical sawing method and laser sawing method. The mechanical sawing method uses diamond blades to saw the wafers. Most wafer sawing tasks could be achieved perfectly by the proper

blade selection. The laser sawing method is also known as the stealth dicing method. It is because the saw straight of laser sawing is extremely tiny. Therefore, the laser sawing method can offer an extreme low kerf loss. The step cut and laser grooving process can reduce and avoid chippings effectively.

The fracture analysis of silicon die includes the fracture pattern analysis and the initial fracture point analysis. The fracture pattern and initial fracture point have the close relationship with the assembly process and strength evaluation method. The wafer grinding process and wafer sawing process create surface defects and edge defects on the silicon die. The surface defect and edge defect decide the initial fracture point, and the surface defect affects the fracture pattern. The wafer grinding surface is not perfectly flat. It is because of the limitation of grinding machine or grinding process. We can find the grinding patterns easily on the ground surface after the wafer grinding process. The grinding pattern leads to the directional behavior of silicon die strength. The initial fracture point may appear on the silicon die surface and edge. The emergent frequency of initial fracture point on the silicon die surface is higher than that on the silicon die edge after the 3PB test. The initial fracture point sometimes appears on the silicon die sidewall. The reason is the wafer sawing method. However, silicon is a brittle and sensitive material, and its fracture is due to the tension stress rather than the compression stress. Therefore, the initial fracture point always appears on the opposite side of the loading force.

The distribution of silicon strength is wide because the defects appear on the silicon surface and edge randomly. The average value method can judge the quality of a set of data. However, it is not suited to judge the quality of silicon die strength data. Weibull distribution is considered as one of the best methods to describe the silicon die strength. Weibull distribution is widely used to describe the strength of

brittle material such as ceramics and silicon. There are two kinds of Weibull distribution – two-parameter Weibull distribution and three-parameter Weibull distribution. The three-parameter Weibull distribution can provide a better data fitting than the two-parameter Weibull distribution, especially in the lower region of failure probability. However, the two-parameter Weibull distribution is good enough to describe the data, and it is simple to use.

There is a board level reliability (BLR) test done by the 4PB test. This BLR test is recognized by JEDEC (Joint Electron Device Engineering Council) and regulated by the standard JESD22B113 – Board Level Cyclic Bend Test Method for Interconnect Reliability Characterization of Components for Handheld Electronic Products. The specimens are attached to a customized PCB in this test. The loading force works on the PCB periodically. However, the loading force is less than the fracture force of PCB because this BLR test is used to evaluate the solder joint reliability rather than the IC chip strength.

The advantages and limitations of current IC chip strength study can be summarized as follows:

Advantages of current IC chip strength study are:

1) Implementing the detailed research on the pure silicon die strength.
2) Evaluating major strength test methods and potential effect factors on the silicon die strength.
3) Proving the wafer grinding process and wafer sawing process are the most critical processes to the silicon die strength.
4) Conducting the detailed fracture pattern study of silicon die.
5) Applying advanced statistical methods to analyze the strength data.

6) Establishing a standard of BLR test.

Limitations of current IC chip strength study include the following:

1) The research about the package level strength is little, and there is not any research about the FOWLP strength.
2) The potential effect factors on the FOWLP strength are uncertain.
3) The assembly process and reliability test effects on the FOWLP strength are uncertain.
4) The finite element method is never used to evaluate the FOWLP strength.
5) The theoretical model of FOWLP strength and fatigue crack growth is not comprehensive.
6) The BLR test focuses on the solder joint reliability rather than the package reliability.

3.2 PROPOSED RESEARCH

Figure 3-1 shows the proposed research flow chart. The proposed research consists of evaluating the FOWLP strength, creating simulation models of FOWLP strength and developing mathematical models of FOWLP strength and FOWLP fatigue crack growth. The whole research is planned to be implemented in three stages.

Stage one

• Conduct experiment to evaluate the FOWLP strength.
• Analyze the FOWLP strength behavior and fracture pattern.
• Evaluate the thermal effect on FOWLP strength.

Stage two

• Develop FOWLP simulation models by ANSYS.
• Validate the FOWLP simulation models.
• Evaluate the strength of proposed FOWLP specimen by ANSYS.

Stage three

• Develop the theoretical model of FOWLP strength.
• Validate the theoretical model of FOWLP strength.
• Propose the theoretical model of FOWLP fatigue crack growth.

Figure 3-1 Proposed research flow chart.

Stage one aims to gain an overall impression of FOWLP strength. The FOWLP strength will be evaluated by the experimental method. The three-point bending test method will be used to evaluate the FOWLP strength. There are several factors hypothesized to affect the FOWLP strength. The proposed effect factors include the package structure, passivation layer, backside protection tape, die to package ratio, package geometry, PCB bar, grinding process and thermal. The thermal effect can be divided into two aspects according to the thermal duration. One aspect is the FOWLP assembly process especially the thermal related assembly process such as the post-mold curing process, passivation curing process and reflow process. The other aspect is the package reliability test especially the thermal related reliability test such as the temperature cycling test and high temperature storage test. Vickers hardness test and 3PB test will be used to evaluate the thermal effect on the

FOWLP strength. The evaluation work of FOWLP strength is important. We can collect valuable FOWLP strength data from the experiment. The strength data will be used in the following stages.

Stage two focuses on the numerical study of FOWLP strength. The ANSYS software will be used to assist with the research. The experiment of 3PB test will be simulated by the ANSYS software. The aims of simulation work include three aspects: create the simulation model of FOWLP strength test, assist fracture analysis and ready for further and deeper development. There is also a proposed FOWLP specimen built by the different assembly processes. The strength of this new FOWLP specimen is hypothesized to be better than that of other specimens with the same thickness level. The author will use simulation method to prove this hypothesis.

Stage three focuses on the theoretical work. The first proposed the theoretical model is the FOWLP strength model. This model is used to describe the failure probability of FOWLP strength, and it is based on the classical two-parameter Weibull distribution. This strength model will be validated with the previous strength data from the experiment work and simulation work. The second proposed theoretical model is the FOWLP fatigue crack growth model. This model is used to describe the crack growth status in a package under the thermal fatigue condition, and it is based on Paris law. Because the FOWLP is made up of various materials, the mismatched CTE of different materials leads to the differences in expansion and shrinkage between different materials. Therefore, the FOWLP fatigue crack growth model should contain two parts. One part is the monomial normal fatigue model. The other part is used to describe the effect of thermal factor on the crack growth. Therefore, a binomial fatigue crack growth model should be more accurate.

3.3 PROPOSED RESEARCH METHODOLOGY

The study of FOWLP strength is unclear and uncertain at the present stage. In order to achieve the research objectives, the author proposes the following methods. He also believes these methods would show novel contributions to the research of FOWLP reliability especially the aspect of FOWLP strength.

1. To evaluate the FOWLP strength

The thinner and thinner FOWLPs are developed to fulfill the requirement of volume sensitive electronic device. The thin FOWLPs may face crack issues. Therefore, the evaluation work of FOWLP strength is necessary. The three-point bending test method is chosen as the evaluation method of FOWLP strength. The 3PB test method has been proved that it is an effective method to evaluate the silicon strength. The 3PB test is similar to the real loading situation because it applies line loading force to the samples. There are three critical devices in the 3PB test, and they are universal tester machine, static load cell and 3PB fixture. In this work, the universal tester machine is Instron universal tester 5566. The load cell is Instron 2530-427 static load cell with the maximum capacity of ±100 N. The universal tester machine is used to do static testing such as the tensile test, compression test, flexure test and bending test. However, the fixture decides the testing type. The fixture in this work is a customized fixture, and it could achieve a very narrow span to support IC chips.

2. To investigate the thermal effect on the FOWLP strength

The FOWLP is made up of various material and thus the proper design of FOWLP structure and material selection are important. The wafer or package

warpage is a serious issue to their reliability. The reason of warpage is the mismatched CTE of different material. Therefore, the investigation of thermal effect on the FOWLP strength is essential. We hypothesize the EMC is the main effect factors on the FOWLP strength during the thermal processes. Therefore, we use pure EMC specimens in this work. The thermal effect comes from two aspects. One aspect is the thermal related assembly process (post-mold curing process, PSV curing process and reflow process), and the other aspect is the thermal related reliability tests (temperature cycling test and high temperature storage test). Both aspect effects will be evaluated in this work. Beyond the 3PB test method, Vickers hardness test method is also used to this work. The FUTURE-TECH microhardness tester FM-300e is used to conduct the microindentation work.

3. To simulate the experiment of FOWLP strength

The finite element method (FEM) is an efficient way to simulate complex problems by the numerical mathematics technique. The FEM can save workforce and time when we deal with huge, complex and long duration problems compared with the experimental methods. In this work, ANSYS software is used to create simulation models and explore the solutions. The simulation models are created based on the FOWLP specimens in the experimental work. The specimen materials include silicon die, EMC, PSV layer and BSP tape. The simulation work is used to simulate the experiment of 3PB test and thus the 3PB fixture material should be included, and it is defined as structural steel.

4. To develop the FOWLP strength model and fatigue crack growth model

The proposed FOWLP strength model is developed based on the two-parameter Weibull distribution. However, the novelty of the proposed FOWLP

strength model is the proposed FOWLP strength model is based on the location of initial fracture point. The initial fracture point is possible to appear in two regions – the package surface and the package interior. The proposed FOWLP fatigue crack growth model is developed based on Paris law. However, the proposed FOWLP fatigue crack growth model includes the thermal effect on the fatigue crack growth. Therefore, the proposed FOWLP fatigue crack growth model is a binomial.

CHAPTER 4 EVALUATION OF FOWLP STRENGTH BY 3PB TEST METHOD

4.1 EXPERIMENT OF 3PB TEST

The three-point bending (3PB) test requires three key apparatuses – the universal tester, static load cell and 3PB fixture. In this work, the universal tester is Instron universal tester 5566 (as shown in Figure 4-1). This machine is used to do static tests such as the tensile test, compression test, flexure test and bending test. The machine load cell is digitalized, and it is controlled by the computer software such as Instron Bluehill3. In this work, the Instron 2530-427 static load cell with the maximum capacity of ±100 N is applied.

Figure 4-1 Instron universal tester 5566.

The last key apparatus is the 3PB fixture. The universal tester and load cell can implement various testing. However, the fixture decides the testing type and method. Vector Scientific Pte Ltd helps to fabricate the fixture (as shown in Figure 4-2) with a fabrication tolerance ±0.05 mm. The 3PB fixture is able to achieve a minimum 4 mm span, and the maximum specimen width should be less than 40 mm. The maximum load capacity of fixture is not required too high because the IC chips are tiny and brittle. However, the fixture must achieve a very narrow span to support the IC chips.

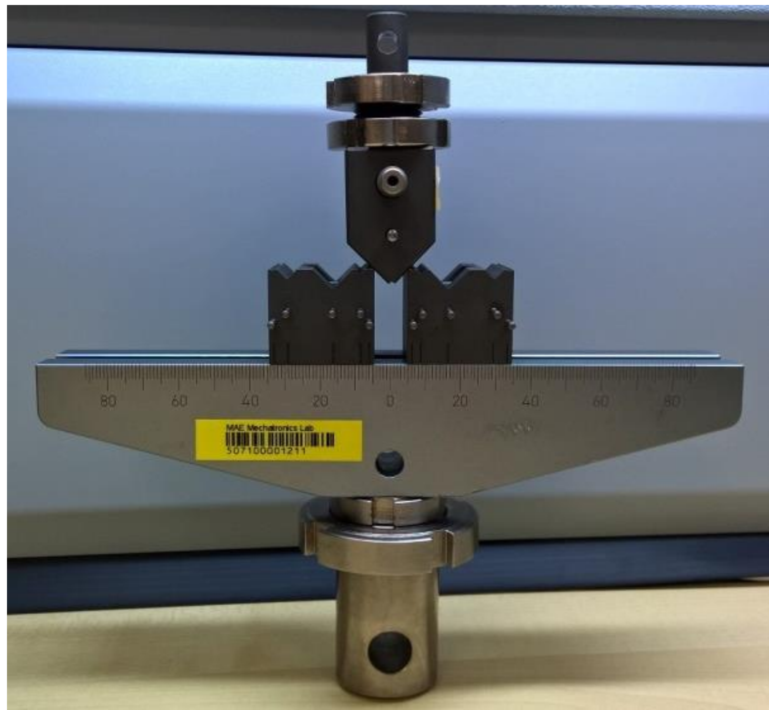

Figure 4-2 Customized 3PB fixture.

The whole experiment is conducted in the biological lab, School of Mechanical and Aerospace Engineering, Nanyang Technological University. The environment temperature is 25°C. There is not any pre-conditioning or heating device

attached to the machine to process the specimens before or during the experiment. The default speed of loading force is 0.6 mm/min (0.01 mm/s).

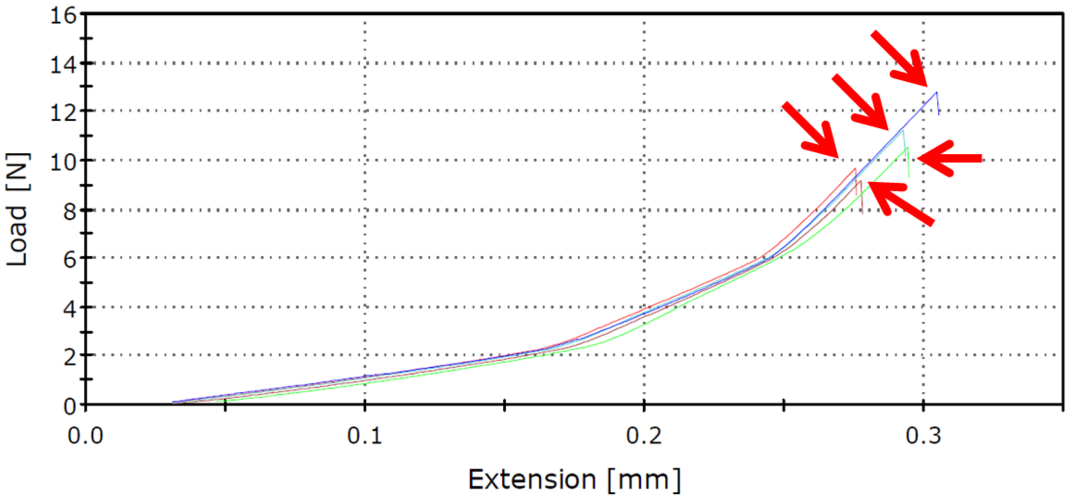

Figure 4-3 Example of load versus extension curves of 3PB test.

Figure 4-3 shows an example of load-extension curves of 3PB test, and it contains five specimens. The arrows point the fracture point of each specimen. We can find the value of specimen fracture load and fracture extension from the testing curves. The specimen fracture load is a key variable to calculate the specimen flexure strength. The FOWLP strength is measured and evaluated by the value of flexure strength. The flexure strength can be calculated by the following equation

$$\sigma_{3PB} = \frac{3LF}{2BW^2} \tag{4.1}$$

where F is the fracture load, L is the fixture span, B is the specimen width and W is the specimen thickness.

The specimen flexure strength is represented by the box plot graph. The t-test and F-test are used to judge whether the differences of specimen flexure strength mean and variance are significant. The t-test and F-test equations are

$$t = \frac{\overline{X_1} - \overline{X_2}}{\sqrt{\frac{s_1^2}{n_1} + \frac{s_2^2}{n_2}}} \tag{4.2}$$

$$F_0 = \frac{S_1^2}{S_2^2} \tag{4.3}$$

where X is the mean of specimen flexure strength, S is the standard deviation of specimen flexure strength and n is the sample size.

The specimens are built by the conventional fan-out wafer level packaging assembly process, and they are considered and designed carefully to fulfill the research objective. The specimens are only built by the dummy silicon die, epoxy molding compound (EMC), backside protection (BSP) tape and passivation (PSV) layers. The functional dies, redistribution layers and solder balls are not used. Therefore, these specimens are not functional, and they are also called bare FOWLPs.

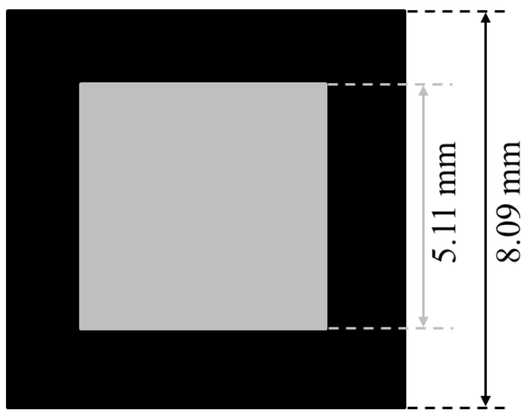

Figure 4-4 FOWLP specimen layout.

The specimen package size is 8.09 mm × 8.09 mm, and the dummy silicon die size is 5.11 mm × 5.11 mm (as shown in Figure 4-4). The dummy silicon wafers are ground to 370 μm and the silicon dies are placed at the geometrical center of package. There is only lithographed one PSV layer, and the PSV layer thickness is 10 μm. The molded artificial wafer is ground to the thickness of 200 μm and thus all the die backsides are exposed. The backside protection tape is laminated on the wafer backside. The backside protection tape has the similar function with the EMC, and it is used to protect the wafer grinding surface. The molded artificial wafer is sawed into the size of 8.09 mm × 8.09 mm. Figure 4-5 shows the detailed process flow illustration of specimen.

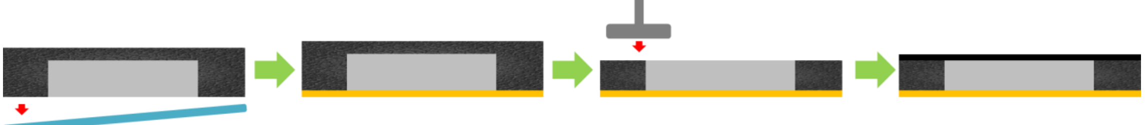

Figure 4-5 FOWLP specimen assembly process flow: debonding, lithographing PSV, backside grinding and laminating BSP tape.

The specimens are equally collected from five different regions in a wafer. Figure 4-6 shows the definition of wafer five regions – top, left, center, right and bottom.

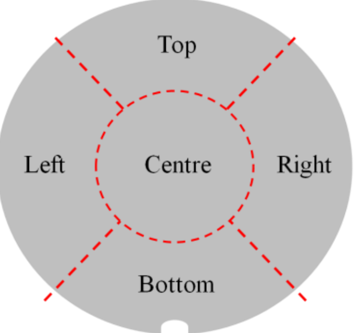

Figure 4-6 Wafer region code.

4.2 EVALUATION OF FOWLP STRENGTH

4.2.1 STRUCTURE EFFECT ON FOWLP STRENGTH

The aim of this work is to find out the structure effect on the FOWLP strength. In order to minimize the effect of other factors on this evaluation, the FOWLP specimens are without PSV layers. The specimens are named as specimen A-1, specimen A-2 and specimen A-3 (or group A specimens), and they represent three kinds of representative FOWLP structure. Figure 4-7 shows the detailed assembly process flow illustration of group A specimen.

Figure 4-7 Assembly process flow of group A specimens: debonding, backside grinding and laminating BSP tape.

The wafer of specimen A-1 is sawed directly after the wafer debonding process. There is a 120 μm thick EMC layer above the silicon die. The structure of specimen A-1 is named as the over-molded structure. The wafer of specimen A-2 is ground after the wafer debonding process. The silicon die backside of specimen A-2 is exposed after the wafer grinding process. The structure of specimen A-2 is named as the die-exposed structure. The silicon die backside of specimen A-3 is laminated a BSP tape after the wafer grinding process, and the BSP tape thickness is 25 μm. The structure of specimen A-3 is named as the BSP tape protected structure. The specimen specifications and the testing machine setup parameters are listed in Table 4-1.

Table 4-1 FOWLP specimens and 3PB test specifications (structure effect).

Specimen ID	Die dimension (mm)			Package dimension (mm)			Sample size	Fixture span (mm)
	X	Y	Z	X	Y	Z		
A-1	5.11	5.11	0.37	8.09	8.09	0.49	25	6
A-2	5.11	5.11	0.2	8.09	8.09	0.2	25	6
A-3	5.11	5.11	0.2	8.09	8.09	0.225	25	6

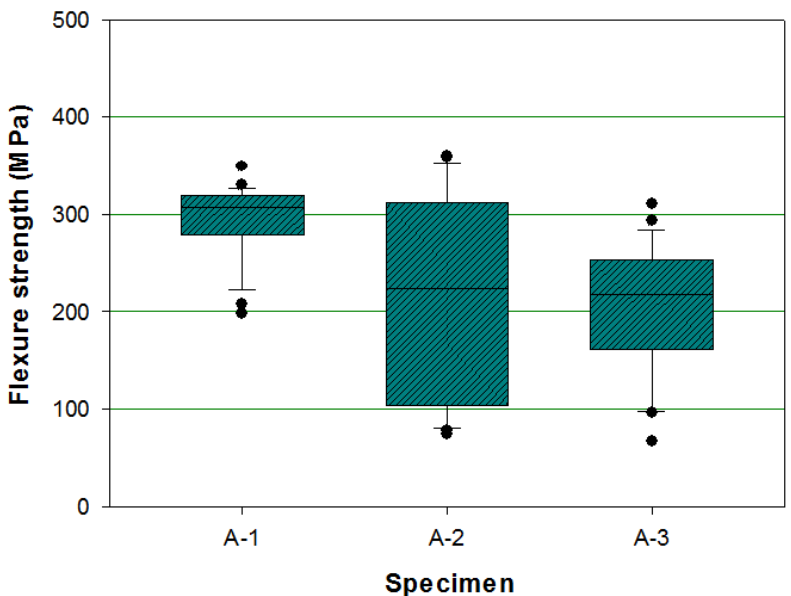

Figure 4-8 Comparison of flexure strength among specimen A-1, specimen A-2 and specimen A-3.

Figure 4-8 shows the comparison of flexure strength among specimen A-1, specimen A-2 and specimen A-3. The average flexure strength of specimen A-1 is much higher than that of specimen A-2 and specimen A-3. The average flexure strength of specimen A-2 drops significantly after the wafer grinding process. Meanwhile, the flexure strength distribution of specimen A-2 is discrete. The t-test verifies that the strength mean of specimen A-1 is larger than the strength mean of specimen A-2 significantly at the 99.5% significance level. The F-test verifies that

the strength variances of specimen A-1 and specimen A-2 have a significant difference. Both validations match the above observation.

The average flexure strength of specimen A-3 is almost as the same as the average flexure strength of specimen A-2. The flexure strength distribution of specimen A-3 becomes concentrated significantly after laminating the BSP tape. The t-test verifies that the strength means of specimen A-2 and specimen A-3 do not have a significant difference. The F-test verifies that the strength variances of specimen A-2 and specimen A-3 have the significant difference at the 99.9% significance level. Both validations match the above observation.

Specimen A-1 is an over-molded structure FOWLP. The liquid state EMC covers the silicon die surface defects and forms a smooth and steady surface on top of the silicon die backside. This kind of structure could minimize the wafer grinding effect on the FOWLP strength. Therefore, the flexure strength of specimen A-1 is concentrated and high. The structure effect on the FOWLP strength also can be considered as the wafer grinding process effect on the FOWLP strength. The strength of over-molded structure FOWLP should always be better than that of die-exposed structure FOWLP.

The previous research of silicon die strength [104, 108] finds out the silicon wafer surface condition is critical to the silicon die strength. This phenomenon is obvious when the grinding side faces down during the 3PB test. The processed silicon strength is far lower than the ideal single crystalline silicon strength. The reason is the wafer grinding process. The grinding machine and grinding wheel grit size have limitations. The grinding pattern always appears on the wafer surface after the grinding process. The grinding pattern looks like grooves by the surface analysis

machine. The grinding pattern can assist the loading force once the loading force is parallel to the grinding pattern. Hence the average flexure strength of specimen A-2 drops significantly after the wafer grinding process. Meanwhile, the grinding pattern can afford the loading force once the loading force is perpendicular to the grinding pattern. It is the reason for the wide flexure strength distribution of specimen A-2.

The BSP tape is a kind of adhesive tape, which is used to protect and reinforce the package backside. The BSP tape has the feature of stability and reliability in the environment of high temperature and high humidity. The structure of BSP tape protected FOWLP is similar to the over-molded structure FOWLP. Both surfaces of BSP tape and EMC could afford the laser marking. The BSP tape has the outstanding performance on its uniformity in thickness compared with the EMC. Therefore, the BSP tape also can cover the grinding pattern and form a smooth surface on top of the wafer backside. Although the BSP tape has a minor contribution to the flexure strength of FOWLP, it reduces the grinding pattern effect on the flexure strength distribution significantly. Therefore, the flexure strength distribution of specimen A-3 becomes concentrated after laminating the BSP tape.

For the fracture analysis aspect, all the specimens break into two parts after the 3PB test. The initial fracture point only appears on the silicon die surface or silicon die edge regardless the specimen structure. Figure 4-9 to Figure 4-12 show the fractured view of specimen A-1, specimen A-2 and specimen A-3, and the images are taken by the scanning electron microscope (SEM).

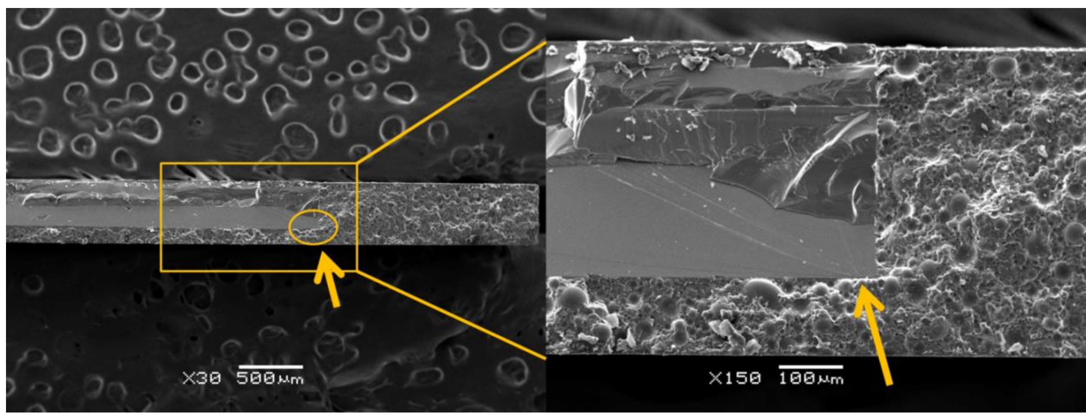

Figure 4-9 The initial fracture point appears on the silicon die edge of specimen A-1.

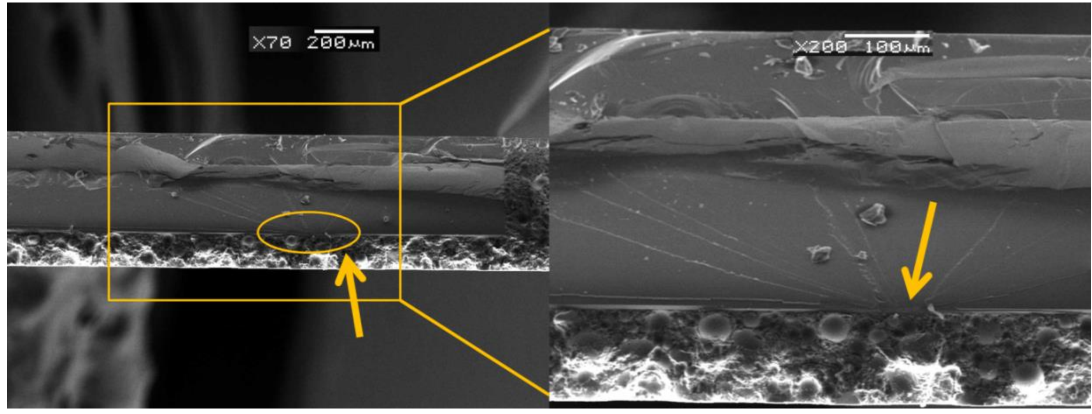

Figure 4-10 The initial fracture point appears on the silicon die surface of specimen A-1.

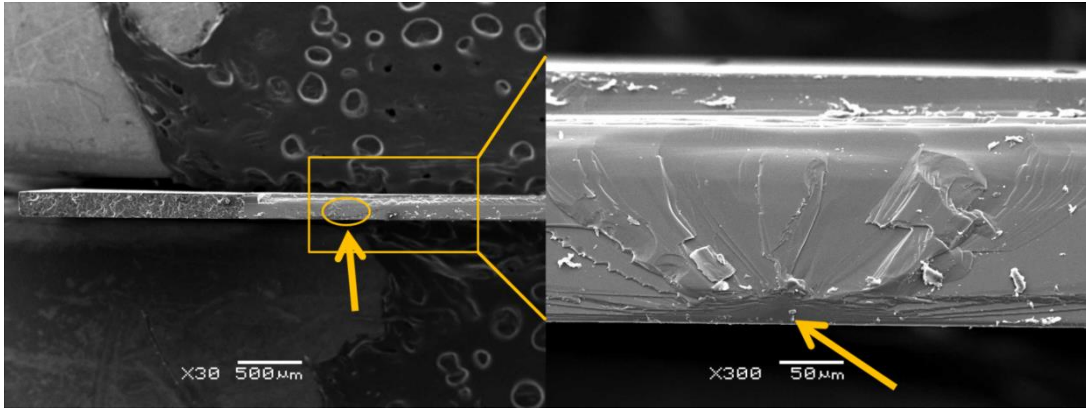

Figure 4-11 The initial fracture point appears on the silicon die surface of specimen A-2.

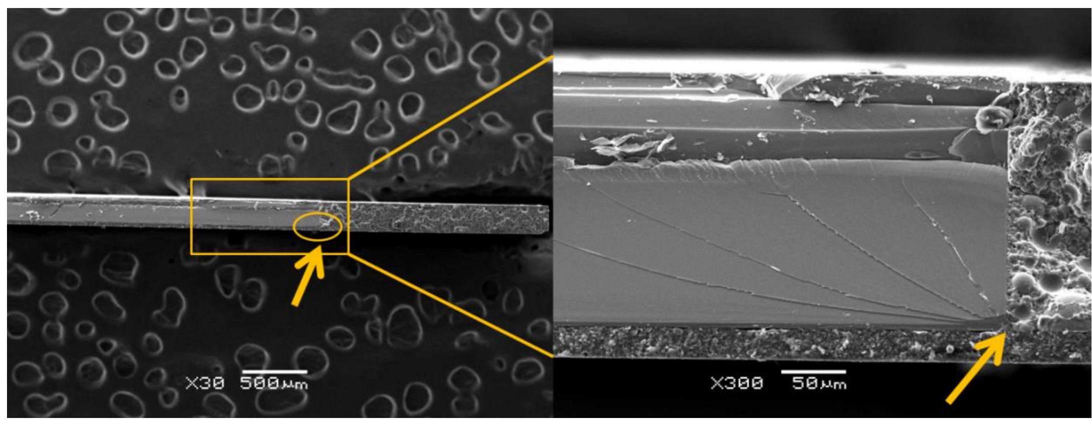

Figure 4-12 The initial fracture point appears on the silicon die edge of specimen A-3.

4.2.2 PSV EFFECT ON FOWLP STRENGTH

The aim of this work is to find out the PSV effect on the FOWLP strength. Group B specimens (specimen B-1, specimen B-2 and specimen B-3) are used for this evaluation work. Their structures are corresponding to specimen A-1, specimen A-2 and specimen A-3 respectively. The only difference is group B specimens are lithographed a 10 µm thick PSV layer on their front side. Therefore, the thickness of group B specimen is 500 µm, 210 µm and 235 µm respectively. The specimen specifications and the testing machine setup parameters are listed in Table 4-2.

Table 4-2 FOWLP specimens and 3PB test specifications (PSV effect).

Specimen ID	Die dimension (mm)			Package dimension (mm)			Sample size	Fixture span (mm)
	X	Y	Z	X	Y	Z		
B-1	5.11	5.11	0.37	8.09	8.09	0.5	25	6
B-2	5.11	5.11	0.2	8.09	8.09	0.21	25	6
B-3	5.11	5.11	0.2	8.09	8.09	0.235	25	6

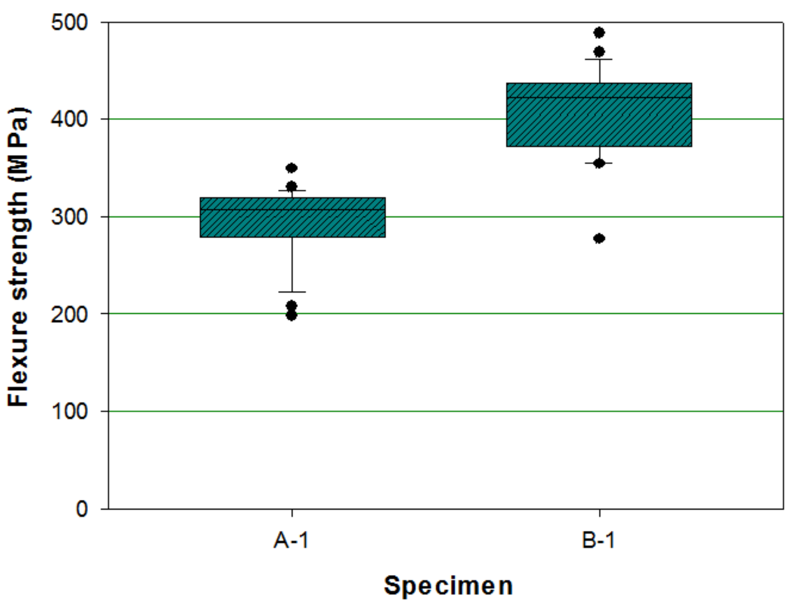

Figure 4-13 Comparison of flexure strength between specimen A-1 and specimen B-1.

Figure 4-13 shows the comparison of flexure strength between specimen A-1 and specimen B-1. The only difference between specimen B-1 and specimen A-1 is the PSV layer. However, the flexure strength of specimen B-1 is higher than the flexure strength of specimen A-1. This phenomenon is interesting because the 10 μm thick PSV layer leads to the average flexure strength grows 40%. The flexure strength distributions of specimen A-1 and specimen B-1 are almost the same. The t-test verifies that the strength mean of specimen B-1 is larger than the strength mean of specimen A-1 significantly. However, the F-test verifies that the strength variances of specimen A-1 and specimen B-1 do not have a significant difference. Both validations matched the above observation.

The PSV layer is lithographed on the specimen front side and thus the specimen backside surface condition never changes. Therefore, we cannot explain this phenomenon through the surface condition factor. The reason should be the PSV

layer lithographing process. The PSV layer lithographing process requires the wafer to store in a high temperature oven to cure. The oven temperature is 225℃, and the curing duration is two hours. The duration excludes the time of temperature rising and falling. The curing process should affect the FOWLP strength. The EMC takes the principal place in the package. The EMC of specimen A-1 and specimen B-1 occupies about 70% of the total package volume. Therefore, the changes in FOWLP strength should be due to the changes in the EMC strength after the curing process. The detailed thermal effect on the EMC strength will be discussed in Chapter 4.3.

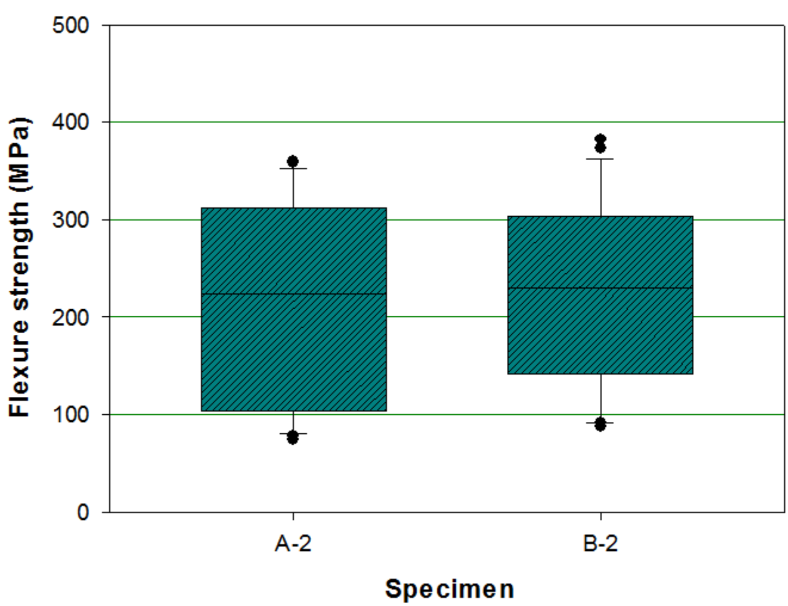

Figure 4-14 Comparison of flexure strength between specimen A-2 and specimen B-2.

Figure 4-14 shows the comparison of flexure strength between specimen A-2 and specimen B-2. Their average flexure strength is almost the same, and the flexure strength distribution of specimen B-2 centralizes a little bit. However, the t-test and F-test verify that the strength mean and variance of specimen A-2 and specimen B-2 do not have a significant difference.

The silicon die backsides of this pair specimen are exposed. The PSV layers are lithographed on their front side and thus the specimen backside condition is not changed. Therefore, the flexure strength distributions of both specimens are almost the same. The EMC volume in both specimens is much less than the EMC volume in specimen A-1 and specimen B-1. The EMC is helpless to enhance the FOWLP strength. Therefore, the PSV effect on the die-exposed structure FOWLP strength is minor.

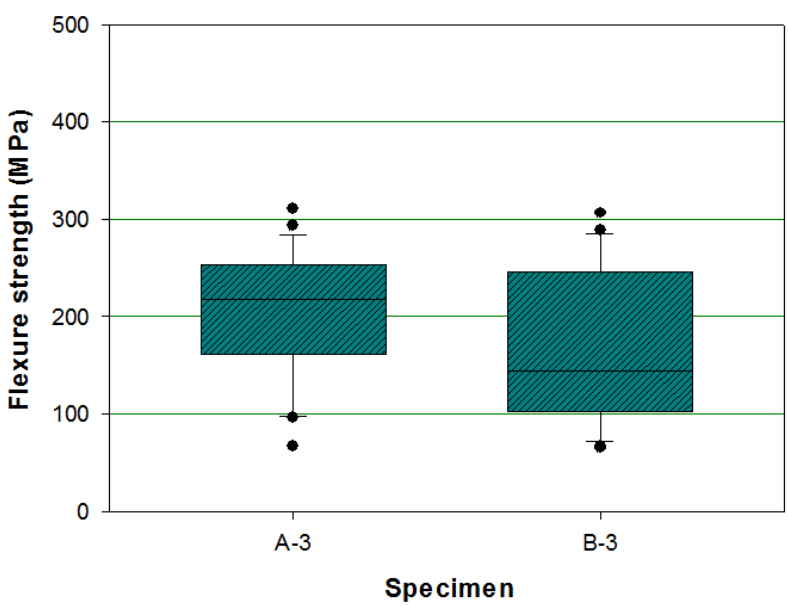

Figure 4-15 Comparison of flexure strength between specimen A-3 and specimen B-3.

Figure 4-15 shows the comparison of flexure strength between specimen A-3 and specimen B-3. The average flexure strength of specimen B-3 drops and the flexure strength distribution of specimen B-3 diffuses after lithographing PSV layers. The t-test verifies that the strength mean of specimen A-3 is larger than that of specimen B-3 significantly. The F-test verifies that the strength variances of specimen A-2 and specimen A-3 do not have a significant difference.

The average flexure strength of BSP tape protected specimen drops after lithographing PSV layers. However, the flexure strength distributions of both specimens almost remain the same. The reason could be the curing process after lithographing PSV layers. The BSP tape has the feature of stability and reliability in the environment of high temperature. However, the curing process may affect the BSP tape function in this work. Further research is required to verify it. In summary, the PSV layer only has the significant effect on the flexure strength of over-molded structure FOWLP specimen (specimen A-1 and specimen B-1).

For the fracture analysis aspect, all the specimens break into two parts after the 3PB test. The initial fracture point only appears on the silicon die surface or silicon die edge regardless the specimen structure. Figure 4-16 to Figure 4-18 show the fractured view of specimen B-1, specimen B-2 and specimen B-3, and the images are taken by the SEM.

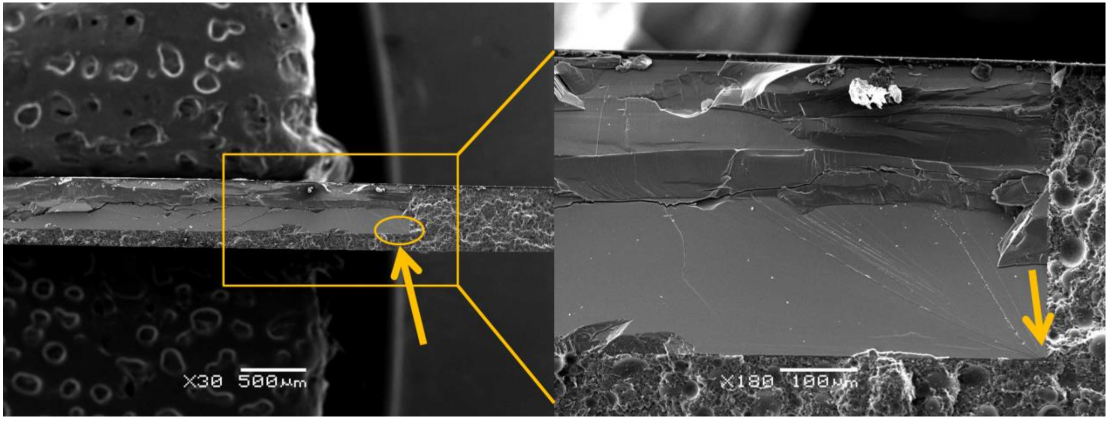

Figure 4-16 The initial fracture point appears on the silicon die edge of specimen B-1.

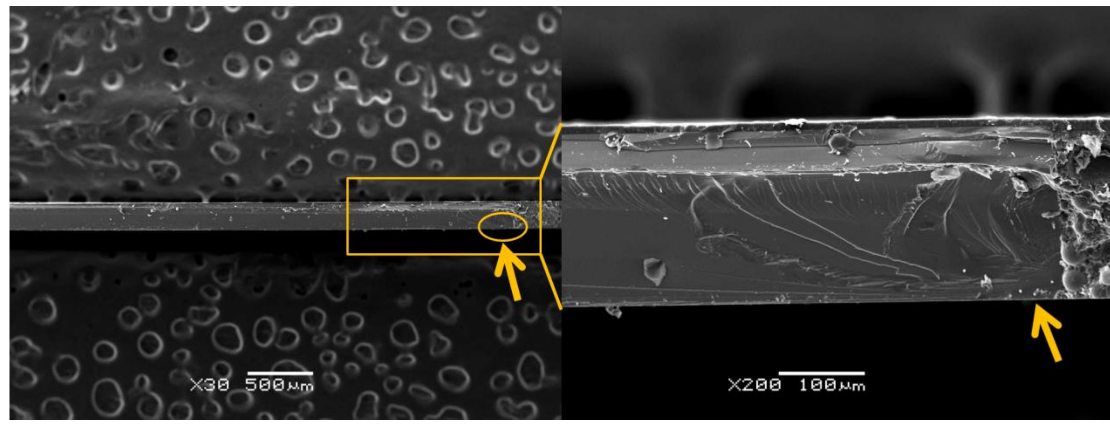

Figure 4-17 The initial fracture point appears on the silicon die surface of specimen B-2.

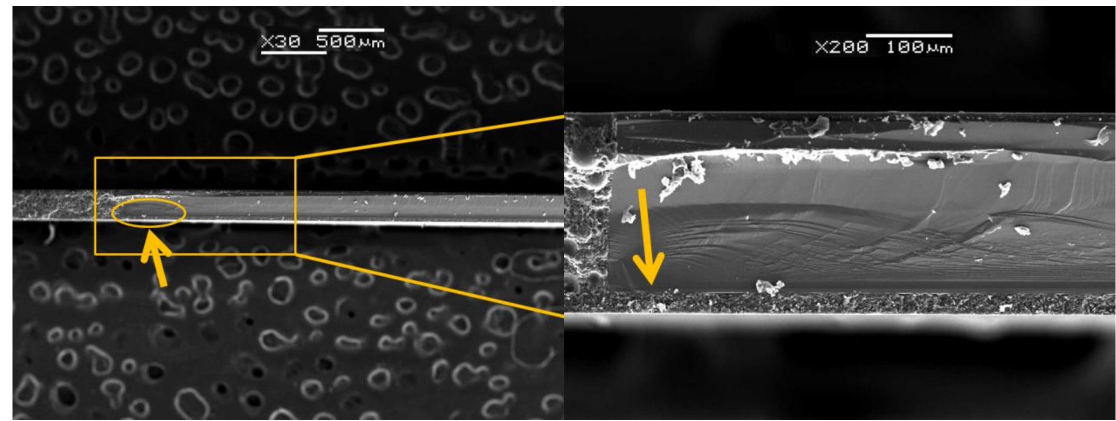

Figure 4-18 The initial fracture point appears on the silicon die surface of specimen B-3.

4.2.3 TEMPERATURE CYCLING TEST EFFECT ON FOWLP STRENGTH

The temperature cycling (TC) test is used to evaluate the specimen reliability through periodically changing in between two extreme temperatures. The common failure modes of specimen are the electrical failure, delamination, solder joint cracking and structural deformation. The TC test in this work follows the JEDEC standard JESD22-A104D. The TC test condition is condition B. The temperature

changes between -55°C and +125°C. The temperature cycling rate is two cycles per hour. The duration of TC test is 500 cycles and 1000 cycles. In other words, the TC test spends 250 hours and 500 hours. We use group B specimens in this evaluation work. There are 50 specimens collected from each specimen wafer, and they are equally divided into two batches. The first batch specimen is used for the 500 cycles TC test while the second batch specimen is used for the 1000 cycles TC test.

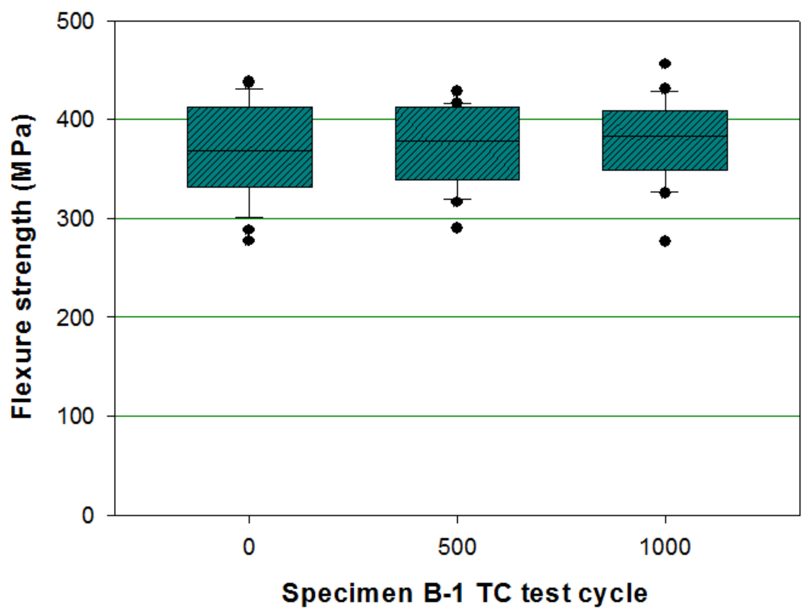

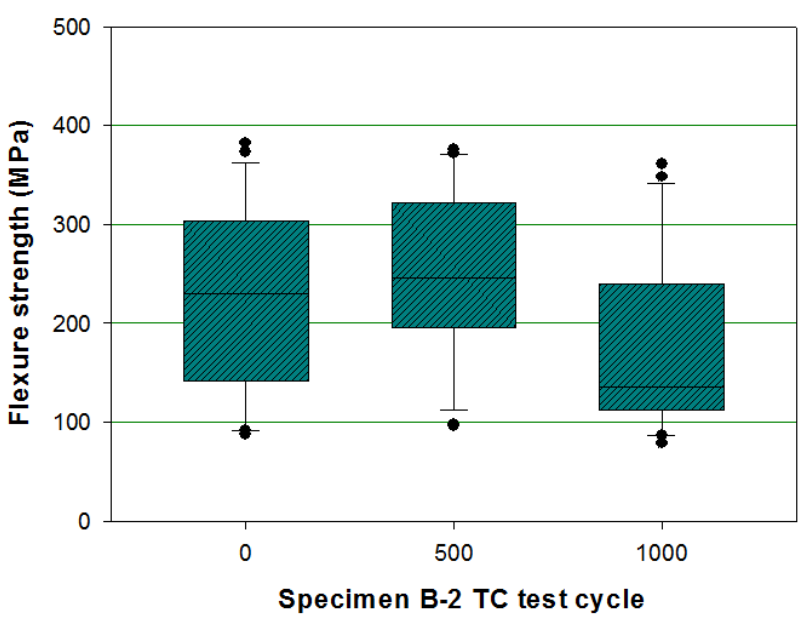

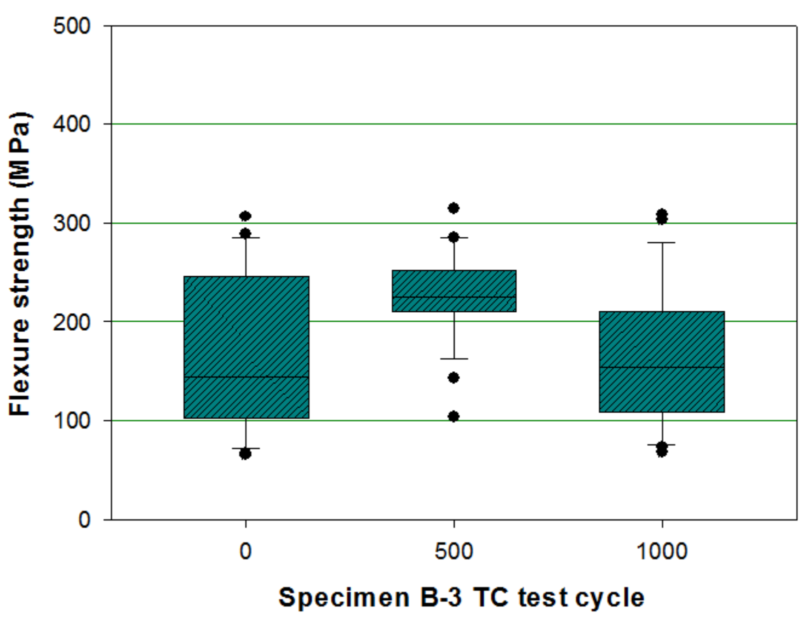

Figure 4-19 Flexure strength of group B specimen after the TC test.

Figure 4-19 shows the flexure strength of group B specimen after the TC test. The 3PB test results show two different trends. The flexure strength of specimen B-1 almost remains the same throughout the test. The flexure strength of specimen B-2 and specimen B-3 increases after the 500 cycles TC test and drops back after the 1000 cycles TC test.

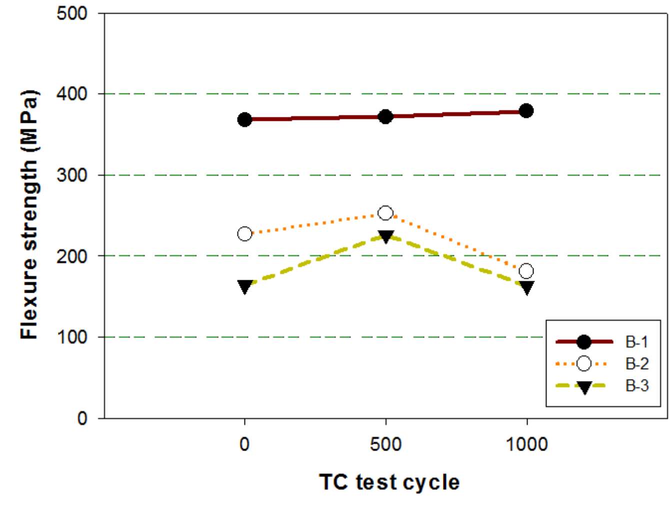

Figure 4-20 Average flexure strength of group B specimen after the TC test.

The average flexure strength of group B specimen is summarized in Figure 4-20. The flexure strength of specimen B-1 is always higher than the flexure strength of other group B specimen. The flexure strength distribution of specimen B-1 is also much narrower than the flexure strength distribution of other group B specimen throughout the test. The TC test does not affect the flexure strength distribution of specimen B-1 obviously. Therefore, the structure of specimen B-1 is quite stable and reliable. The key point of this structure is the EMC. There is a 120 μm thick EMC layer above the silicon die in specimen B-1. This EMC layer can protect the silicon die backside defects and enhance the package strength.

The structure of specimen B-2 and specimen B-3 is closer to the finished FOWLP. The difference between specimen B-2 and specimen B-3 is the BSP tape. The trends of average flexure strength of specimen B-2 and specimen B-3 are almost the same. The flexure strength of specimen B-2 and specimen B-3 drops significantly after the 1000 cycles TC test, and their flexure strength is even lower than their initial flexure strength. Therefore, the TC test affects the FOWLP strength significantly especially the die-exposed structure FOWLP and the BSP tape protected FOWLP. The BSP tape is treated as a substitution of EMC. However, we find the BSP tape does not show an obvious effect on the flexure strength and flexure strength distribution of FOWLP in this work.

4.2.4 HIGH TEMPERATURE STORAGE TEST EFFECT ON FOWLP STRENGTH

The high temperature storage (HTS) test is used to evaluate the specimen reliability in an extreme temperature environment. The common failure modes of specimen are the electrical failure, delamination, solder joint cracking and structural deformation. The HTS test in this work follows the JEDEC standard JESD22-A103. The high temperature storage test condition is condition B, and the temperature is 150℃. The duration of HTS test is 500 hours and 1000 hours. We use group B specimens in this evaluation work. There are 50 specimens collected from each specimen wafer, and they are equally divided into two batches. The first batch specimen is used for the 500 hours HTS test while the second batch specimen is used for the 1000 hours HTS test.

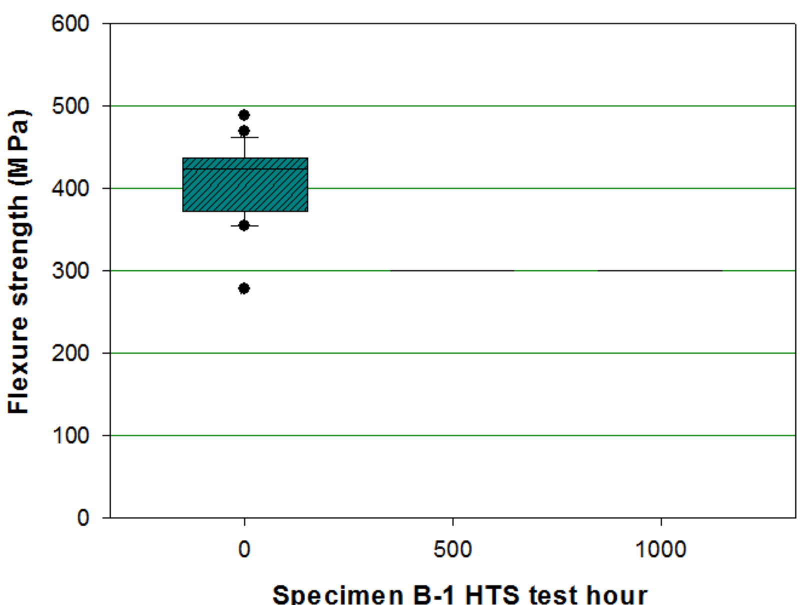

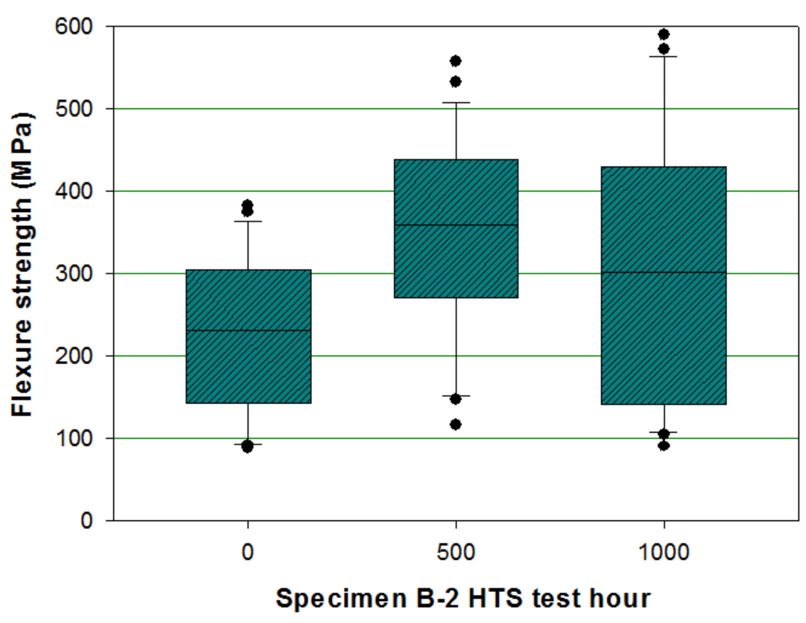

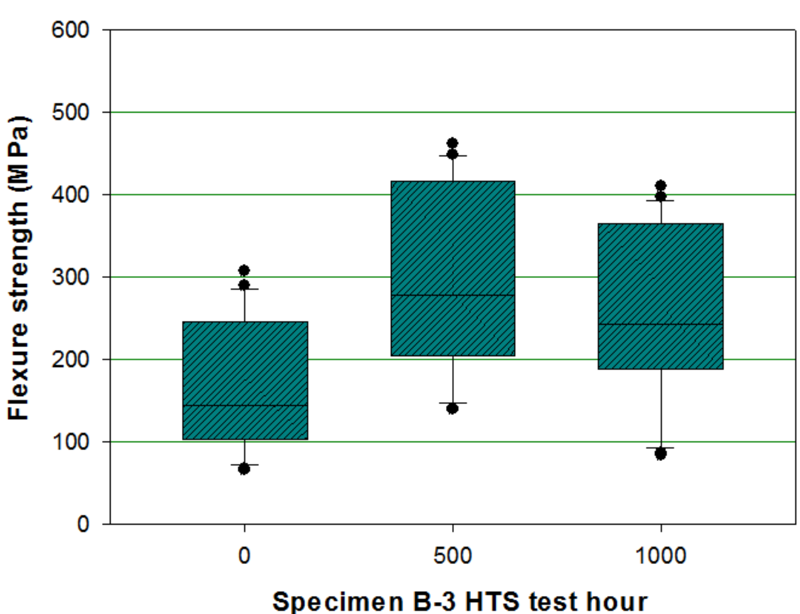

Figure 4-21 Flexure strength of group B specimen after the HTS test.

Figure 4-21 shows the flexure strength of group B specimen after the HTS test. The flexure strength of specimen B-1 after the 500 hours and the 1000 hours HTS test does not appear on the graph. It is because our load cell maximum capacity is only 100N, and the flexure load of specimen B-1 is much larger than this limit.

The flexure strength of specimen B-2 and specimen B-3 increases after the 500 hours HTS test and drops back after the 1000 hours HTS test.

The HTS test does not affect the flexure strength of specimen B-1 obviously. The performance of flexure strength and flexure strength distribution of specimen B-1 is always the best throughout the test. The flexure distribution of specimen B-1 is much narrower than other specimens throughout the test, and the HTS test does not affect the flexure strength distribution of specimen B-1. Therefore, the structure of specimen B-1 is quite stable and reliable again.

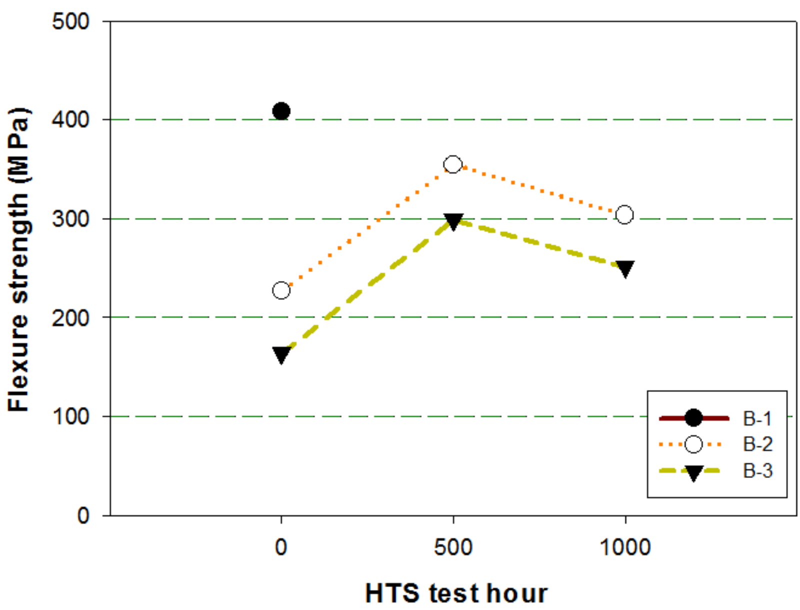

Figure 4-22 Average flexure strength of group B specimen after the HTS test.

The average flexure strength of group B specimen is summarized in Figure 4-22. The flexure strength of specimen B-2 and specimen B-3 drops after the 1000 hours HTS test. However, their flexure strength after the 1000 hours HTS test is still higher than their flexure strength at time zero. This phenomenon is different from the TC test result. This work does not consider the package functional failure and

structural failure such as electrical failure and PSV delamination. The HTS test affects the FOWLP strength significantly especially the die-exposed structure FOWLP and the BSP tape protected structure FOWLP.

The difference between specimen B-2 and specimen B-3 is the BSP tape. The BSP tape function is similar to the EMC function. They are both used to protect the silicon die backside and enhance the package strength. The BSP tape is good at its uniformity thickness compared with the EMC. The BSP tape is considered as it has the ability to enhance the package strength. However, we only find the BSP tape may reduce the flexure strength distribution. There is not any evidence show that the BSP tape could enhance the FOWLP flexure strength. Therefore, the BSP tape cannot enhance the FOWLP strength beyond tightening the strength distribution.

4.3 EVALUATION OF EMC STRENGTH

In the previous evaluation work of FOWLP strength, we find that the FOWLP strength significantly increases once specimens are lithographed passivation layers. The passivation layer thickness is only 10 μm and thus it should not affect the FOWLP strength seriously. The FOWLP wafers are stored in a high temperature oven after the passivation layer lithographing process to cure for a few hours. We hypothesize the curing process affects the certain material strength. The major components of FOWLP are the silicon die and EMC. Silicon is a quite stable material. Therefore, the EMC should be affected by the thermal process. In this section, we are

going to find out the effect of short-term thermal process (thermal related assembly process) and long-term thermal process (thermal related reliability test) on the EMC strength.

4.3.1 EXPERIMENT CONFIGURATION

The three-point bending test is used for this evaluation work. The testing apparatuses are Instron universal tester 5569 and a maximum capacity of ±1kN load cell. The support span increases to 8 mm to fit the new specimens. The loading speed increases to 6 mm/min. The test is conducted under the room temperature 25°C.

We add Vickers hardness test to evaluate the EMC hardness in this work. The Vickers hardness test method is developed by Robert L. at al. in 1921 to replace the Brinell method. The indenter of Vickers hardness test can be used to all kinds of materials regardless their hardness. Therefore, Vickers hardness test is popular and easy to use. The unit of Vickers hardness test is Vickers pyramid number (HV). The hardness is obtained by the load over the indentation area [179, 180]

$$A = \frac{d^2}{2\sin(136°/2)} \approx \frac{d^2}{1.8544} \tag{4.4}$$

$$HV = \frac{F}{A} = \frac{1.8544F}{d^2} \tag{4.5}$$

Where A is the area of resulting indentation, F is the load and d is the average diagonal lengths of resulting indentation. The FUTURE-TECH microhardness tester FM-300e (as shown in Figure 4-23) is used to conduct the hardness test in this evaluation work.

Figure 4-23 FUTURE-TECH microhardness tester FM-300e.

Figure 4-24 shows the indentation location of Vickers hardness test in a specimen. Each specimen is performed ten times indentation, and the indentation load is 100 g.

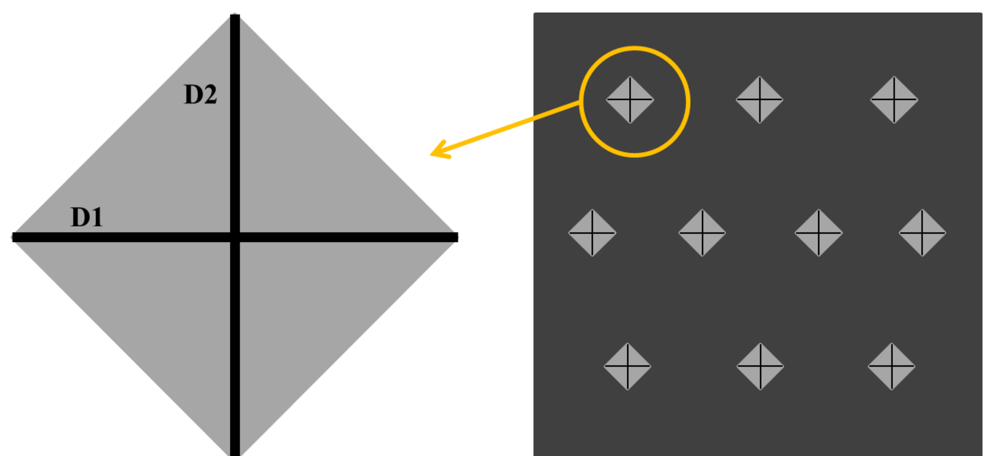

Figure 4-24 Proposed indentation locations of Vickers hardness test in a specimen and the definition of resulting indentation diagonal D1 and D2.

The specimen is made up of pure EMC in this evaluation work. The pure EMC specimen can minimize the effect of other materials. There are four kinds of EMC used to build the specimen. The specimens are named as EMC-1, EMC-2, EMC-3 and EMC-4. The material properties of specimens are listed in Table 4-3.

Table 4-3 The material properties of pure EMC specimens.

Specimen ID	Dimension (mm)			Viscosity (Pa*s)	CTE by TMA (ppm) α1/α2	Tg by DMA (℃)	Flexure Modulus by DMA (GPa)
	X	Y	Z				
EMC-1	10	10	0.65	650	7.0/25	160	18
EMC-2	10	10	0.65	650	7.3/32	165	23
EMC-3	10	10	0.65	600	9.0/42	165	18
EMC-4	10	10	0.45	300	12/45	165	14

Figure 4-25 shows an EMC specimen before debonding. The specimen size is 10 mm × 10 mm. The thickness of EMC-1, EMC-2 and EMC-3 is 650 μm, and the thickness of EMC-4 is 450 μm. There are five observation points designed to trace the specimen hardness and strength. Table 4-4 lists the five observation point details.

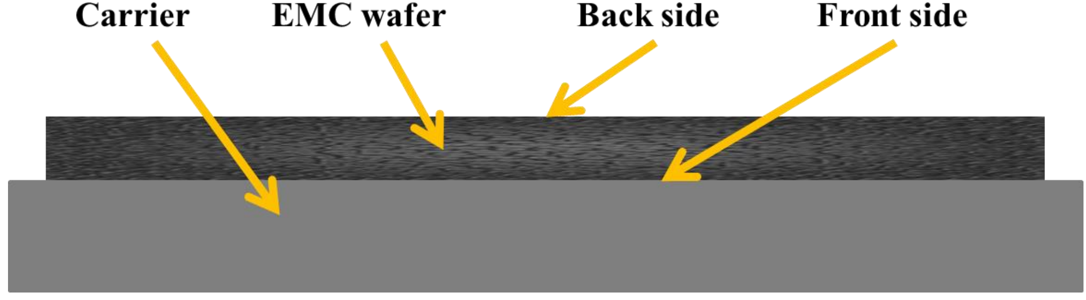

Figure 4-25 An EMC specimen wafer before debonding.

Table 4-4 Observation points in the thermal related assembly processes.

Observation point	Completed process				
	Post-mold curing	1 × PSV curing	3 × PSV curing	1 × Reflow	2 × Reflow
1	Yes				
2	Yes	Yes			
3	Yes	Yes	Yes		
4	Yes	Yes	Yes	Yes	
5	Yes	Yes	Yes	Yes	Yes

There are two rounds of curing process after the molding process. The first round curing process occurs immediately after the molding process, and it is completed within the molding machine. The curing time is 10 minutes, and the curing temperature is 125°C. The second round curing process is conducted in a separate oven. The curing time is one hour, and the curing temperature is 150°C. The second round curing process is named as the post-mold curing (PMC) process.

The passivation lithographing process is conducted after the molding process. The typical FOWLP has three passivation layers and two redistribution layers. The low-cost FOWLP only has two passivation layers and one redistribution layers. The wafer is required to cure after each passivation lithographing process. The curing temperature of passivation layer is 225°C, and the duration is two hours. However, we do not lithograph real passivation layer on the EMC specimens.

There is a reflow process after the PSV curing process. The peak temperature of reflow oven is between 255°C and 260°C, and the reflow time is 72 seconds.

4.3.2 THERMAL RELATED ASSEMBLY PROCESS EFFECT ON EMC STRENGTH

The aim of this work is to find out the effect of short-term thermal related assembly process on the EMC hardness and strength. The Vickers hardness test is used to evaluate the EMC hardness, while the three-point bending test is used to evaluate the EMC strength.

Table 4-5 lists the specimen specifications and the testing machine setup parameters of Vickers hardness test. There are two specimens collected from each specimen group. There are ten indentation points for each specimen at different locations. The indentation side is the specimen backside. It is because the specimen backside is the initial fracture side during the three-point bending test.

Table 4-5 EMC specimens and Vickers hardness test specifications.

Specimen ID	Sample size	Indentation point (per sample)	Indentation Load (g)	Remark
EMC-1	2	10	100	Force on sample backside
EMC-2	2	10	100	
EMC-3	2	10	100	
EMC-4	2	10	100	

Figure 4-26 shows the comparison of average Vickers pyramid number among EMC specimens. All the specimen curves show the same trend. The hardness of EMC specimen increases about 20% after the one time PSV curing process, and it becomes stable after the three times PSV curing process. The hardness of EMC specimen almost remains the same in the following observation points. EMC-2

always has the highest hardness throughout the test, and EMC-4 has the lowest hardness.

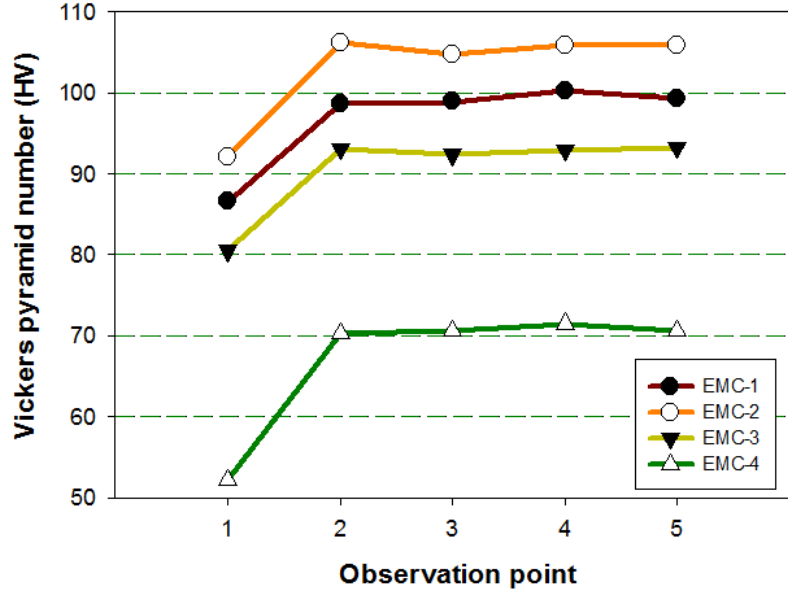

Figure 4-26 Comparison of average Vickers pyramid number among EMC specimens.

Table 4-6 lists the specimen specifications and the testing machine setup parameters of three-point bending test. There are ten specimens collected from each specimen group. The specimens come from five regions – top, left, center, right and bottom as per wafer. Therefore, two specimens are collected from each region and combined into ten specimens. The loading side is the specimen front side.

Table 4-6 EMC specimens and 3PB test specifications.

Specimen ID	Sample size	Width (mm)	Thickness (mm)	Span (mm)	Loading Speed (mm/min)	Remark
EMC-1	10	10	0.65	8	6	Sample backside face down
EMC-2	10	10	0.65	8	6	
EMC-3	10	10	0.65	8	6	
EMC-4	10	10	0.45	8	6	

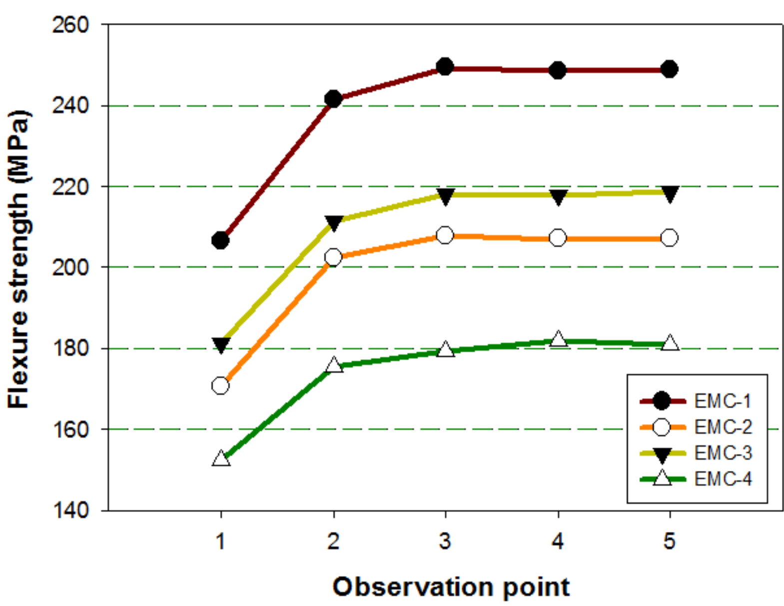

Figure 4-27 Comparison of average flexure strength among EMC specimens.

Figure 4-27 shows the comparison of average flexure strength among EMC specimens. All the specimen curves still show the same trend. The flexure strength of EMC specimen increases about 20% after the one time PSV curing process. However, the flexure strength of EMC specimen still increases slightly in the following observation points. The flexure strength of EMC specimen may still have the chance to increase after the three times PSV curing process if we change the reflow process to a long-term thermal process such as the PSV curing process. EMC-1 always has the highest flexure strength throughout the test. EMC-4 still has the lowest flexure strength. EMC-2 has the second lowest flexure strength, although it has the highest hardness.

The hardness and strength of EMC specimen increase rapidly after the one time PSV curing process. It seems the hardness and strength are enhanced by the PSV curing process. This phenomenon matches the previous research [161, 181-183]. The increased glass transition could lead to the increasing in the flexural modulus of

EMC. The hardness of EMC specimens becomes stable after the one time PSV curing process and it does not increase obviously after the three times PSV curing process. However, the flexure strength of EMC specimens still shows the growth trend after the three times PSV curing process. We cannot judge whether the flexure strength of EMC specimens becomes stable based on the current experiment because the duration of reflow process is too short.

For the relationship between the hardness and strength, the hardness and strength are two independent material properties, and it has been proved that there is not any relationship between the hardness and strength. For example, the steel hardness is high, and its strength is low. In this work, EMC-2 has the highest hardness and the second lowest strength. Therefore, we cannot use one test to predict the other test result.

The other finding from this work is the flexure strength distribution of pure EMC specimen is much tighter than the flexure strength distribution of FOWLP specimen. Figure 4-28 shows the three-point bending test curves of EMC and FOWLP specimen. Each graph contains five specimen curves. The curves of pure EMC specimen almost overlap from the beginning to fracture points. The curves of FOWLP specimen show different fracture points although the curves overlap each other at the beginning. The different fracture load points lead to the flexure strength distribution wide.

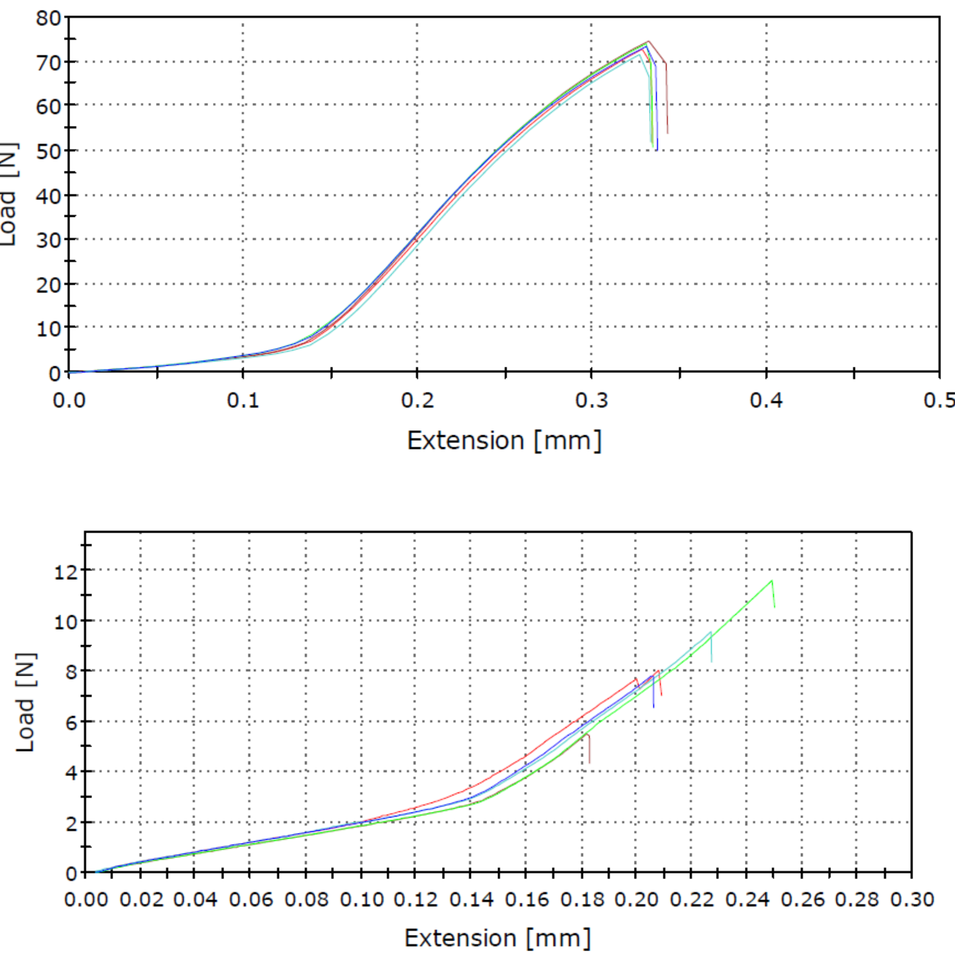

Figure 4-28 3PB test curves (load versus extension) of EMC (top) and FOWLP (bottom) specimens.

Figure 4-29 shows the comparison of flexure strength between pure EMC specimens and FOWLP specimens. The flexure strength distributions are clear in Figure 4-29. The flexure strength distribution of pure EMC specimen is extremely tight compared with the flexure strength distribution of FOWLP specimen. The flexure strength distribution of specimen A-1 is the best among FOWLP specimens. However, it still has a big difference with the flexure strength distribution of EMC specimens.

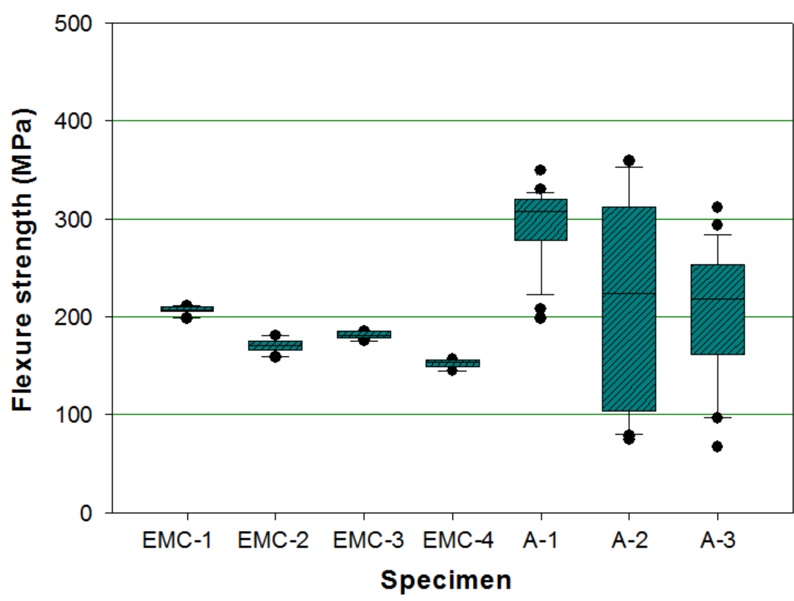

Figure 4-29 Comparison of flexure strength between EMC specimens and FOWLP specimens.

4.3.3 THERMAL RELATED RELIABILITY TEST EFFECT ON EMC STRENGTH

The aim of this work is to find out the effect of long-term thermal related reliability test on the EMC strength. We choose the high temperature storage test to process the EMC specimens. The three-point bending test is used to evaluate the EMC strength.

Table 4-7 lists the specimen specifications and the testing machine setup parameters of three-point bending test. The loading side is the specimen front side. The loading speed is 6 mm/min. There are two observation points in the HTS test. The specimens are collected and tested after the 500 hours and 1000 hours HTS test respectively.

Table 4-7 EMC specimens and 3PB test specifications (HTS test effect).

Specimen ID	Width (mm)	Thickness (mm)	Span (mm)	500 hrs HTS test sample size	1000 hrs HTS test sample size
EMC-1	10	0.65	8	4	3
EMC-2	10	0.65	8	6	5
EMC-3	10	0.65	8	4	3
EMC-4	10	0.45	8	2	2

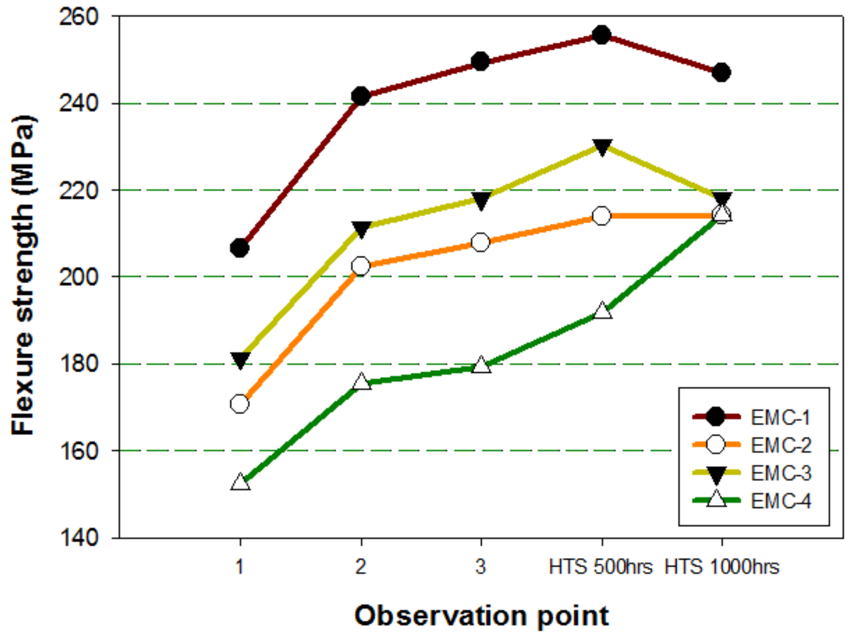

Figure 4-30 Comparison of average flexure strength among EMC specimens after the HTS test.

Figure 4-30 shows the comparison of average flexure strength among EMC specimens after the HTS test. The curves of average flexure strength show three trends. The average flexure strength of EMC-1 and EMC-3 specimen increases first and then decreases. The average flexure strength of EMC-2 almost remains the same after the HTS test. The average flexure strength of EMC-4 always increases

throughout the HTS test. The average flexure strength of EMC-4 has caught up with the average flexure strength of EMC-2 and EMC-3 after the 1000 hours HTS test.

The flexure strength of EMC specimen increases significantly after the 500 hours HTS test. This phenomenon proves that the flexure strength of EMC does not become stable after the three times PSV curing process (observation point 3). The flexure strength of EMC increases with extending the thermal process time. However, the flexure strength of some EMC specimens (EMC-1 and EMC-3) shows the downward trend after the 1000 hours HTS test. The flexure strength of EMC-1 and EMC-3 drops significantly. The change of flexure strength of EMC-2 is not obvious. A longer HTS test may be required to evaluate whether the flexure strength of EMC-2 becomes stable. However, based on the current evaluation work, the performance of EMC-2 is superior, and EMC-2 may be a good choice for the FOWLPs.

Figure 4-31 Side view of EMC-4 specimen after the 1000 hours HTS test.

The flexure strength of EMC-4 shows a rapid growth trend throughout the HTS test. The growth rate of EMC-4 flexure strength is incredible. The flexure strength of EMC-4 is almost as the same as the flexure strength of EMC-2 and EMC-3. However, EMC-4 is not a good choice. The warpage of EMC-4 is too high after the HTS test. Figure 4-31 shows the side view of EMC-4 specimen after the 1000 hours HTS test. The warpage performance of EMC-4 specimen is terrible. The FOWLP function fails definitely after the HTS test if EMC-4 materials are used.

Therefore, the finding of high flexure strength growth rate of EMC-4 is not very exciting.

4.4 OPTIMIZED DESIGN OF FOWLP STRUCTURE

In the previous evaluation work of FOWLP strength, we find that the over-molded structure FOWLP always shows the highest flexure strength. The over-molded EMC layer shows an obvious enhancement of the FOWLP strength. However, the thickness of over-molded structure FOWLP is an issue. The BSP tape protected structure FOWLP is introduced to meet the requirement of minimal volume and thickness. The BSP tape cannot enhance the FOWLP strength beyond reducing the flexure strength distribution. In this section, we are going to find out some additional factors, which could affect the FOWLP strength.

All the specimens are functional FOWLPs in this evaluation work, and they are sponsored by STATS ChipPAC Pte. Ltd. Although the specimens are functional chips, their solder balls are removed by the chemical liquid. However, this batch specimen contains more components than the bare FOWLP specimens.

4.4.1 FOWLP DIMENSION

There are two factors needed to consider in the aspect of FOWLP dimension. The first factor is the silicon die to package ratio. The second factor is the package size. The former concerns the effect of die size on the FOWLP strength with the

same package size. The latter concerns the effect of package size on the FOWLP strength with the same die to package ratio.

Group C specimens are used to evaluate the effect of die to package ratio on the FOWLP strength. Table 4-8 lists group C specimen specifications. There are three kinds of specimen in group C. Their package sizes are 9.9 mm × 9.9 mm. However, their die sizes are different. There are three different die sizes: 8.05 mm × 8.05 mm, 8.4 mm × 8.4 mm and 8.75 mm × 8.75 mm. Therefore, there are three different die to package ratios. The die thickness is 340 μm, while the package thickness is 420 μm. The dies are always placed at the geometrical center of package. All the specimens are laid on the 3PB fixture with their smooth and flat active side facing down. The reason is to isolate and minimize the effect of wafer grinding process on the FOWLP strength. The sample size is 25. The fixture span is 6 mm, and the loading speed is 6 mm/min.

Table 4-8 Group C specimen specifications.

Specimen ID	Die dimension (mm)			Package dimension (mm)			Die to package ratio
	X	Y	Z	X	Y	Z	
C-1	8.05	8.05	0.34	9.9	9.9	0.42	0.535
C-2	8.40	8.40	0.34	9.9	9.9	0.42	0.583
C-3	8.75	8.75	0.34	9.9	9.9	0.42	0.632

Figure 4-32 shows the comparison of flexure strength among group C specimens. The average flexure strength shows the decreasing trend from specimen C-1 to specimen C-3. Specimen C-1 has the highest average flexure strength, while specimen C-3 has the lowest. The low die to package ratio FOWLP should have the highest flexure strength

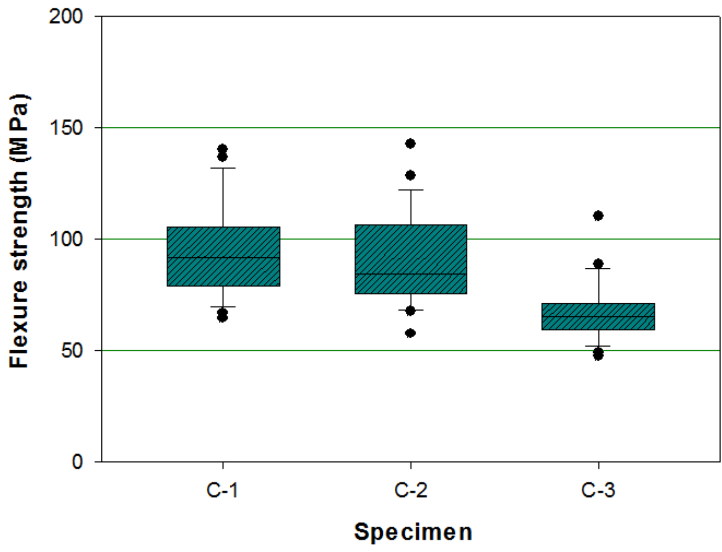

Figure 4-32 Comparison of flexure strength among group C specimens.

Specimen C-1 has the smallest die to package ratio. In other words, the silicon die of specimen C-1 is the smallest. The flexure strength decreases with the silicon die size increases. Group C specimens are the over-molded structure FOWLP. Their silicon dies are encapsulated by the EMC. The EMC volume increases after decreasing the silicon die size. The high volume EMC specimen shows the high flexure strength. Therefore, the EMC volume has the significant effect on the FOWLP strength in the over-molded structure FOWLP. The reason is the shifting of bending neutral surface.

A neutral surface must exist in a bending object. The neutral surface should parallel to the upper and lower surfaces of specimen. The bending stress varies linearly with the distance from the neutral surface. Therefore, the maximum stress must appear on the upper and lower surfaces of specimen. The upper surface (loading surface) of specimen suffers the compression stress, while the lower surface of specimen suffers the tension stress in the bending test. Silicon is the sensitive and

brittle material, and its fracture is due to the tension stress rather the compression stress. Therefore, the fracture always appears on the opposite side of loading force. The neutral surface shifts to the lower surface of silicon die when the EMC thickness increases. Therefore, the tension stress at the lower surface of silicon die reduces, and the package strength increases.

Group D specimens are used to evaluate the effect of package size on the FOWLP strength. Table 4-9 lists group D specimen specifications. There are two kinds of specimen in group D. Specimen D-1 package size is 6.43 mm × 6.43 mm, and its die size is 5.66 mm × 5.66 mm. Specimen D-2 package size is 6.14 mm × 6.14 mm, and its die size is 5.395 mm × 5.395 mm. The die thickness is 340 μm, while the package thickness is 420 μm. The dies are always placed at the geometrical center of package.

The dimension difference is small. However, both package and die are enlarged or narrowed in the same proportion. The reason is to maintain the same die to package ratio. All the specimens are laid on the 3PB fixture with their smooth and flat active side facing down. The reason is to isolate and minimize the effect of wafer grinding process on the FOWLP strength. The sample size is 25. The fixture span is 4 mm, and the loading speed is 6 mm/min.

Table 4-9 Group D specimen specifications.

Specimen ID	Die dimension (mm)			Package dimension (mm)			Die to package ratio
	X	Y	Z	X	Y	Z	
D-1	5.395	5.395	0.34	6.14	6.14	0.42	0.625
D-2	5.66	5.66	0.34	6.43	6.43	0.42	0.627

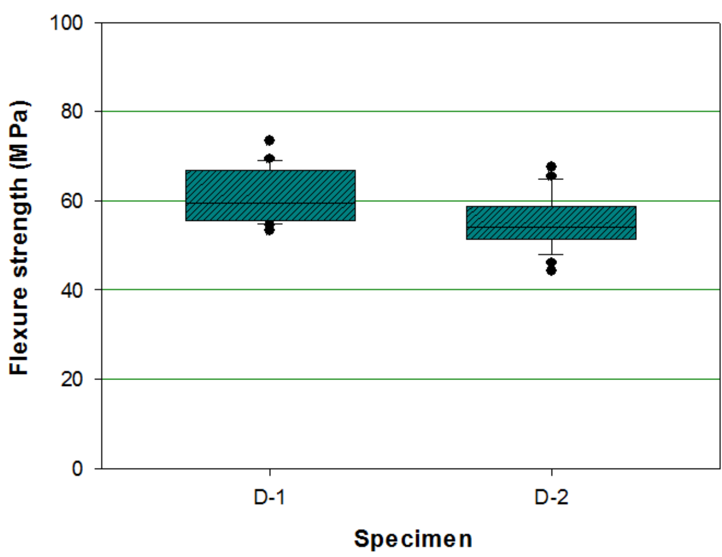

Figure 4-33 Comparison of flexure strength among group D specimens.

Figure 4-33 shows the comparison of flexure strength among group D specimens. The average flexure strength of specimen D-1 is higher than the average flexure strength of specimen D-2. The flexure strength distribution of specimen D-2 is a little bit tighter than the flexure strength distribution of specimen D-1.

Group D specimens are selected carefully. We cannot just select any two different dimension specimens because the FOWLP is not a homogeneous object. In order to gain an accuracy experiment result, the specimens must maintain the same die to package ratio. However, there is still a 0.32% die to package ratio difference between specimen D-1 and specimen D-2. The flexure strength of specimen D-1 is 10% higher than that of specimen D-2. The t-test verifies that the flexure strength mean of specimen D-1 is greater than the flexure strength mean of specimen D-2 significantly at the 99.5% confidence level. Therefore, the smaller over-molded structure FOWLP has higher flexure strength. The reason for this phenomenon is also due to the shifting of bending neutral surface.

4.4.2 PCB BAR PLACEMENT

The PCB bar is a tiny PCB with prefabricated electrical circuits, and it is used to improve the package interconnection ability. The PCB bars are added to the artificial wafer during the pick and place process, and they are encapsulated by the EMC during the molding process.

Group E specimens are used to evaluate the effect of PCB bar on the FOWLP strength. Table 4-10 lists group E specimen specifications. There are two kinds of specimen in group E. The package size of specimen E-1 is 7 mm × 7 mm, and the package thickness is 191 μm. The package size of specimen E-2 is 14 mm × 14 mm, and the package thickness is 300 μm. The dies are always placed at the geometrical center of the packages.

Table 4-10 Group E specimen specifications.

Specimen ID	Die dimension (mm)			Package dimension (mm)			Remark
	X	Y	Z	X	Y	Z	
E-1	5.079	5.079	0.191	7	7	0.191	Contain 2 PCB bar
E-2	11	11	0.3	14	14	0.3	Contain 4 PCB bar

Figure 4-34 shows the layout of specimen E-1 and specimen E-2. For specimen E-1, there are only two PCB bars on the package peripheral, and the PCB bars face to each other. For specimen E-2, there are four PCB bars on the package peripheral, and one pair of them is a little bit longer than the other pair. The thickness of PCB bar is 150 μm.

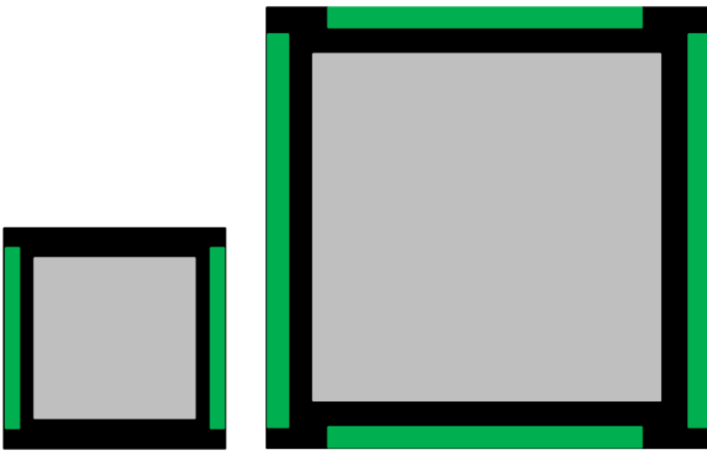

Figure 4-34 Group E specimen layout (Green columns are PCB bar).

There are two rounds of 3PB test. For example: for specimen E-1, the loading force of the first round 3PB test is parallel to the PCB bar and the loading force of the second round 3PB test is perpendicular to the PCB bar. Specimen E-1 is used to evaluate the effect of PCB bar on the FOWLP strength. Specimen E-2 is used to evaluate the effect of PCB bar size on the FOWLP strength. All the specimens are laid on the 3PB fixture with their smooth and flat active side facing down. The reason is to isolate and minimize the backside grinding effect on the FOWLP strength. The sample size is 50. The fixture span is 4 mm for specimen E-1, and 10 mm for specimen E-2. The loading speed is 6 mm/min.

Figure 4-35 shows the comparison of specimen E-1 flexure strength. The average flexure strength of EMC direction is higher than the average flexure strength of PCB bar direction. The latter flexure strength distribution is a little bit wider than the former flexure strength distribution.

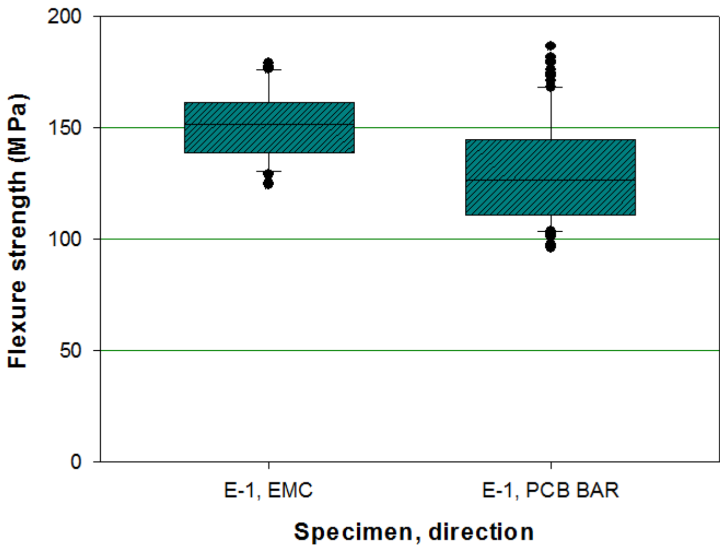

Figure 4-35 Comparison of specimen E-1 flexure strength.

The flexure strength of EMC direction (loading force on the EMC) is higher than the flexure strength of PCB bar direction (loading force on the PCB bar). The reason for this phenomenon is the low Young's modulus of PCB bar. The Young's modulus of PCB bar is less than that of EMC too much.

The EMC volume reduces once the PCB bar is added to the package. The EMC volume on the EMC sides is high, while the EMC volume on PCB bar sides is low. The PCB bar is made up of the glass fiber reinforced epoxy resin, and its strength is lower than the EMC strength. Therefore, the decreasing of strength on the PCB bar side is reasonable.

Figure 4-36 shows the comparison of specimen E-2 flexure strength. The average flexure strength of short PCB bar direction is higher than the average flexure strength of long PCB bar direction. The former flexure strength distribution is tighter than the latter flexure strength distribution.

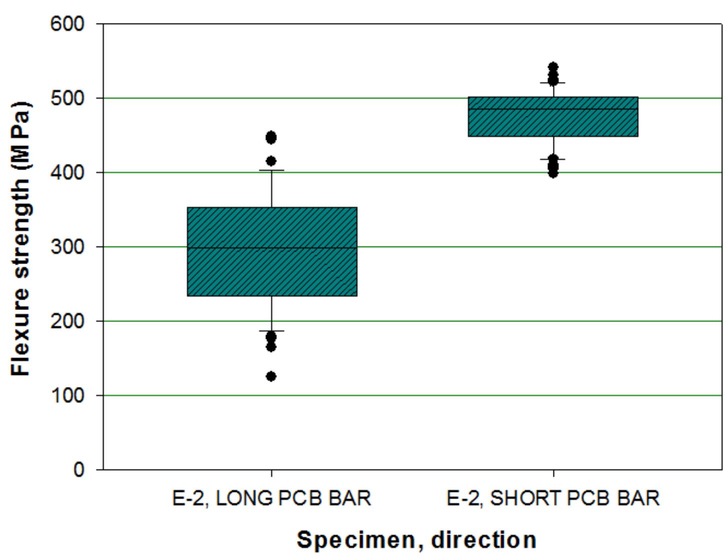

Figure 4-36 Comparison of specimen E-2 flexure strength.

The flexure strength trend of specimen E-2 aligns with the flexure strength trend of specimen E-1. The EMC volume on the short PCB bar sides is high, while the EMC volume on the long PCB bar sides is low. Therefore, the effect of PCB bar on the FOWLP package is significant and directional. The short and thin PCB bar are preferred by the FOWLP.

4.4.3 GRINDER WHEEL SELECTION

The silicon die is required to grind to a thin level to build a thin over-molded structure FOWLP. However, we cannot align the molding thickness of artificial wafer with the silicon die thickness. It is because the EMC filler size is larger than the thickness of over-molded layer. Therefore, the grinding process of molded artificial wafer cannot be neglected. The effect of wafer grinding process on the

silicon wafer strength is investigated and proved before. In this section, we are going to find out whether the grinding process still affects the mold wafer strength.

Group F specimens are used to evaluate the effect of wafer grinding process on the FOWP strength. Table 4-11 lists group F specimen specification. The package size of Group F specimen is 8 mm × 8 mm, and the die size is 4.264 mm × 4.614 mm. The package thickness is 348 μm. The dies are always placed at the geometrical center of package.

Table 4-11 Group F specimen specifications.

Specimen ID	Die dimension (mm)			Package dimension (mm)			Grinding wheel
	X	Y	Z	X	Y	Z	
F-1	4.264	4.264	0.32	8	8	0.348	W1
F-2	4.264	4.264	0.32	8	8	0.348	W2
F-3	4.264	4.264	0.32	8	8	0.348	W3
F-4	4.264	4.264	0.32	8	8	0.348	W2+Si etch

There are four kinds of specimen, and they are ground by different grinding wheels or grinding methods. There are three kinds of grinding wheel: W1, W2 and W3. W3 has the finest grits and W1 has the roughest grits. The silicon etching process is added to polish the wafer surface further. The silicon etching process smooths the wafer surface by the chemical method, and it could make up the grinding wheel limitation and gain a smooth wafer surface. The final thicknesses of specimens are the same even the four specimens are ground by different wheels and processes. All the specimens are placed on the 3PB fixture with their backside facing down. The sample size is 63. The fixture span is 6 mm, and the loading speed is 6 mm/min.

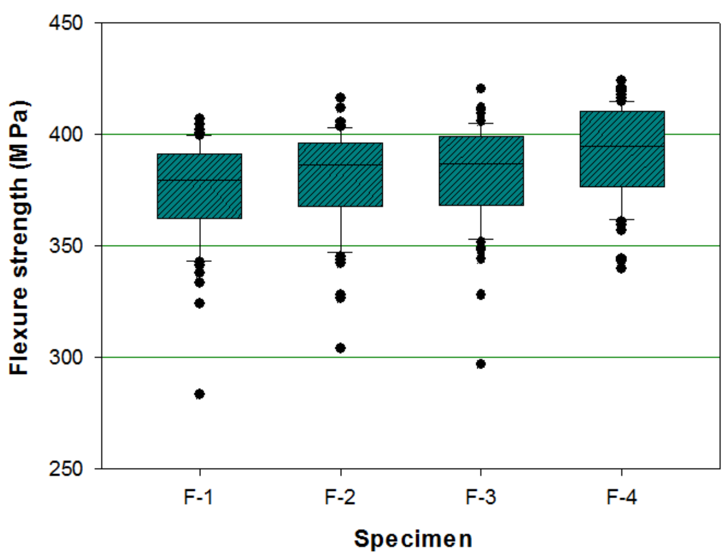

Figure 4-37 Comparison of flexure strength among group F specimens.

Figure 4-37 shows the comparison of flexure strength among group F specimens. The average flexure strength increases from specimen F-1 to specimen F-4. Specimen F-4 has the highest flexure strength, and specimen F-1 has the lowest flexure strength. The flexure strength distributions of specimens are almost the same.

Group F specimens are ground by the different grinding wheels or the grinding methods. The expected grinding outcome is specimen F-4 has the finest grinding surface, and specimen F-1 has the roughest grinding surface. The grinding surface roughness is measured and listed in Table 4-12. The flexure strength has the opposite trend with the wafer surface roughness. The wafer with the finest surface has the highest flexure strength, and the wafer with the roughest surface has the lowest flexure strength. Therefore, the wafer grinding process still has the significant effect on the FOWLP strength.

Table 4-12 Wafer surface roughness of Group F specimen.

Specimen ID	Surface roughness Ra (μm)
F-1	0.0127
F-2	0.0098
F-3	0.0056
F-4	0.0033

4.5 SUMMARY

The 3PB test is conducted by Instron universal tester 5566. The static load cell of Instron 2530-427 is used, and its maximum capacity is ±100 N. The 3PB fixture is customized with a fabrication tolerance ±0.05 mm. The whole experiment is conducted in the biological lab, School of Mechanical and Aerospace Engineering, Nanyang Technological University. The environment temperature is 25°C. There is not any pre-conditioning or heating device attached to the machine to process the specimens before or during the experiment. The default speed of loading force is 0.6 mm/min (0.01 mm/s). The specimens are built by the conventional fan-out wafer level packaging assembly process, and they are considered and designed carefully to fulfill the research objective. The dummy silicon die size of specimen is 5.11 mm × 5.11 mm, and the package size is 8.09 mm × 8.09 mm.

The FOWLPs have three kinds of typical structure, and they are the over-molded structure, die-exposed structure and BSP tape protected structure. The 3PB test results show that the flexure strength of over-molded structure FOWLP is much

higher than the flexure strength of other two kinds of structure FOWLP. However, the flexure strength distribution of these three kinds of structure FOWLP shows the different trend. The flexure strength distribution of over-molded structure FOWLP is much tight. The flexure strength distribution of die-exposed structure FOWLP is the widest. The flexure strength distribution of BSP tape protected structure FOWLP is tighter than the flexure strength distribution of die-exposed structure FOWLP even they have the same average flexure strength. The reason is the condition of FOWLP backside. The BSP tape covers the backside defects and forms a smooth surface on top of the wafer backside. Although the BSP tape has a minor contribution to the FOWLP strength, it reduces the effect of wafer grinding process on the flexure strength distribution significantly. Therefore, the over-molded structure and BSP tape protected structure FOWLP is recommended. For the aspect of FOWLP fracture analysis, all the specimens break into two parts after the 3PB test. The initial fracture point only appears on the silicon die surface or silicon die edge regardless the specimen structure.

The PSV layers are lithographed on the three kinds of typical structure FOWLP. The 3PB test results show two trends. The flexure strength of over-molded structure FOWLP increases significantly after lithographing the PSV layers. The thickness of PSV layer is 10 μm. Hence the PSV layer should not affect the FOWLP strength seriously. The reason should be the PSV lithographing process. The PSV lithographing process requires the wafer to store in a high temperature oven for curing. The oven temperature is 225℃, and the storage duration is two hours. The EMC takes the principal place in the FOWLP and thus the increase in the FOWLP strength should be due to the increase in the EMC strength after the PSV curing process. The flexure strength of die-exposed and BSP tape protected structure

FOWLP almost remains the same. The reason is the PSV layer is lithographed on the specimen front side, and the surface condition of specimen backside never changes. Therefore, the over-molded structure FOWLP is recommended.

The PSV curing process is only a short-term thermal process. The temperature cycling test and high temperature storage test are used to evaluate the long-term thermal test effect on the FOWLP strength. The cycling rate in this work is two cycles per hour. The durations of TC test are 500 cycles and 1000 cycles. The temperature of high temperature storage test is 150℃. The durations of HTS test are 500 hours and 1000 hours. The 3PB test results show two trends. The flexure strength of over-molded structure FOWLP increases slightly after both TC test and HTS test. The EMC physical property especially the strength should be affected by the thermal test. The flexure strength of die-exposed and BSP tape protected structure FOWLP increases at the middle point of test and drops at the end of test.

The flexure strength of over-molded structure FOWLP always increases significantly after the thermal process. We hypothesize that the increase in the FOWLP strength comes from the increase in the EMC strength and the EMC strength must be affected by the thermal process seriously. We collect four kinds of EMC specimen. The 3PB test and Vickers hardness test is used to evaluate the strength and hardness of EMC specimen. The Instron universal tester 5569 and a maximum capacity of ±1kN load cell are used to conduct the 3PB test. The FUTURE-TECH microhardness tester FM-300e is used to conduct the Vickers hardness test. The experiment results show that the flexure strength and hardness of EMC specimens increase rapidly after the one time PSV curing process. However, the growth trends of flexure strength and hardness of EMC specimens become stable after the three times PSV curing process. The reason is the thermal process temperature is higher

than the EMC glass transition. The increasing of EMC glass transition and EMC flexural modulus is due to the thermal process. However, the EMC flexure strength still increases significantly after the 500 hours HTS test, and this phenomenon proves that the EMC flexure strength does not become stable after the three times PSV curing process. The strengths of EMC specimens drop after the 1000 hours HTS test except for EMC-2. All the FOWLP specimens use EMC-2 in this research and thus the previous phenomenon of flexure strength up and down is not related to the EMC material. For the relationship between the strength and hardness, it has been proved that there is not any relationship between the strength and hardness. The strength and hardness are two independent material properties.

In order to get a reliable FOWLP, the over-molded structure FOWLP is recommended. The thin over-molded structure FOWLP can fulfill the requirement of volume sensitive device. There are some matters needed attention when we build the over-molded structure FOWLP. The FOWLP with small silicon die and thin PCB bar gains high strength. The reason is the shifting of bending neutral surface. The changing of material volume and material Young’s modulus leads to the shifting of neutral surface. The wafer grinding process still affects the FOWLP strength. The FOWLP with the finest molding surface has the highest flexure strength.

CHAPTER 5 NUMERICAL STUDY OF FOWLP STRENGTH

5.1 SIMULATION OF 3PB TEST

The finite element method (FEM) is a numerical method, which solves complex engineering problems [184]. There is much commercial computer software used to solve the finite element problems such as ANSYS (as shown in Figure 5-1), Abaqus and COMSOL. In this work, ANSYS is used to implement the numerical study of FOWLP strength.

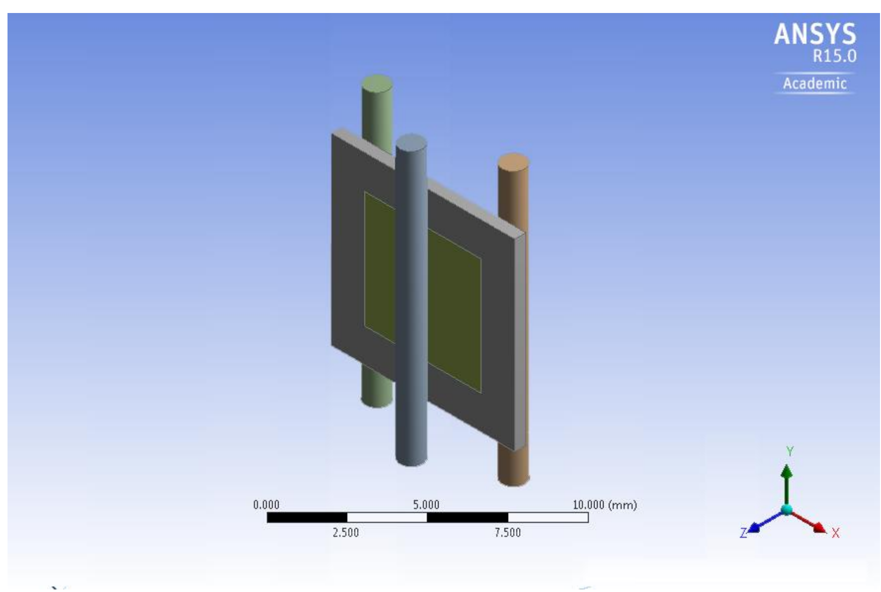

Figure 5-1 ANSYS simulation software.

The 3PB test on FOWLP specimens is planned to be simulated by ANSYS. Figure 5-2 shows the 3PB test for a FOWLP specimen. The effective parts are the

3PB fixture and the specimen. Therefore, the simulation models only include the 3PB fixture and the FOWLP specimen. The three rollers of 3PB fixture are made up of stainless steel with 1 mm diameter. These rollers are defined as the structural steel in ANSYS.

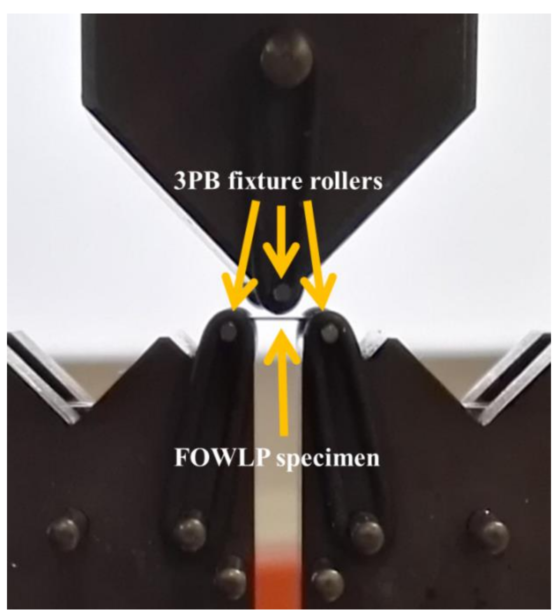

Figure 5-2 The experiment of 3PB test for a FOWLP specimen.

The FOWLP specimen has four kinds of materials, and they are silicon die, EMC, PSV and BSP tape. Table 5-1 lists the material properties of simulation models. Moreover, they are assumed as isotropic elasticity materials in ANSYS.

Table 5-1 The material properties of simulation models.

Part	Material	Young's Modulus (GPa)	Poisson's ratio
FOWLP specimen	Silicon die	131	0.28
	EMC	23	0.3
	PSV layer	2	0.4
	BSP tape	6.2	0.3
3PB fixture	Structure steel	200000	0.3

The ANSYS static structural toolbox is used in this simulation work. ANSYS Geometry is used to create the simulation models. There are four components in the simulation model (as shown in Figure 5-3). Three rollers represent the 3PB fixture and a FOWLP specimen located in between the top and bottom rollers. Therefore, there are three contact points in the simulation model, and all the contact points are defined as the frictionless contact. The surfaces of lower two rollers are defined as the fixed support.

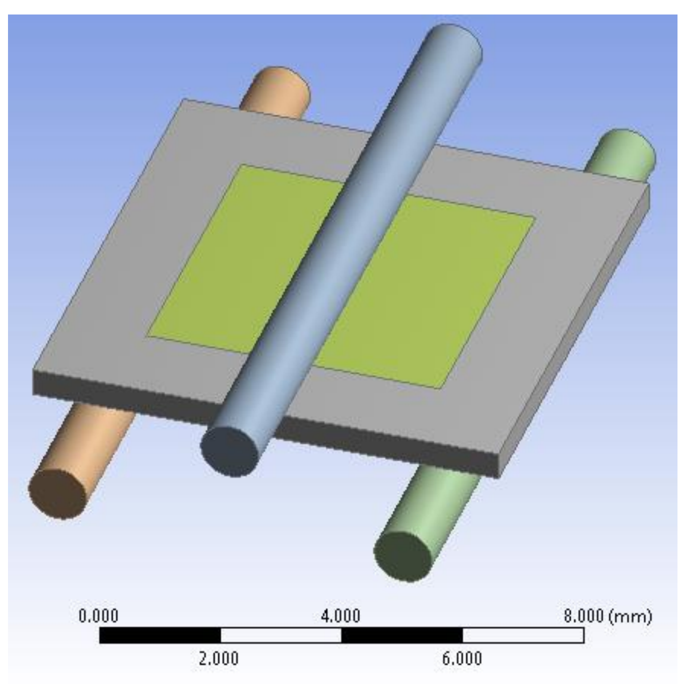

Figure 5-3 The simulation model of 3PB test for a FOWLP specimen.

Two different mesh methods are applied. For the 3PB fixture rollers, the round edges of roller are divided into ten divisions by the edge sizing method (as shown in Figure 5-4). For the FOWLP specimen, the body surface of FOWLP specimen is meshed by the body sizing method with the 0.5 mm element size. All the vertical direction edges of FOWLP specimen are divided into four layers by the edge sizing method (as shown in Figure 5-5).

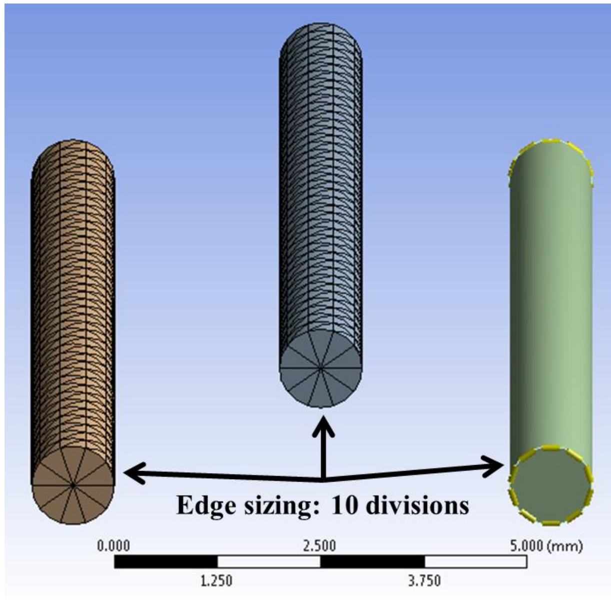

Figure 5-4 Meshed 3PB fixture rollers.

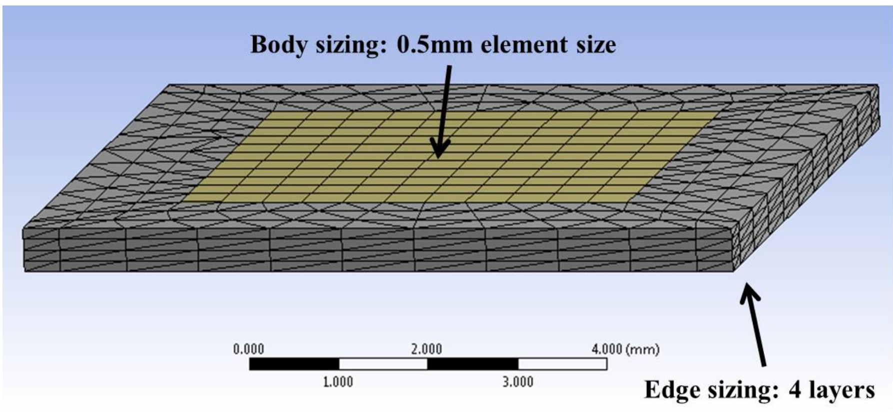

Figure 5-5 Meshed FOWLP specimen.

There are two methods can be used to solve the simulation model. The first method is named as the velocity method. The velocity method controls the movement of 3PB roller by the velocity. This method is much complicated, and the impulse factors must be considered. This method should be solved by the ANSYS explicit

dynamics toolbox. However, this toolbox imports too many variables and leads to the simulation work complicate. Therefore, we do not recommend this method.

The second method is named as the displacement method. The displacement method defines the movement of 3PB fixture roller by the displacement. This approach focuses on the specimen deflection rather than the loading force speed. The actual loading speed of 3PB test is required as slow as possible to reduce the effect of roller movement on the FOWLP specimen. The displacement method only concerns the specimen deformation at a certain deflection position. The stress and strain of FOWLP specimen are calculated based on the deflection value. In this work, we choose the displacement method. The upper roller of 3PB fixture is instructed a downward displacement (as shown in Figure 5-6).

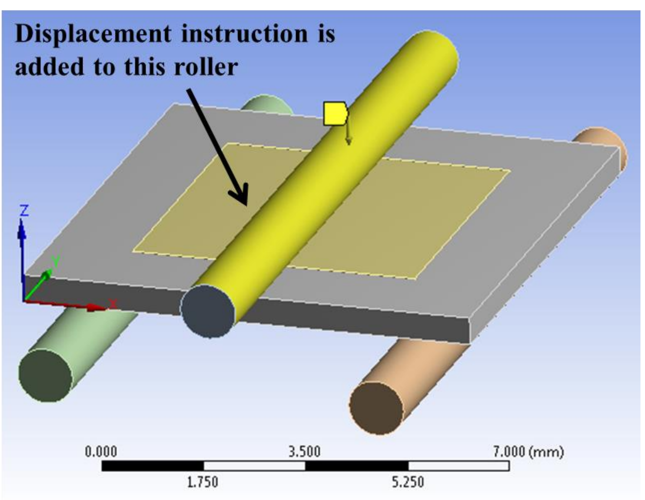

Figure 5-6 The upper roller is instructed a downward displacement.

The displacement range should refer to the experiment data to avoid unpractical results and save the computational time. Figure 5-7 shows one of the displacement step control graphs. In this graph, only step 2 is the effective step, and its displacement range is from 0.15 mm to 0.25 mm.

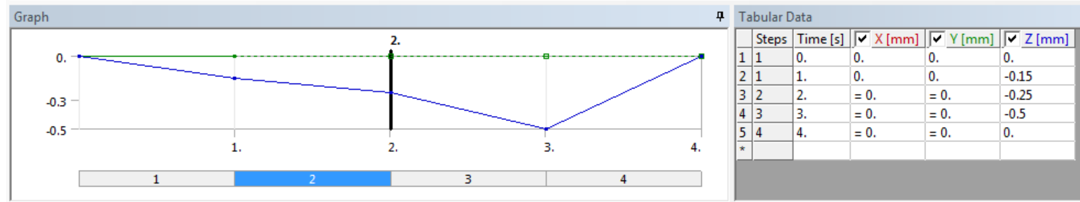

Figure 5-7 The displacement step control graph with an effective range from 0.15 mm to 0.25 mm.

The maximum principal stress (within the effective deflection range) of FOWLP specimen is recorded as the simulation result. The comparison of experiment result and simulation result is represented by the two-parameter Weibull distribution

$$P = 1 - exp\left[-\left(\frac{\sigma}{\sigma_0}\right)^m\right] \tag{5.1}$$

where P is the failure probability, σ is the flexure strength (or maximum principal stress in ANSYS), σ_0 is the scale parameter and m is the shape parameter or Weibull modulus.

5.2 Evaluation of FOWLP strength by numerical method

We face some issues in the previous evaluation work of FOWLP strength by the experimental method. Firstly, the specimen preparation takes too much time. The changes of specimen parameters or materials require serval days to rebuild the new specimen. Secondly, the experiment can be affected by human factors easily since

the specimens are very thin and small. In this section, we are going to use the finite element method to simulate the experiment of 3PB test. The aim of this work is to build the simulation model of 3PB test for the FOWLP.

5.2.1 SIMULATION CONDITIONS

The simulation model comes from group A and group B specimens in Chapter 4. Specimen A-2 and specimen A-3 are not used to this simulation work because they are not built by the conventional FOWLP assembly process. The package size of specimen is 8.09 mm × 8.09 mm, and the silicon die size is 5.11 mm × 5.11 mm. There are four kinds of specimen created in the simulation work. Each one of them represents one specimen status after a process. Figure 5-8 shows the specimen status after each assembly process.

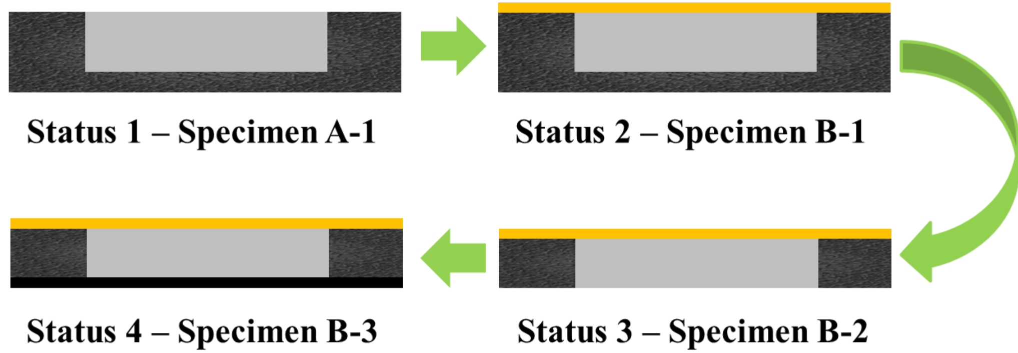

Figure 5-8 The FOWLP specimen status after each assembly process.

Figure 5-9 shows the illustration of specimen A-1 simulation model, and there are only two kinds of material – silicon die and EMC. The thickness of

specimen A-1 is 490 μm, and the thickness of silicon die is 370 μm. The node number and element number of specimen A-1 are 16365 and 8289.

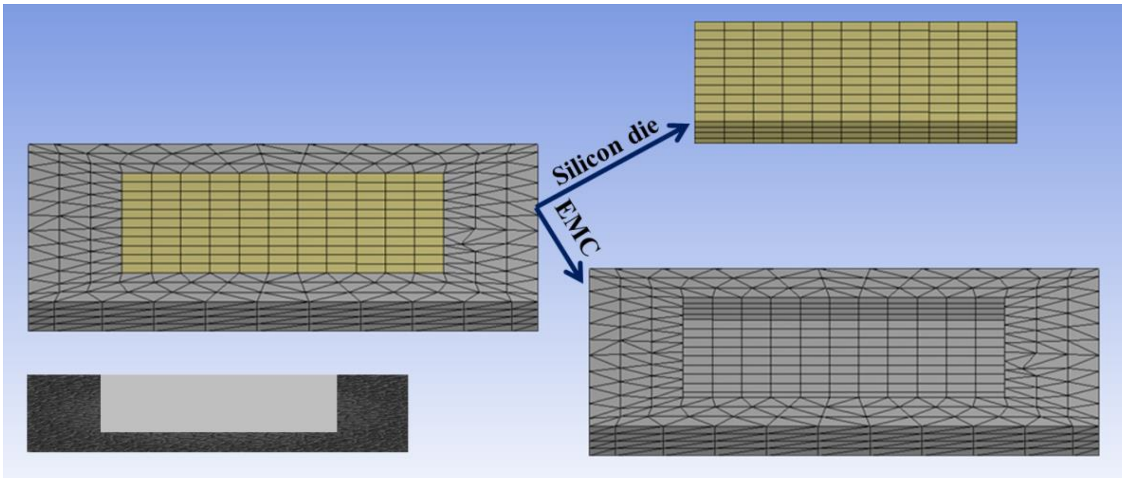

Figure 5-9 Specimen A-1 simulation model.

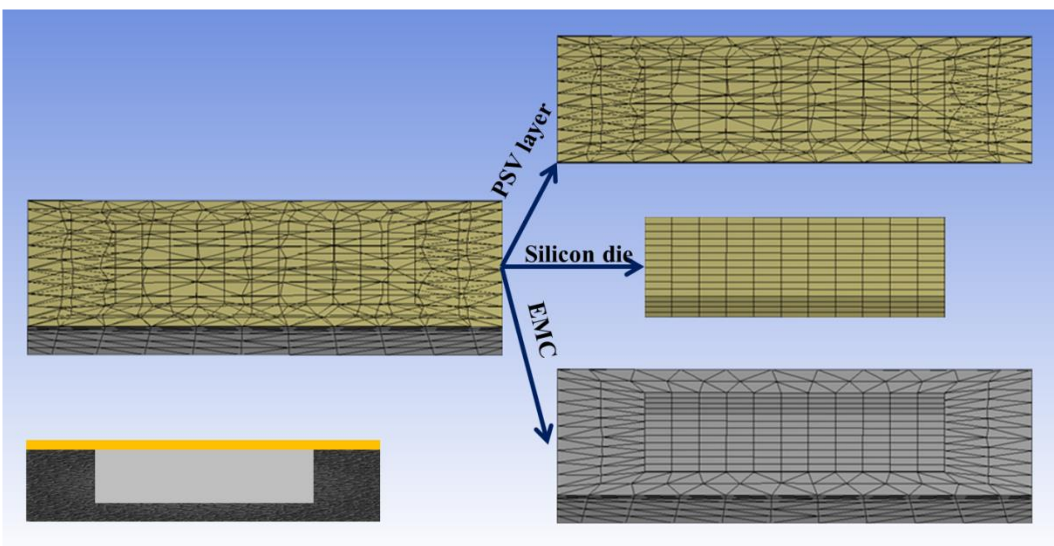

Figure 5-10 Specimen B-1 simulation model.

Figure 5-10 shows the illustration of specimen B-1 simulation model, and there are three kinds of materials – silicon die, EMC and PSV layer. Specimen B-1 is

lithographed a 10 μm thick PSV layer, and its total thickness is 500 μm. The node number and element number of specimen B-1 are 18638 and 9853.

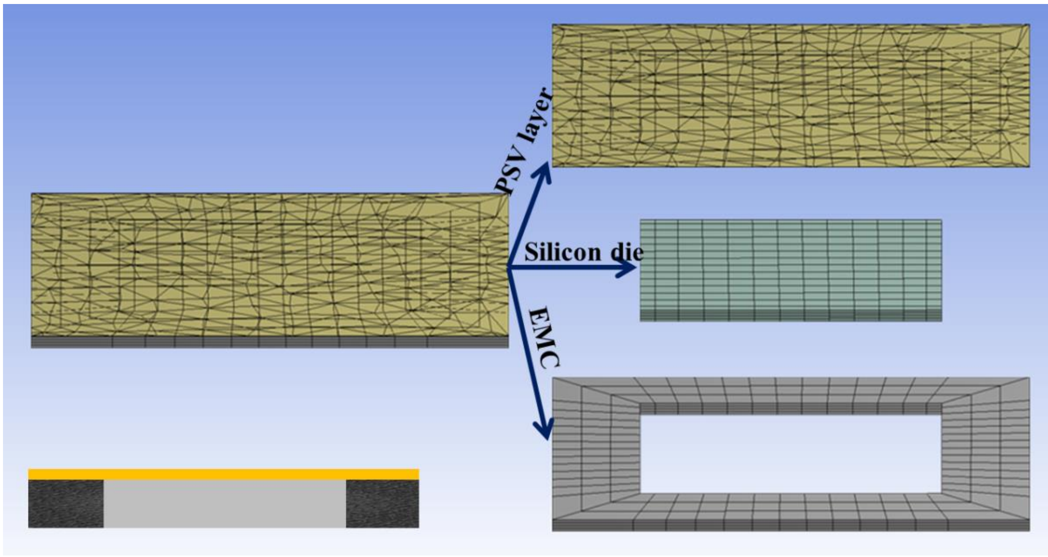

Figure 5-11 Specimen B-2 simulation model.

Figure 5-11 shows the illustration of specimen B-2 simulation model, and there are three kinds of materials – silicon die, EMC and PSV layer. Specimen B-2 is ground to the thickness of 210 μm, and its backside is exposed. The node number and element number of specimen B-2 are 17735 and 7267.

Figure 5-12 shows the illustration of specimen B-3 simulation model, and there are four kinds of materials – silicon die, EMC, PSV layer and BSP tape. Specimen B-3 is laminated a 25 μm thick BSP tape on its backside, and its total thickness is 235 μm. The node number and element number of specimen B-3 are 20251 and 8923.

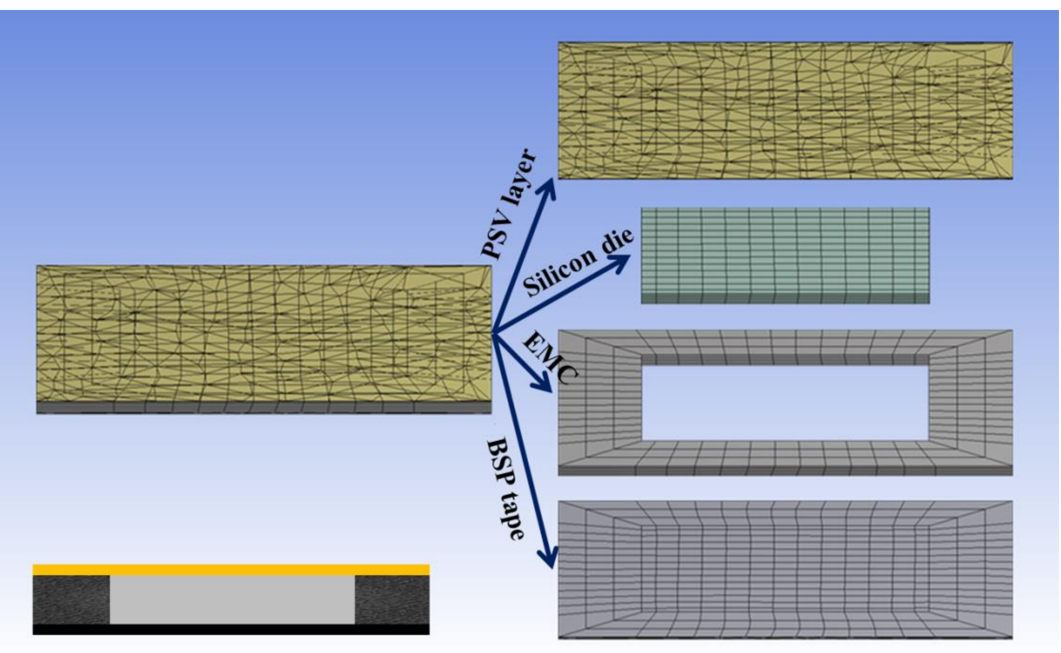

Figure 5-12 Specimen B-3 simulation model.

The displacement method is used for the simulation work. The displacement range of roller should refer to the experiment data to avoid unpractical results and save the computational time. Table 5-2 and Table 5-3 list the flexure strength and extension of specimen A-1, specimen B-1, specimen B-2 and specimen B-3 after the experiment of 3PB test. We take about 30 sampling points in the effective displacement range, and the corresponding maximum principal stress (flexure strength) value is recorded.

Table 5-2 The flexure strength and extension of specimen A-1 and specimen B-1 after the experiment of 3PB test.

S/N	Specimen A-1		Specimen B-1	
	Flexure strength (MPa)	Extension (mm)	Flexure strength (MPa)	Extension (mm)
1	207.94	0.202	379.24	0.239
2	198.27	0.194	427.30	0.256
3	255.16	0.205	368.37	0.230
4	255.39	0.201	423.67	0.255
5	231.63	0.190	355.49	0.231
6	307.44	0.210	436.38	0.255
7	307.45	0.213	488.18	0.268
8	323.81	0.213	427.44	0.252
9	307.16	0.208	371.58	0.237
10	323.84	0.212	422.36	0.254
11	349.52	0.227	277.15	0.209
12	325.35	0.220	354.33	0.233
13	315.56	0.214	414.00	0.248
14	275.01	0.207	436.68	0.261
15	317.72	0.220	412.08	0.252
16	290.13	0.201	449.79	0.260
17	321.43	0.220	355.01	0.231
18	330.36	0.212	424.26	0.247
19	311.23	0.209	410.24	0.247
20	317.84	0.220	422.87	0.248
21	306.59	0.211	373.20	0.239
22	294.83	0.205	438.68	0.256
23	307.82	0.212	456.69	0.269
24	287.65	0.202	410.68	0.248
25	281.99	0.205	468.39	0.274
Max	**349.52**	**0.227**	**488.18**	**0.274**
Min	**198.27**	**0.190**	**277.15**	**0.209**
Ave	**294.04**	**0.209**	**408.16**	**0.248**

The extension range of specimen A-1 is between 0.190 mm and 0.227 mm, while the extension range of specimen B-1 is between 0.209 mm and 0.274 mm.

Table 5-3 The flexure strength and extension of specimen B-2 and specimen B-3 after the experiment of 3PB test.

S/N	Specimen B-2 Flexure strength (MPa)	Specimen B-2 Extension (mm)	Specimen B-3 Flexure strength (MPa)	Specimen B-3 Extension (mm)
1	109.18	0.190	66.94	0.176
2	267.57	0.277	75.47	0.180
3	229.96	0.271	112.92	0.227
4	204.71	0.262	94.13	0.213
5	157.85	0.245	105.77	0.222
6	244.57	0.275	137.27	0.245
7	231.90	0.277	98.11	0.211
8	266.38	0.294	199.22	0.266
9	283.72	0.292	306.53	0.313
10	322.90	0.304	249.09	0.281
11	326.03	0.313	120.27	0.233
12	230.53	0.290	64.98	0.182
13	91.30	0.249	122.92	0.233
14	88.15	0.258	144.10	0.267
15	205.82	0.289	166.87	0.260
16	340.61	0.308	266.68	0.295
17	241.37	0.274	288.80	0.304
18	355.67	0.308	268.24	0.286
19	373.67	0.323	283.48	0.294
20	382.32	0.322	241.92	0.285
21	92.25	0.196	110.54	0.222
22	158.20	0.244	189.85	0.269
23	126.11	0.223	148.56	0.252
24	118.42	0.219	146.67	0.250
25	226.37	0.272	93.74	0.211
Max	**382.32**	**0.323**	**306.53**	**0.313**
Min	**88.15**	**0.190**	**64.98**	**0.176**
Ave	**227.02**	**0.271**	**164.12**	**0.247**

The extension range of specimen B-2 is between 0.190 mm and 0.323 mm, while the extension range of specimen B-3 is between 0.176 mm and 0.313 mm.

5.2.2 SIMULATION RESULT AND DISCUSSION

The flexure strength and maximum principal stress of FOWLP specimen are represented by the two-parameter Weibull distribution. We use Minitab software to plot the two-parameter Weibull distribution graph. The scale parameter and shape parameter of two-parameter Weibull distribution are solved by the maximum likelihood estimation method automatically in Minitab. Table 5-4 lists the summary of specimen scale parameters and shape parameters.

Table 5-4 Summary of scale parameters and shape parameters of specimens.

S/N	Scale parameter (σ_0)		Shape parameter (m)	
	Experiment	Simulation	Experiment	Simulation
Specimen A-1	308.924	316.350	11.053	27.725
Specimen B-1	426.825	427.246	11.394	19.394
Specimen B-2	255.740	217.260	2.795	3.373
Specimens B-3	186.164	193.731	2.361	3.475

Figure 5-13 shows the comparison of two-parameter Weibull distributions between experiment results and simulation results. The x-axis represents the flexure strength of FOWLP specimen and the y-axis represents the failure probability of FOWLP specimen.

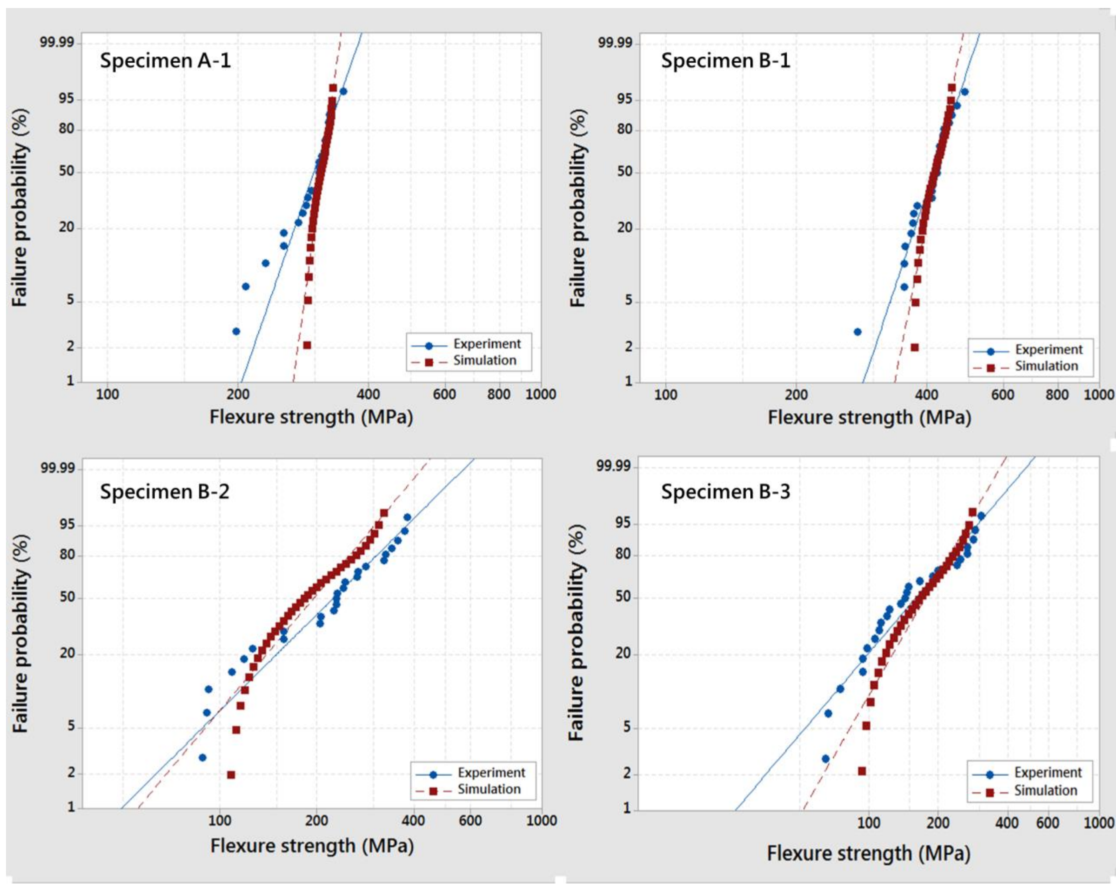

Figure 5-13 Comparison of two-parameter Weibull distribution between experiment results and simulation results.

Figure 5-13 shows that the experiment curve and simulation curve match each other in the upper region of failure probability closely. However, the simulation curves sometimes overestimate the FOWLP flexure strength in the lower region of failure probability compared with the experiment curve. Specimen B-2 simulation curve underestimates the FOWLP flexure strength in the upper region of failure probability compared with the experiment curve.

The comparisons between experiment results and simulation results are quite close for all the specimens. The simulation result of specimen B-3 is the most important and valuable result since the structure of specimen B-3 is the closest to finished FOWLPs. The missing components in specimen B-3 are redistribution layers

and solder balls. However, the outcome of applying ANSYS simulation software to evaluate the FOWLP strength is ideal and satisfactory. The current simulation models have the potential to replace the experimental method to implement the evaluation work of FOWLP strength.

One of the advantages of simulation method is stability. The simulated 3PB test is not affected by human factors such as the placement of specimen. The small and tiny specimen is required to be placed in the center of 3PB fixture manually. The specimen position is observed and judged by human eyes. Hence the specimen placement position is not 100% accurate at every time, and the perfect placement is impractical. The fracture point should appear along the specimen centerline in order to gain the accurate specimen flexure strength. However, the deviating of specimen placement position leads to the fracture point shifting. The fracture point may appear on the border between the EMC and silicon die. In that case, the flexure strength represents the border strength of EMC and silicon die. This border strength has the significant difference in the actual package strength.

The other advantage of simulation method is completely eradicating the environment effect on specimens. The specimens can be affected by the humidity and oxidized if it is not stored properly. Therefore, the specimens are packed and sealed in a damp proof bag or kept in a nitrogen-filled cabinet to minimize the environmental effect. However, the simulation method can isolate this kind of environment effect totally.

The simulation model can be further developed to implement more complicated evaluation work of FOWLP strength. There is one proposed future plan. We can apply reliability tests to the simulation model before the 3PB test. The aim of

this plan is to evaluate the FOWLP strength after long-term reliability tests. The potential reliability tests are the temperature cycling test, high temperature storage test and unbiased highly accelerated stress test. All of these reliability tests require a long time to complete. For example, the normal HTS test time is 1000 hours, which equals to 42 days approximately. However, the long-term reliability test can be implemented through the simulation method in a few hours.

5.2.3 STUDY THE EFFECT OF MESH ELEMENT SIZE

In this section, we are going to study the effect of mesh element size on the simulation results. The mesh method is critical. There are two mesh methods applied. For the 3PB fixture rollers, the round edges of roller are divided into ten divisions by the edge sizing method. For the FOWLP specimen, all the vertical direction edges of FOWLP specimen are divided into four layers by the edge sizing method again. The body surface of FOWLP specimen is meshed by the body sizing method with the 0.5 mm element size. We only modify the element size of specimen body surface in this study.

We use the simulation model of specimen A-1 in this work. The default element size of specimen A-1 simulation model is 0.5 mm, and the simulation result matches with the experiment result very well at this element size. We add and test six more element size – 0.15 mm, 0.2 mm, 0.3 mm, 0.4 mm, 0.7 mm and 1 mm. Table 5-5 lists the summary of node number, element number and elapsed time of simulation model. The elapsed time of simulation model is proportional to its node number and

element number. The larger the node number and the element number, the longer the elapsed time.

Table 5-5 Summary of node number, element number and elapsed time of simulation models.

Model ID	Element size (mm)	Node number	Element number	Elapsed time (Second)
1	0.15	153337	95079	18962
2	0.20	80571	48465	15134
3	0.30	30197	15847	4310
4	0.40	22229	11991	3400
5	0.50	16365	8289	3204
6	0.70	12592	6338	2234
7	1.00	10702	5368	1759

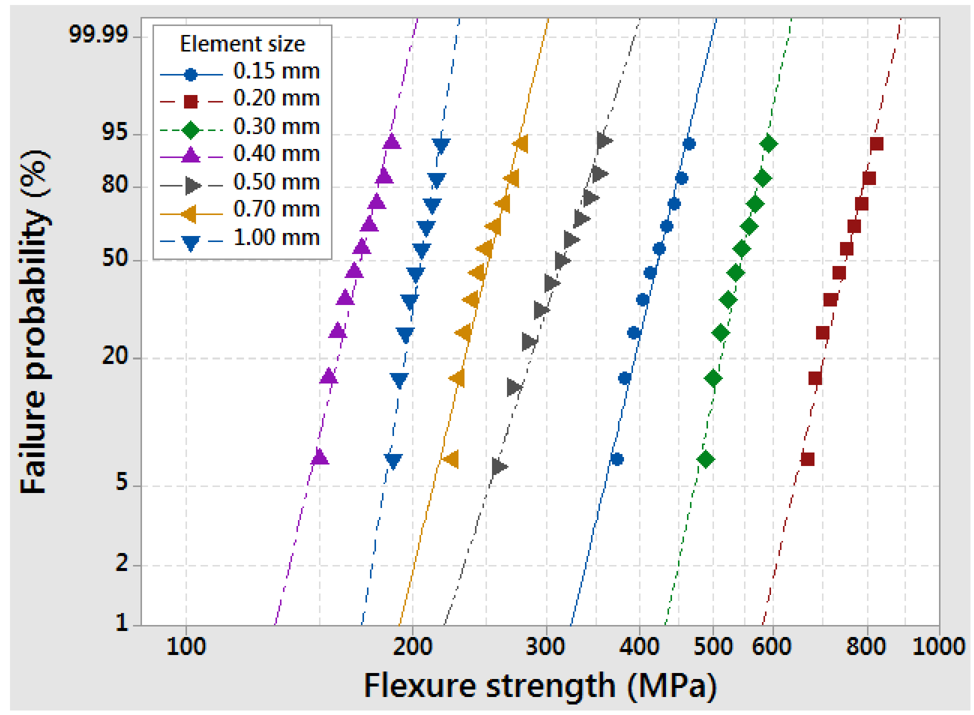

Figure 5-14 Comparison of two-parameter Weibull distribution among simulation models with different element sizes.

Figure 5-14 shows the comparison of two-parameter Weibull distribution among simulation models with different element sizes. The curve of model 5 (0.5 mm element size) is the benchmark curve. The models with smaller element size than 0.5 mm deviate too much to the benchmark curve. However, the curve of model 1 (0.15 mm element size) has a trend of regression to the benchmark curve. The curve of simulation model with less than 0.15 mm element size may match with the benchmark curve again. The elapsed time of model 1 is 18962 seconds, which equals to five and a half hours approximately. The elapsed time should increase exponentially if we further reduce the simulation model element size. Therefore, the simulation model (specimen A-1) with 0.5 mm element size shows a good balance between the result and the elapsed time.

5.3 EVALUATION OF PROPOSED FOWLP STRENGTH BY NUMERICAL METHOD

In the previous evaluation work of FOWLP strength by the experimental method, we find the strength of over-molded structure FOWLP is superior. Therefore, we propose a new FOWLP. However, the strength of this proposed FOWLP is not evaluated by the experimental method. In this section, we are going to use the finite element method to evaluate the FOWLP strength. The aim of this work is to prove the strength of our proposed FOWLP is superior.

5.3.1 DESIGN OF PROPOSED FOWLP

Chapter 4 introduces the evaluation of FOWLP strength by the experimental method. The main findings are:

1. The backside condition of FOWLP affects the FOWLP flexure strength distribution.

The performance of flexure strength distribution of over-molded structure FOWLP is superior. The flexure strength distribution of FOWLP drops significantly once the backside of silicon die is exposed. The BSP tape may reduce the flexure strength distribution. Therefore, the silicon die is sensitive to the wafer grinding process, and the wafer grinding process generates defects on the silicon surface easily.

2. The wafer grinding process affects the FOWLP flexure strength.

The performance of flexure strength of over-molded structure FOWLP with the fine grinding process is superior. The wafer grinding process still has the effect on the mold wafer. However, the EMC is not as sensitive as the silicon to the wafer grinding process. The flexure strength and flexure strength distribution of over-molded structure FOWLP do not change significantly after the wafer grinding process.

3. The thermal process affects the FOWLP flexure strength.

The performance of over-molded structure FOWLP stability is superior. The flexure strength of over-molded structure FOWLP never drops after the thermal process or the thermal test. However, the flexure strength of die-exposed structure FOWLP and BSP tape protected structure FOWLP drops after the long-term thermal test. The phenomenon of decreasing of flexure strength is not only due to the

FOWLP structure, and the EMC also has the effect on it. EMC-2 is the best molding material in this work. The reason is the high glass transition and high flexure modulus of EMC-2.

4. The package geometry affects the FOWLP flexure strength.

The performance of flexure strength of FOWLP with the small silicon die is superior. The reason is the shifting of bending neutral surface. The neutral surface should exist in a bending object, and it always parallels to the upper and lower surfaces of specimen. The bending stress varies linearly with the distance from the neutral surface. Therefore, the maximum stress must appear on the upper and lower surfaces of specimen. The EMC volume increases if the silicon die volume decreases with the same package size. The neutral surface shifts down once the silicon die volume decreases. Therefore, the tension stress on the lower surface of silicon die reduces and the FOWLP strength increases.

In summary, the over-molded structure FOWLP shows the best performance of flexure strength and flexure strength distribution. Therefore, we propose a new over-molded structure FOWLP to prove our findings.

The new FOWLP specimen has the over-molded structure, and it contains silicon die, EMC and PSV layer. The package size and silicon die size of proposed FOWLP are similar to group A and group B specimens in Chapter 4. The package size is 8.09 mm × 8.09 mm, and the silicon die size is 5.11 mm × 5.11 mm. The assembly process of this new specimen is different. Figure 5-15 shows the new specimen assembly process flow.

Figure 5-15 The assembly process flow of proposed new FOWLP specimen.

The new specimen is molded to the thickness of 260 μm at status 1. However, the silicon die thickness of new specimen is thinner than the previous specimens. The silicon die thickness of new specimen is only 150 μm, which is far thinner than the thickness of normal specimen 370 μm. The new specimen is lithographed a 10 μm thick PSV layer at status 2. The new specimen is ground to the thickness of 210 μm at status 3. Therefore, the thickness of over-molded EMC layer is 50 μm

The new specimen can be transformed to a homogeneous specimen by the technique of transformed section. The new length of transformed section

$$L_{new} = L_{original} \times n \tag{5.2}$$

$$n = \frac{E'}{E_{base}} \tag{5.3}$$

where E is Young's modulus of material.

We used the material properties in Table 5-1. The base material is EMC, and the rest materials are transformed to the EMC. The new length of transformed material is

$$L_{silicon\ die} = 5.11 \times \frac{131}{23} = 29.105\ mm \tag{5.4}$$

$$L_{PSV\ layer} = 8.09 \times \frac{2}{23} = 0.703\ mm \tag{5.5}$$

$$L_{BSP\ tape} = 8.09 \times \frac{6.2}{23} = 2.181\ mm \tag{5.6}$$

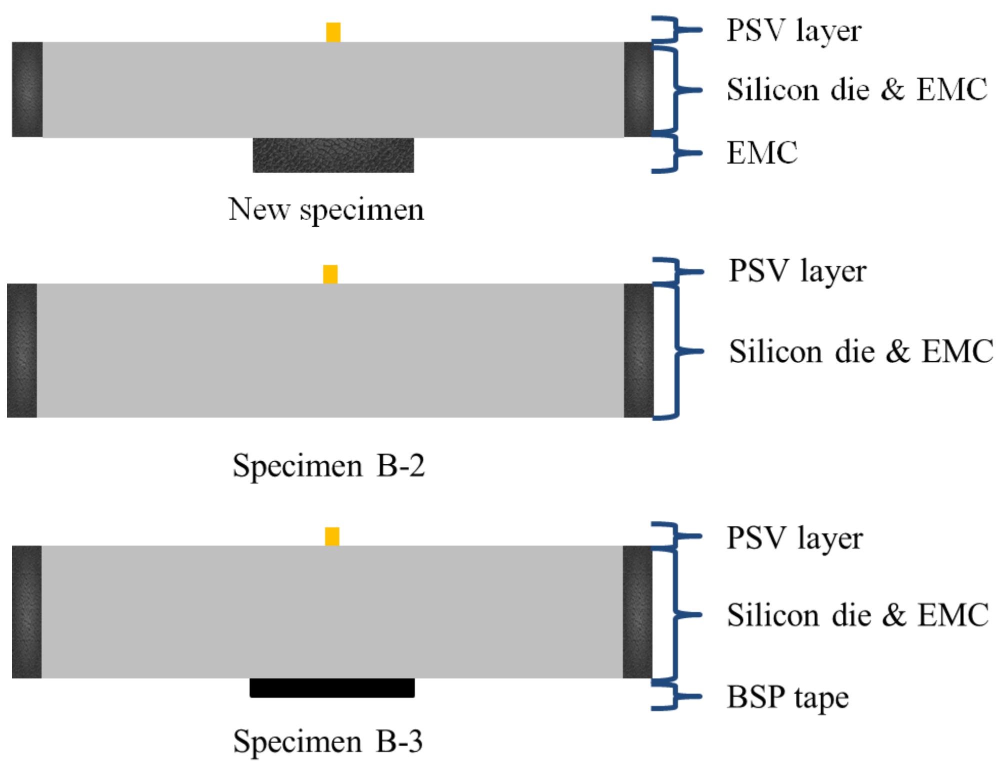

Figure 5-16 Transformed section of proposed new specimen, specimen B-2 and specimen B-3.

.

Table 5-6 Calculation process of neutral surface of proposed new specimen.

Section	Area (mm^2)	y (mm)	yA (mm^3)
PSV layer	0.00703	0.205	0.001441
Si+EMC	4.81275	0.125	0.601594
EMC	0.4045	0.025	0.010113
Total	5.22428		0.613147

Figure 5-16 shows the transformed section of new specimen, specimen B-2 and specimen B-3. Table 5-6 lists the calculation process of neutral surface of proposed new specimen. Therefore, the neutral surface location of new specimen is

$$Y_{new} = 0.613147 \div 5.22428 = 0.117365 \approx 0.117\ mm \qquad (5.7)$$

and the neutral surface location of specimen B-2 and specimen B-3 can be calculated by the same method, and they are

$$Y_{B-2} \approx 0.1\ mm \qquad (5.8)$$

$$Y_{B-3} \approx 0.124\ mm \qquad (5.9)$$

The upper surface (loading surface) of specimen suffers the compression stress, while the lower surface of specimen suffers the tension stress in the bending test. Silicon is the sensitive and brittle material, and its fracture is due to the tension stress rather the compression stress. Therefore, the fracture always appears on the opposite side of loading force. The bending stress varies linearly with the distance from the neutral surface. Therefore, the maximum stress must appear on the upper and lower surfaces of specimen.

Table 5-7 Distances between the FOWLP specimen neutral surface and the lower surface of silicon die.

	Neutral surface, Y (mm)	Lower surface of silicon die, d (mm)	Y-d (mm)
New specimen	0.117	0.05	0.067
Specimen B-2	0.1	0	0.1
Specimen B-3	0.124	0.025	0.099

Table 5-7 lists the distance between the specimen neutral surface and the lower surface of silicon die. The new specimen shows the minimum distance between the specimen neutral surface and the lower surface of silicon die. Therefore, the lower surface of silicon die of new specimen should suffer the minimum tension stress among the three specimens, and the flexure strength of new specimen should be the highest. Figure 5-17 shows the stress distribution of proposed new specimen, specimen B-2 and specimen B-3.

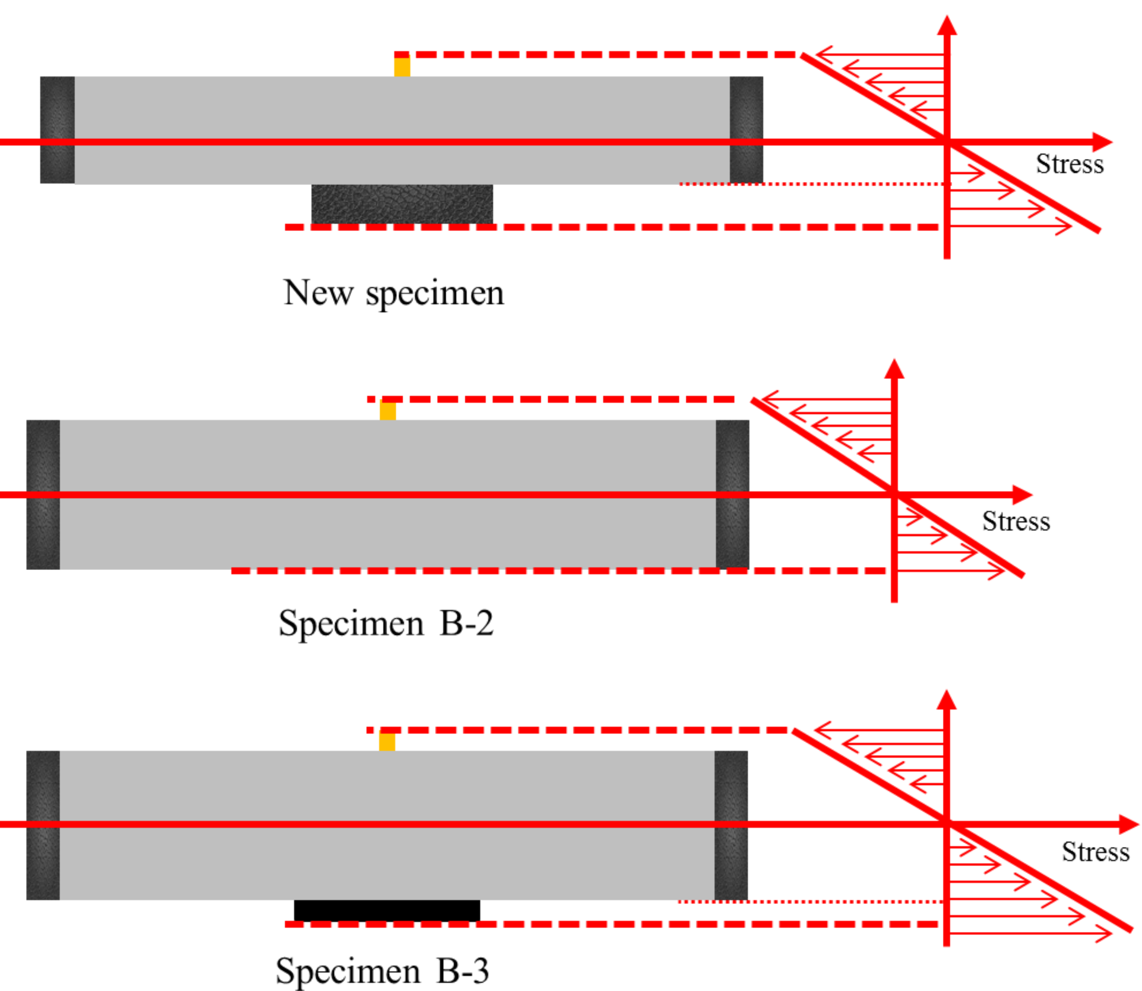

Figure 5-17 Stress distribution of proposed new specimen, specimen B-2 and specimen B-3.

The neutral surface can be further close to the lower surface of silicon die if we reduce the silicon die thickness or increase the EMC thickness. According to the theory of neutral surface, the neutral surface and lower surface of silicon die can coincide once the thickness of silicon die is 60 μm. However, the stability of assembly process may be affected if we grind the silicon die to a thin level.

5.3.2 SIMULATION CONDITIONS

There are three kinds of material – silicon die, EMC and PSV layer in the simulation model of proposed new FOWLP (as shown in Figure 5-18). The node number and element number of new specimen are 17200 and 8847.

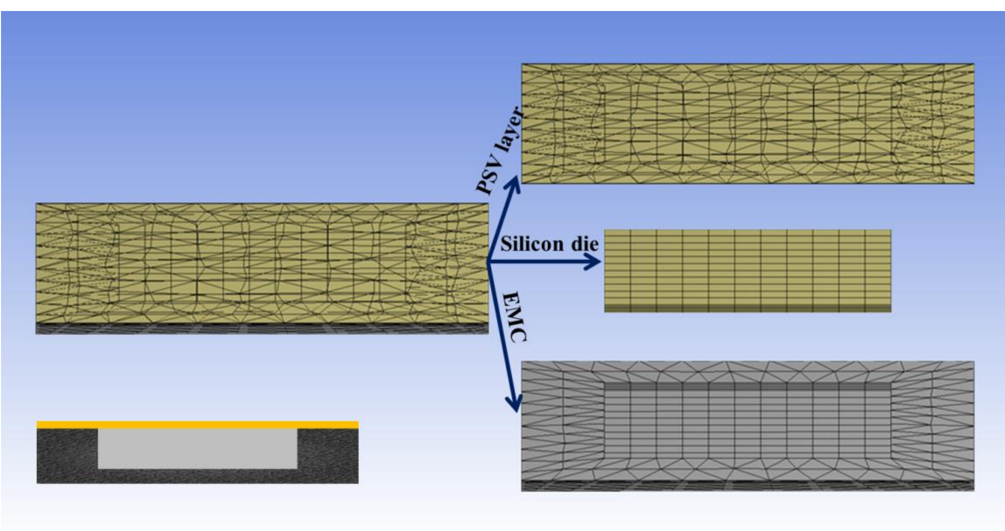

Figure 5-18 The simulation model of proposed new FOWLP.

The simulation model is still solved by the displacement method. Specimen B-2 and specimen B-3 are used to make the strength comparison. However, there is not any experiment data (extension) to refer to this new specimen. We choose the

experiment data of specimen B-2. The reason is the final thicknesses of both specimens are the same, and specimen B-2 shows the widest extension range among all the specimens. The extension range of specimen B-2 is between 0.190 mm and 0.323 mm. The strength of new specimen is really superior if the flexure strength of new specimen is higher than the flexure strength of specimen B-2 and specimen B-3 at the extension range of specimen B-2. We take about 30 sampling points in this effective extension range, and the maximum principal stress (flexure strength) is recorded.

5.3.3 SIMULATION RESULT AND DISCUSSION

The maximum principal stress of new specimen, specimen B-2 and specimen B-3 is processed and represented by the two-parameter Weibull distribution. We use Minitab software to plot the two-parameter Weibull distribution graph. The scale parameter and shape parameter of two-parameter Weibull distribution are solved by the maximum likelihood estimation method automatically in Minitab. The scale parameter and shape parameter of new specimen are 348.251 and 5.043.

Figure 5-19 shows the comparison of two-parameter Weibull distribution among specimen B-2, specimen B-3 and the proposed new specimen. The curve of new specimen is far ahead of specimen B-2 and specimen B-3. The flexure strength of new specimen is always higher than that of specimen B-2 and specimen B-3 with the same failure probability. Although the thicknesses of these three specimens are almost the same, the flexure strength of new specimen is 40% higher than the flexure strength of specimen B-2 and specimen B-3.

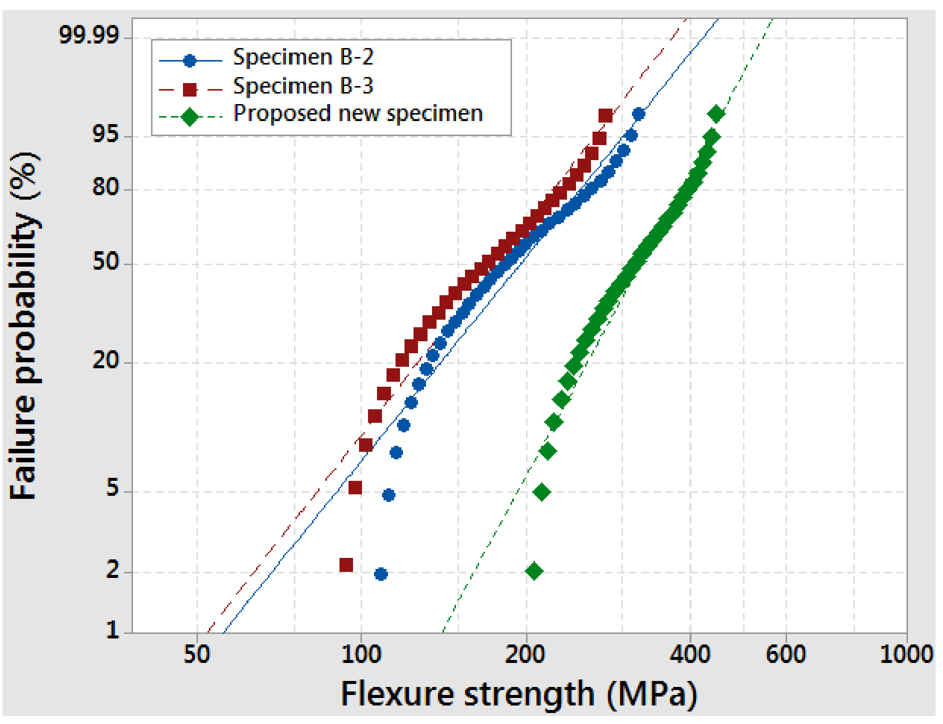

Figure 5-19 Comparison of two-parameter Weibull distribution among specimen B-2, specimen B-3 and the proposed new specimen.

The new FOWLP specimen has shown its superior to other structure FOWLPs with the same thickness. The assembly process of new specimen only has a minor modification to the current process, and there is not any special or new process added. For example, we build a FOWLP specimen with the final thickness of 210 μm (200 μm thick body and 10 μm thick PSV layer plus RDL), and the thickness of over-molded layer is fixed at 50 μm. The incoming silicon wafer should be ground to the thickness of 150 μm. The silicon wafer thickness is much thinner than the usual silicon wafer thickness. The new assembly process only grinds the silicon wafer one time in order to reduce the effect of wafer grinding process on the silicon strength. However, the mold wafer still needs to be ground, and the molding process cannot implement the molding thickness of 200 μm directly. The reason is the size of EMC filler is about 75 μm. If we intend to mold the wafer to the thickness of 200 μm, the

surface of mold wafer becomes bumpy and rough. The safe molding thickness is at least 110 μm thicker than the thickness of artificial wafer. Therefore, the target molding thickness should be around 360 μm for this new specimen. The wafer grinding process needs to remove the redundant EMC after lithographing PSV layers and RDLs. However, the silicon die is never exposed. The new specimen is also not required the BSP tape and thus the cost is saved.

The assembly process of new specimen needs attention to the silicon wafer grinding process. The wafer grinding process quality is critical because the silicon die of new specimen is very thin. The improper selections of grinding parameters and grinding wheels lead to the silicon wafer crack. The pick and place process also may break the silicon die during the die ejection process. Therefore, the poly grind process may be needed to ensure the quality of silicon wafer surface.

In this work, we use the finite element method to evaluate the strength of proposed FOWLP. The simulation method can save much cost and time to evaluate the FOWLP strength compared with the experimental method. A small modification of specimen dimension or thickness could lead to several days or weeks to rebuild the new specimens. However, the specimen modification is a trivial matter by the simulation software. Hence we can save much cost of material and workforce.

There is an issue when we apply the displacement method to solve new simulation models. The effective displacement range is uncertain. In this work, the displacement range can refer to the experiment results. We borrow the extension range of specimen B-2 to evaluate the strength of new specimen. The reason is both specimens have the same thickness, and they are competitors with each other.

However, we do not have any reference when we evaluate a new set of specimen. This problem should be considered in the future.

5.4 SUMMARY

ANSYS software is used to implement the numerical study of FOWLP strength. The ANSYS static structural toolbox is used to create the simulation models and explore solutions. There are two different mesh methods applied. The 3PB fixture rollers are meshed with the edge sizing method. The specimen body surface is meshed with the body sizing method. The movement of 3PB roller is controlled by the displacement method. The maximum principal stress of simulation model is processed by the two-parameter Weibull distribution and plotted by Minitab.

The comparison between experiment results and simulation results shows that the experiment curves and simulation curves match each other in the upper region of failure probability closely. However, the simulation curves sometimes overestimate the FOWLP failure probability in the lower region of failure probability compared with the experiment curves. However, the outcome of applying ANSYS simulation software to evaluate the FOWLP strength is ideal and satisfactory. The current simulation models have the potential to replace the experimental method to implement the evaluation work of FOWLP strength. The simulation method has the advantages of stability, minimal environment effect and saving workforce and time.

The simulation model also can be further developed to implement the more complicated evaluation work of FOWLP strength.

We propose a new FOWLP and this FOWLP has the over-molded structure. We only use the simulation method to evaluate the strength of this new FOWLP specimen. The proposed FOWLP size is 8.09 mm × 8.09 mm and its die size is 5.11 mm × 5.11 mm. The thicknesses of silicon die and package are 150 μm and 210 μm respectively. Hence the thickness of over-molded layer is 50 μm.

The simulation result shows that the flexure strength of proposed FOWLP is higher than the flexure strength of other FOWLP specimens with the same thickness. The reason is the shifting of bending neutral surface. The proposed FOWLP has the minimum distance between the neutral surface and the lower surface of silicon die compared with other specimens. Therefore, the lower surface of silicon die of proposed FOWLP suffers the minimum tension stress in the 3PB test and thus the flexure strength of proposed specimen is high. The assembly process of proposed specimen only has a minor modification to the current process, and there are not any special or new processes added. However, the assembly process of proposed specimen needs attention to the silicon wafer grinding process. The grinding process quality is critical because the silicon die of new specimen is very tiny. There is an issue when we apply displacement method to evaluate new simulation models. The effective displacement range is uncertain. This problem should be considered in the future work.

CHAPTER 6 DEVELOPMENT OF THEORETICAL MODEL OF FOWLP STRENGTH

6.1 THEORETICAL MODEL OF FOWLP STRENGTH

6.1.1 WEIBULL DISTRIBUTION

Weibull distribution is widely used to describe the strength of brittle material such as ceramics and silicon. There are two kinds of Weibull distribution – two-parameter Weibull distribution and three-parameter Weibull distribution. The two-parameter Weibull distribution can be expressed as [132, 133]

$$P = 1 - exp\left[-\left(\frac{\sigma}{\sigma_0}\right)^m\right] \quad (6.1)$$

where σ is the flexure strength of specimen, σ_0 is the scale parameter and m is the shape parameter or Weibull modulus. The two-parameter Weibull distribution has been proved that it is an effective method to describe the strength.

The failure probability list should be established to solve the scale parameter and shape parameter of equation (6.1). The most widely used failure probability estimation equation is [143]

$$P_i = \frac{i - 0.3}{n + 0.4} \tag{6.2}$$

where i is the ith sample flexure strength (in the ascending order) and n is the sample size.

The scale parameter and shape parameter can be solved by two different estimation methods – least square estimation (LSE) method and maximum likelihood estimation (MLE) method. The least square estimation method takes the logarithm on the two-parameter Weibull distribution equation (6.1) twice and thus we have

$$1 - P = exp\left[-\left(\frac{\sigma}{\sigma_0}\right)^m\right]$$

$$\ln(1 - P) = -\left(\frac{\sigma}{\sigma_0}\right)^m$$

$$\ln\ln\left(\frac{1}{1 - P}\right) = \ln\left(\frac{\sigma}{\sigma_0}\right)^m$$

$$\ln\ln\left(\frac{1}{1 - P}\right) = m\ln\sigma - m\ln\sigma_0$$

$$\ln\ln\left(\frac{1}{1 - P}\right) = \ln\left(\frac{1}{\sigma_0}\right)^m + m\ln\sigma \tag{6.3}$$

According to the equation

$$Y = a + bX \tag{6.4}$$

we can define

$$Y = \ln\ln\left(\frac{1}{1 - P}\right) \tag{6.5}$$

$$X = \ln \sigma \tag{6.6}$$

$$a = \ln\left(\frac{1}{\sigma_0}\right)^m = -m \ln \sigma_0 \tag{6.7}$$

$$b = m \tag{6.8}$$

Therefore, the scale parameter and shape parameter are [144]

$$m = \frac{N \sum_{i=1}^{N} x_i y_i - \sum_{i=1}^{N} x_i \sum_{i=1}^{N} y_i}{N \sum_{i=1}^{N} x_i^2 - \sum_{i=1}^{N} x_i \sum_{i=1}^{N} x_i} \tag{6.9}$$

$$\ln \sigma_0 = -\frac{1}{m} \frac{\sum_{i=1}^{N} y_i \sum_{i=1}^{N} x_i^2 - \sum_{i=1}^{N} x_i \sum_{i=1}^{N} x_i y_i}{N \sum_{i=1}^{N} x_i^2 - \sum_{i=1}^{N} x_i \sum_{i=1}^{N} x_i} \tag{6.10}$$

where x_i and y_i are the value of ith $\ln \sigma$ and the value of ith $\ln \ln\left(\frac{1}{1-P}\right)$ respectively.

The least square estimation method is quite straightforward, and it can be solved manually without computer assistance compared with the maximum likelihood estimation method. The maximum likelihood estimation method takes the derivative and logarithm on the two-parameter Weibull distribution equation (6.1) and thus we have

$$P' = \frac{m}{\sigma_0}\left(\frac{\sigma}{\sigma_0}\right)^{m-1} exp\left[-\left(\frac{\sigma}{\sigma_0}\right)^m\right] \tag{6.11}$$

$$\ln P' = N \ln(m) - Nm \ln(\sigma_0) + (m-1) \sum \ln \sigma - \sum \left(\frac{\sigma}{\sigma_0}\right)^m \tag{6.12}$$

To derive equation (6.12) with respect to σ_0 and m respectively, and let the derivative equation equals to zero. Therefore, the scale parameter and shape parameter are

$$\sigma_0 = \left(\frac{1}{N}\sum_{i=1}^{N}\sigma_i^m\right)^{\frac{1}{m}} \tag{6.13}$$

$$\frac{N}{m} + \sum_{i=1}^{N}\ln\sigma_i - N\frac{\sum_{i=1}^{N}\sigma_i^m \ln\sigma_i}{\sum_{i=1}^{N}\sigma_i^m} = 0 \tag{6.14}$$

The shape parameter (m) needs the assistance of computer to be solved, and it cannot be solved manually. However, σ_0 is quite easy to be solved once we have the value of m.

The graph of Weibull distribution plot highly depends on the specimen geometry and evaluation method. The specimen geometry includes the specimen shape, volume and dimension. The evaluation method includes 3PB test, 4PB test, BOR test and ball breaker test. The flexure strength of specimen is different by different evaluation methods. For example, the silicon flexure strength of 4PB test must be lower than the silicon flexure strength of 3PB test. In practical, the loading area of 4PB test is much larger than the loading area of 3PB test. In theory, the tensile stress region of 4PB test is much wider than that of 3PB test.

Weibull proposed three fundamental properties [185] about using Weibull distribution to describe the strength of brittle material. These rules provide the guideline when we propose our FOWLP strength model.

1. A brittle material is statistically homogeneous and isotropic.
2. Subvolume and subsurface of a specimen are statistically independent.
3. Subvolume and subsurface of a specimen follow the weakest line concept.

6.1.2 ANALYTICAL MODEL FORMULATION

A classical approach was proposed by Behnken et al. [186] to describe the silicon wafer strength. This approach relates the silicon wafer strength to its volume. The failure probability for a wafer is given by [186]

$$P_v(\sigma) = exp\left[-\int_V \left(\frac{\sigma - \gamma V}{\alpha_V}\right)^{\omega V} dV\right] \quad (6.15)$$

where γV is the location parameter, α_V is the scale parameter and ωV is the shape parameter. This approach describes that the defects of specimen are distributed randomly in a wafer. That means the number of defects is proportional to the wafer volume. Therefore, this approach only considers the effect of defects especially the defects inside the specimen body on the specimen strength.

Except for the weak planes of silicon crystal lattice, the silicon die surface defects and silicon die edge defects are considered as the main effect factors on the silicon die strength. Therefore, the silicon strength model should consider the surface defects and edges defects except for the body defects. However, the number of surface defects should be proportional to the area of wafer surface (A), and the number of edge defects should be proportional to the edge length (L). Therefore, the final failure probability for a wafer should be

$$P(\sigma) = P_V(\sigma) \cdot P_A(\sigma) \cdot P_L(\sigma) \quad (6.16)$$

The critical effect factors of FOWLP strength are quite different from the silicon die. There are three representative FOWLP structures, and they are over-molded structure, BSP tape protected structure and die-exposed structure. The silicon

die backside of over-molded structure FOWLP is encapsulated by the EMC. The silicon die backside of BSP tape protected structure FOWLP is laminated with the BSP tape. The silicon die backside of die-exposed structure FOWLP is exposed. However, the fracture analysis results of FOWLP show that the initial fracture point only expands from the silicon die surface or silicon die edge. Therefore, the initial fracture point locates inside the FOWLP (over-molded structure FOWLP and BSP tape protected structure FOWLP), while the initial fracture point locates on the surface of die-exposed structure FOWLP.

Therefore, two theoretical models of FOWLP strength are proposed

$$P_V = 1 - exp\left[-\iiint\limits_V \left(\frac{\sigma}{\sigma_0}\right)^m dV\right] \tag{6.17}$$

$$P_S = 1 - exp\left[-\iint\limits_A \left(\frac{\sigma}{\sigma_0}\right)^m dA\right] \tag{6.18}$$

where σ is the flexure strength, σ_0 is the scale parameter, m is the shape parameter or Weibull modulus, V is the specimen volume and A is the area of specimen surface.

Equation (6.17) and equation (6.18) is based on the two-parameter Weibull distribution, and they are used to describe the strength of FOWLP with different initial fracture points. Equation (6.17) is used to describe the strength of over-molded structure FOWLP and BSP tape protected structure FOWLP. It is because the initial fracture point locates inside the FOWLP. Equation (6.18) is used to describe the strength of die-exposed structure FOWLP. It is because the initial fracture point locates on the surface of FOWLP.

6.1.3 DERIVATION OF GOVERNING EQUATION

The FOWLP surface is square, and the cross section of FOWLP is rectangular. The FOWLP strength is evaluated by the 3PB test method. We need to introduce the stress-density function to assist in solving the FOWLP strength models. The stress-density function is first introduced by Nadler et al. [185]. This function is used to simplify the integral process. The FOWLP strength models can be expressed as

$$P_V = 1 - exp\left[-\frac{V}{V_0}\left(\frac{\sigma}{\sigma_0}\right)^m \int_{s_{min}}^{1} s^m f(s)ds\right] \tag{6.19}$$

$$P_S = 1 - exp\left[-\frac{A}{A_0}\left(\frac{\sigma}{\sigma_0}\right)^m \int_{s_{min}}^{1} s^m g(s)ds\right] \tag{6.20}$$

$$s_{min} = \frac{\sigma_{min}}{\sigma} \tag{6.21}$$

where σ_{min} is the smallest stress in the specimen and it may or may not be equal to zero. σ is the flexure strength of specimen. V_0 is the specimen volume and V is the specimen volume under the loading force. A_0 is the specimen surface area and A is the specimen surface area under the loading force. The stress-density functions f(s) and g(s) can be obtained from the following equations [185]

$$\int_{s_{min}}^{1} f(s)ds = \frac{V(s)}{V} \;=>\; f(s) = -\frac{d}{ds}\frac{V(s)}{V} \tag{6.22}$$

$$\int_{s_{min}}^{1} g(s)ds = \frac{A(s)}{A} \;=>\; g(s) = -\frac{d}{ds}\frac{A(s)}{A} \tag{6.23}$$

The specimen geometry and evaluation method should be clear before solving the FOWLP strength models. The governed stress-density functions for the three-point bending test with the rectangular cross section specimen are [185]

$$f(s) = -\frac{1}{2}\ln s \tag{6.24}$$

$$g(s) = \frac{1}{4}(1 - \ln s) \tag{6.25}$$

The superiority of stress-density function is obvious. It can reduce the complex two and three times integral function to the one time integral function. Therefore, equation (6.19) and equation (6.20) can be expressed as

$$P_V = 1 - exp\left[-\frac{V}{V_0}\left(\frac{\sigma}{\sigma_0}\right)^m \int_{s_{min}}^{1} s^m \left(-\frac{1}{2}\ln s\right) ds\right] \tag{6.26}$$

$$P_S = 1 - exp\left[-\frac{A}{A_0}\left(\frac{\sigma}{\sigma_0}\right)^m \int_{s_{min}}^{1} s^m \frac{1}{4}(1 - \ln s) ds\right] \tag{6.27}$$

The integral function can be solved by the technique of integration by parts. For example, we have the following integral function in equation (6.26)

$$\int_{s_{min}}^{1} s^m \ln s \, ds \tag{6.28}$$

and thus we can define u, du, dv and v as

$$u = \ln s, du = \frac{1}{s}dx, dv = s^m, v = \frac{1}{m+1}s^{m+1} \tag{6.29}$$

According to the integration by parts formula, we have

$$uv - \int vdu = \frac{\ln(s)\, s^{m+1}}{m+1} - \int \frac{s^m}{m+1} ds$$
$$= \left[\frac{\ln(s)\, s^{m+1}}{m+1} - s^{m+1}\right]_{s_{min}}^{1} \tag{6.30}$$

Equation (6.27) can be solved in the same way

$$\int_{s_{min}}^{1} s^m (1 - \ln s) ds = \int_{s_{min}}^{1} s^m ds - \int_{s_{min}}^{1} s^m \ln s \, ds$$
$$= \left[\frac{s^{m+1}(m - \ln s + 2)}{m+1}\right]_{s_{min}}^{1} \tag{6.31}$$

Therefore, equation (6.26) and equation (6.27) can be expressed as

$$P_V = 1 - exp\left\{\left[\frac{\sigma}{\sigma_0}\right]^m \cdot \frac{V}{2V_0}\left[\frac{\ln(s)\, s^{m+1}}{m+1} - s^{m+1}\right]_{s_{min}}^{1}\right\} \tag{6.32}$$

$$P_S = 1 - exp\left\{\left[\frac{\sigma}{\sigma_0}\right]^m \cdot \frac{-A}{4A_0}\left[\frac{s^{m+1}(m - \ln s + 2)}{m+1}\right]_{s_{min}}^{1}\right\} \tag{6.33}$$

For the integral part of equation (6.32)

$$\left[\frac{\ln(s)\, s^{m+1}}{m+1} - s^{m+1}\right]_{s_{min}}^{1}$$
$$= \left[\frac{\ln(1)\, 1^{m+1}}{m+1} - 1^{m+1}\right] \tag{6.34}$$
$$- \left[\frac{\ln(s_{min})\, {s_{min}}^{m+1}}{m+1} - {s_{min}}^{m+1}\right]$$

$$s_{min} = \frac{\sigma_{min}}{\sigma} \tag{6.35}$$

where σ_{min} is the smallest stress in the specimen and it may or may not be equal to zero. We assume it closes to zero

$$\sigma_{min} \to 0, s_{min} \to 0 \tag{6.36}$$

$$\lim_{x \to 0} x \ln x = 0 \tag{6.37}$$

and thus equation (6.32) becomes

$$P_V = 1 - exp\left\{\left[\frac{\sigma}{\sigma_0}\right]^m \cdot \frac{V}{2V_0}\left[(0-1) - \left(\frac{0}{m+1} - 0\right)\right]\right\}$$

$$P_V = 1 - exp\left[-\frac{V}{2V_0} \cdot \left(\frac{\sigma}{\sigma_0}\right)^m\right] \tag{6.38}$$

For equation (6.33)

$$P_S = 1 - exp\left\{\left[\frac{\sigma}{\sigma_0}\right]^m \cdot \frac{-A}{4A_0}\left[\left(\frac{1^{m+1}(m - \ln 1 + 2)}{m+1}\right) - \left(\frac{{s_{min}}^{m+1}(m - \ln s_{min} + 2)}{m+1}\right)\right]\right\}$$

$$P_S = 1 - exp\left\{\left[\frac{\sigma}{\sigma_0}\right]^m \cdot \frac{-A}{4A_0}\left[\left(\frac{m+2}{m+1}\right) - \left(\frac{0}{m+1}\right)\right]\right\}$$

$$P_S = 1 - exp\left[-\frac{A}{4A_0}\left(\frac{m+2}{m+1}\right) \cdot \left(\frac{\sigma}{\sigma_0}\right)^m\right] \tag{6.39}$$

We introduce a new symbol Δ to simplify equation (6.38) and equation (6.39), and let P_U represent both of them

$$P_U = 1 - exp\left[-\Delta \cdot \left(\frac{\sigma}{\sigma_0}\right)^m\right] \tag{6.40}$$

$$\Delta_V = \frac{V}{2V_0} \tag{6.41}$$

$$\Delta_S = \frac{A}{4A_0}\left(\frac{m+2}{m+1}\right) \tag{6.42}$$

where V_0 is the specimen volume and V is the specimen volume under the loading force. A_0 is the specimen surface area and A is the specimen surface area under the loading force. Figure 6-1 shows the illustration of contact area in the 3PB test.

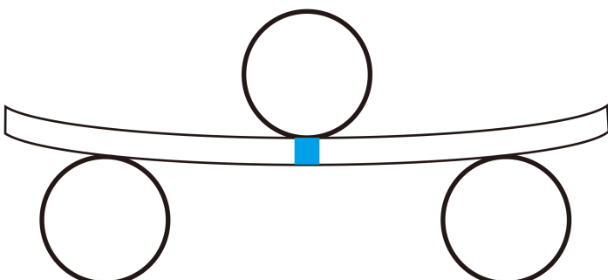

Figure 6-1 Illustration of contact area (dark area) in the 3PB test.

The contact width should equal to the specimen width since the 3PB loading roller is wider than the specimen width. Therefore, we have

$$\frac{V}{V_0} = \frac{contact\ length\ \times contact\ width\ \times speicmen\ height}{specimen\ length\ \times speicmen\ width\ \times specimen\ height} = \frac{contact\ length}{specimen\ length} \quad (6.43)$$

$$\frac{A}{A_0} = \frac{contact\ length\ \times contact\ width}{specimen\ length\ \times speicmen\ width} = \frac{contact\ length}{specimen\ length} \quad (6.44)$$

$$\frac{V}{V_0} = \frac{A}{A_0} = \frac{contact\ length}{specimen\ length} \quad (6.45)$$

The specimen length is a known constant in equation (6.45). The only variable is the contact length. There is a contact length expression proposed by Turner et al. [187, 188]

$$l = 2\left[\frac{3rF(1-v^2)}{4E}\right]^{\frac{1}{3}} \quad (6.46)$$

where r is the loading force radius, F is the loading force, v is Poisson's ratio and E is Young's modulus.

We use the least square estimation method to solve equation (6.40) and thus we take logarithm two times to P_U

$$\ln\ln\left(\frac{1}{1-P_U}\right) = \ln\Delta + m\ln\sigma - m\ln\sigma_0$$
$$= \ln\Delta + \ln\left(\frac{1}{\sigma_0}\right)^m + m\ln\sigma \quad (6.47)$$

According to the equation

$$Y = a + bX \quad (6.48)$$

we can define

$$Y = \ln\ln\left(\frac{1}{1-P_U}\right) \quad (6.49)$$

$$X = \ln\sigma \quad (6.50)$$

$$a = \ln\Delta + \ln\left(\frac{1}{\sigma_0}\right)^m = \ln\Delta - m\ln\sigma_0 \quad (6.51)$$

$$b = m \quad (6.52)$$

Therefore, the scale parameter and shape parameter can be solved by the following equations

$$m = \frac{N\sum_{i=1}^{N} x_i y_i - \sum_{i=1}^{N} x_i \sum_{i=1}^{N} y_i}{N\sum_{i=1}^{N} x_i^2 - \sum_{i=1}^{N} x_i \sum_{i=1}^{N} x_i} \quad (6.53)$$

$$\ln\Delta - m\ln\sigma_0 = \frac{\sum_{i=1}^{N} y_i \sum_{i=1}^{N} x_i^2 - \sum_{i=1}^{N} x_i \sum_{i=1}^{N} x_i y_i}{N\sum_{i=1}^{N} x_i^2 - \sum_{i=1}^{N} x_i \sum_{i=1}^{N} x_i} \quad (6.54)$$

.

6.1.4 EXPERIMENTAL AND NUMERICAL RESULT AND DISCUSSION

The FOWLP strength is evaluated by the 3PB test method, and the detailed experimental procedure is introduced in Chapter 4. The experiment results of specimen B-1, specimen B-2 and specimen B-3 are selected to conduct the validation of FOWLP strength model. These three specimens represent the most significant FOWLP structures. The fracture analysis results show that their initial fracture points initiate from the silicon backside. There are the EMC layer and BSP tape on the backside of specimen B-1 and specimen B-3. Hence the fractures initiate from the package interior. The backside of specimen B-2 is exposed. Hence the fracture initiates from the package surface. Therefore, equation (6.38) is applied to specimen B-1 and specimen B-3, while equation (6.39) is applied to specimen B-2. Table 6-1 lists the 3PB test flexure strength and corresponding failure probability of specimen B-1, specimen B-2 and specimen B-3. The failure probability (P) is calculated by equation (6.2) with the sample size 25. X and Y are calculated by equation (6.50) and equation (6.49) respectively.

The diameter of 3PB fixture rollers is 1 mm and thus the radius is 0.5 mm. The Poisson's ratio of FOWLP is assigned as 0.3. The values of fracture load (F) and Young's modulus (E) are obtained from the 3PB test, and we use the average values of fracture load and Young's modulus. Table 6-2 lists the 3PB test average values of fracture load, extension and Young's modulus of specimens.

Table 6-1 3PB test flexure strength and corresponding failure probability of specimen B-1, specimen B-2 and specimen B-3.

S/N	σ_i – Flexure strength (MPa)			P_i – Failure probability
	Specimen B-1	Specimen B-2	Specimen B-3	
1	277.1514	88.1507	64.9827	0.0276
2	354.3285	91.3047	66.9427	0.0669
3	355.0125	92.2489	75.4705	0.1063
4	355.4866	109.1754	93.7374	0.1457
5	368.3728	118.4202	94.1275	0.1850
6	371.5768	126.1142	98.1124	0.2244
7	373.2047	157.8479	105.7749	0.2638
8	379.2433	158.2036	110.5415	0.3031
9	410.2429	204.7127	112.9215	0.3425
10	410.6753	205.8154	120.2677	0.3819
11	412.0786	226.3713	122.9233	0.4213
12	413.9974	229.9639	137.2656	0.4606
13	422.3647	230.5283	144.0967	0.5000
14	422.8719	231.8978	146.6746	0.5394
15	423.6746	241.3738	148.5645	0.5787
16	424.2572	244.5692	166.8696	0.6181
17	427.2951	266.3839	189.8499	0.6575
18	427.4371	267.5748	199.2213	0.6969
19	436.3789	283.7223	241.9175	0.7362
20	436.6841	322.9014	249.0926	0.7756
21	438.6754	326.0324	266.6766	0.8150
22	449.7861	340.6148	268.2423	0.8543
23	456.6889	355.6711	283.4756	0.8937
24	468.3925	373.6718	288.8022	0.9331
25	488.1806	382.3246	306.5253	0.9724
$\sum X_i$ or $\sum Y$	**150.131**	**133.2899**	**124.8297**	**-13.7376**
$\sum X_i^2$	**901.9098**	**715.807**	**628.7724**	
$\sum X_i Y$	**-79.2254**	**-60.3937**	**-55.5142**	

Table 6-2 3PB test average fracture load, extension and Young's modulus of specimen B-1, specimens B-2 and specimens B-3.

3PB results	Specimen B-1	Specimen B-2	Specimen B-3
Fracture load (N)	91.7231	8.9995	8.1473
Extension (mm)	0.2479	0.2712	0.2469
Young's modulus (MPa)	42999.093	60887.761	39664.902

The contact length and volume or surface area ratio of specimen are listed in Table 6-3. The shape parameters and scale parameters of FOWLP strength model are calculated and listed in Table 6-4. Table 6-5 lists the simulation model flexure strength and corresponding failure probability of specimens.

Table 6-3 The contact length and volume ratio or area ratio of specimen.

3PB results	Specimen B-1	Specimen B-2	Specimen B-3
Contact length (mm)	1.7991	0.7390	0.8246
$\frac{V}{V_0} = \frac{A}{A_0}$	0.2224	0.0913	0.1019
Δ_V or Δ_S	0.1112	0.0294	0.0510

Table 6-4 The shape parameters and scale parameters of FOWLP strength models.

Strength model parameters	Specimen B-1	Specimen B-2	Specimen B-3
Shape parameter (m)	9.7015	2.4908	2.3892
Scale parameter (σ_0)	342.2269	62.5508	53.3749

Table 6-5 Simulation model flexure strength and corresponding failure probability of specimen B-1, specimen B-2 and specimen B-3.

S/N	Specimen B-1		Specimen B-2		Specimen B-3	
	Flexure strength (MPa)	Failure probability	Flexure strength (MPa)	Failure probability	Flexure strength (MPa)	Failure probability
1	374.32	0.0203	108.56	0.0198	93.67	0.0216
2	376.97	0.0494	112.04	0.0480	97.52	0.0525
3	379.61	0.0785	115.62	0.0763	101.48	0.0833
4	382.24	0.1076	119.31	0.1045	105.57	0.1142
5	384.81	0.1366	123.10	0.1328	109.77	0.1451
6	387.36	0.1657	127.00	0.1610	114.11	0.1759
7	389.91	0.1948	131.02	0.1893	118.59	0.2068
8	392.44	0.2238	135.14	0.2175	123.20	0.2377
9	394.97	0.2529	139.38	0.2458	127.95	0.2685
10	397.48	0.2820	143.72	0.2740	132.83	0.2994
11	400.00	0.3110	148.19	0.3023	137.86	0.3302
12	402.50	0.3401	152.77	0.3305	143.03	0.3611
13	404.99	0.3692	157.46	0.3588	148.35	0.3920
14	407.48	0.3983	162.28	0.3870	153.80	0.4228
15	409.96	0.4273	167.21	0.4153	159.40	0.4537
16	412.43	0.4564	172.26	0.4435	165.15	0.4846
17	414.90	0.4855	177.43	0.4718	171.05	0.5154
18	417.36	0.5145	182.72	0.5000	177.10	0.5463
19	419.82	0.5436	188.13	0.5282	183.30	0.5772
20	422.26	0.5727	193.67	0.5565	189.65	0.6080
21	424.71	0.6017	199.33	0.5847	196.15	0.6389
22	427.15	0.6308	205.59	0.6130	202.81	0.6698
23	429.58	0.6599	213.12	0.6412	209.63	0.7006
24	432.01	0.6890	221.00	0.6695	216.61	0.7315
25	434.43	0.7180	229.30	0.6977	223.85	0.7623
26	436.85	0.7471	237.79	0.7260	231.37	0.7932
27	439.27	0.7762	246.44	0.7542	239.06	0.8241
28	441.68	0.8052	255.30	0.7825	246.93	0.8549
29	444.09	0.8343	264.38	0.8107	255.00	0.8858
30	446.50	0.8634	273.60	0.8390	263.29	0.9167
31	448.90	0.8924	282.98	0.8672	271.75	0.9475
32	451.30	0.9215	292.47	0.8955	280.39	0.9784
33	453.70	0.9506	302.12	0.9237		
34	456.09	0.9797	311.98	0.9520		
35			321.98	0.9802		

Therefore, the three FOWLP specimen strength models are

$$P_{V,B-1} = 1 - exp\left[-0.1112\left(\frac{\sigma}{342.2269}\right)^{9.7015}\right] \tag{6.55}$$

$$P_{S,B-2} = 1 - exp\left[-0.0294\left(\frac{\sigma}{62.5508}\right)^{2.4908}\right] \tag{6.56}$$

$$P_{V,B-3} = 1 - exp\left[-0.051\left(\frac{\sigma}{53.3749}\right)^{2.3892}\right] \tag{6.57}$$

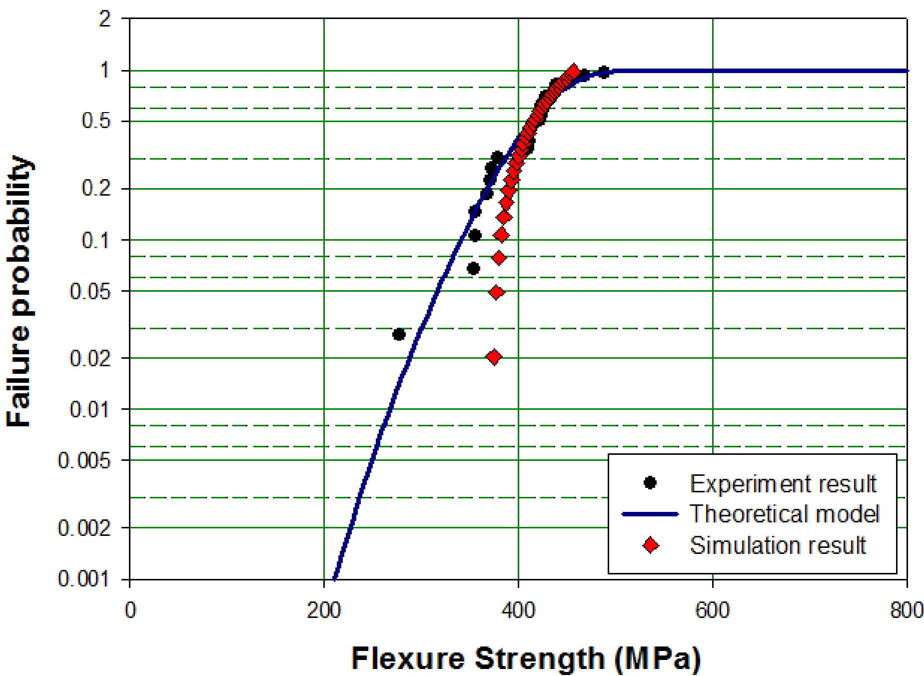

Figure 6-2 Comparison of specimen B-1 strength model with experiment results and simulation results.

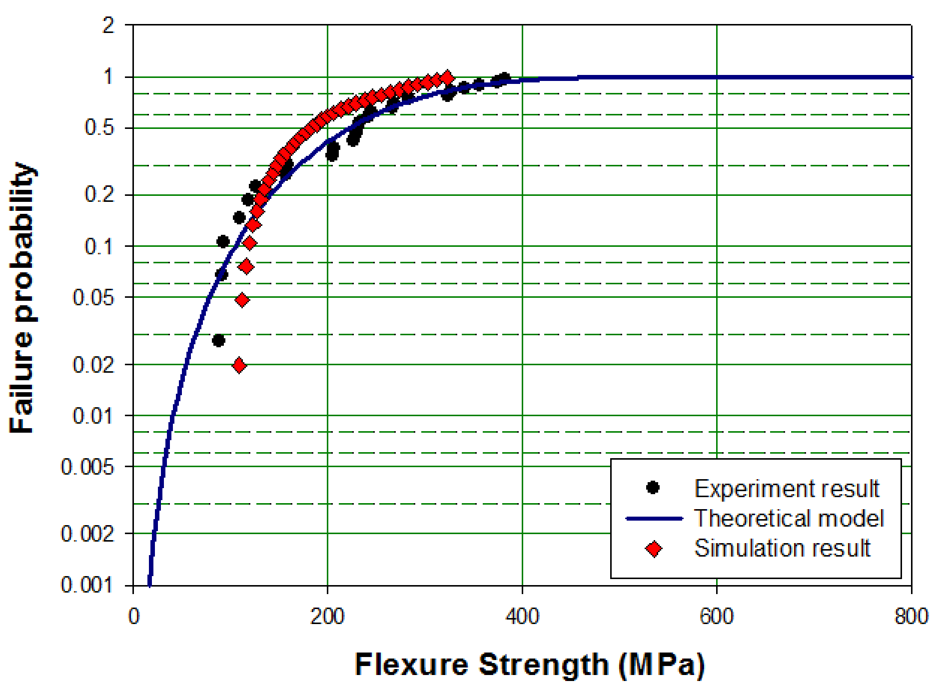

Figure 6-3 Comparison of specimen B-2 strength model with experiment results and simulation results.

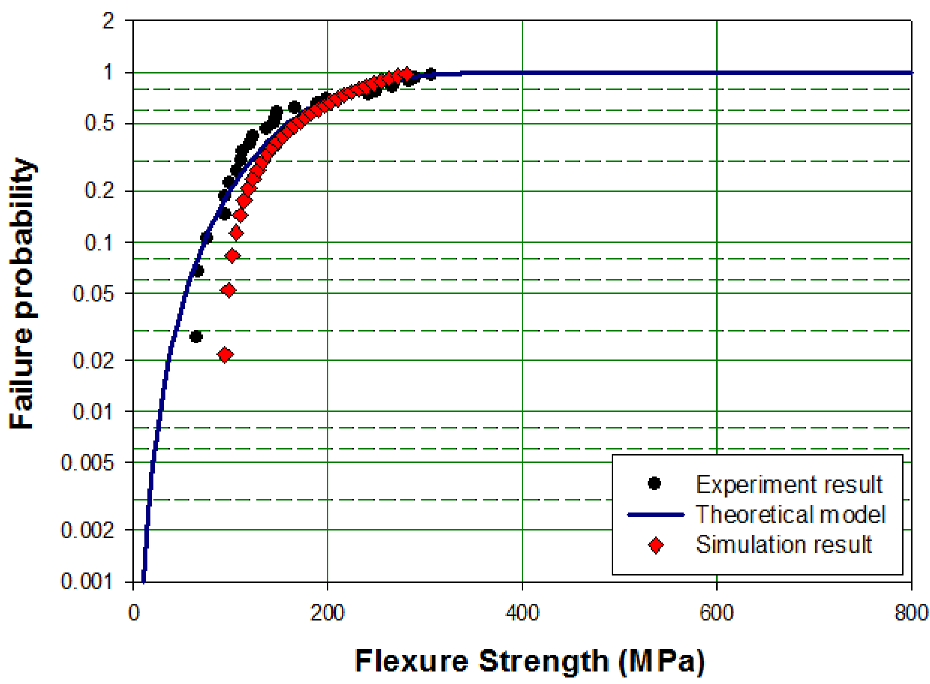

Figure 6-4 Comparison of specimen B-3 strength model with experiment results and simulation results.

Figure 6-2, Figure 6-3 and Figure 6-4 show the comparison of specimen B-1, specimen B-2 and specimen B-3 strength model with experiment results and simulation results. The x-axis represents the specimen flexure strength and the y-axis represents the specimen failure probability. The circle dots represent the experiment result (3PB test flexure strength), while the diamond dots represent the simulation result (simulated 3PB test flexure strength). The curves represent the corresponding specimen strength model.

The differences between specimen experiment results and simulation results are small, and they almost match each other closely. However, all the specimen strength models underestimate their corresponding specimen flexure strength in the lower region of failure probability. The underestimated phenomenon often occurs in the two-parameter Weibull distribution [141, 142]. This is the shortcoming of two-parameter Weibull distribution. The proposed FOWLP strength models are derived from the two-parameter Weibull distribution and thus they also show the underestimated phenomenon more or less. The three-parameter Weibull distribution could minimize the underestimated issue. However, the solving process of three-parameter Weibull distribution is much more complicated than that of two-parameter Weibull distribution. Specimen B-1 strength model underestimates both experiment and simulation results too much in the lower region of failure probability. The reason may be the experiment errors. There is a data point far away from the major stream of data point. This data point should be an experiment error.

The simulation results somewhat overestimate the experiment results in the lower region of failure probability. The reason may be the effect of assembly process is not taken into account in the simulation model. For example, Specimen B-3 has the BSP tape. The lamination process of BSP tape requires the wafer to lie on a hot

chuck table. The lamination roller also has a high temperature. The temperature of chuck table and lamination roller is 90℃. The laminated wafer is required to store in a high temperature oven for two hours, and the oven temperature is 150℃. The high temperature storage process could affect the material properties. However, the above factors are not taken into account in the simulation model of specimen B-3.

6.2 THEORETICAL MODEL OF FOWLP FATIGUE CRACK GROWTH

6.2.1 FOWLP FRACTURE MECHANICS

Fracture mechanics can address the questions about the maximum allowable load for a given material crack length and vice versa. The materials can be classified into two categories – brittle and ductile. The brittle materials do not show plastic deformation, and their crack grows rapidly. The ductile materials show plastic deformation and their crack grows tardiness. The fracture analysis results show that the fracture pattern of FOWLP is brittle and thus we only discuss the fracture mechanics of brittle material in this section.

The very first theory about the fracture mechanics of brittle material is Griffith's criterion. For an infinite plate of unit thickness with a crack length 2a, its surface energy and elastic strain energy are [189]

$$U_s = 2aG, U_e = -\frac{\pi\sigma^2 a^2}{E} k, where\ k = 1 - v^2 \tag{6.58}$$

where k is for the plane strain, and k is for the plane stress when k=1. v is Poisson's ratio. At the critical fracture point, we can obtain the critical strain energy release rate [189]

$$U_s = U_e \tag{6.59}$$

$$G_c = \frac{\pi\sigma^2 a}{E} k \tag{6.60}$$

Griffith's theory only can be applied to brittle materials. Irwin' theory [189] can be applied to both brittle and ductile materials. Irwin's theory takes note of the crack stress, and it introduces the stress intensity factor [189]

$$K_c = \sigma\sqrt{\pi a} \tag{6.61}$$

The critical stress intensity factor has the relationship with the critical strain energy release rate

$$K_c^2 = \sigma^2 \pi a = \frac{E G_c}{k} \tag{6.62}$$

$$K_c = \sqrt{\frac{E G_c}{k}} \tag{6.63}$$

The specimen is defined as an infinite plate so far. We perform the three-point bending test for a cuboid with a finite plate and certain geometries and thus the stress intensity factor should be [189]

$$K = \frac{3FL}{2BW^{\frac{3}{2}}}\left[1.93\left(\frac{a}{W}\right)^{\frac{1}{2}} - 3.07\left(\frac{a}{W}\right)^{\frac{3}{2}} + 14.53\left(\frac{a}{W}\right)^{\frac{5}{2}} - 25.11\left(\frac{a}{W}\right)^{\frac{7}{2}} + 25.8\left(\frac{a}{W}\right)^{\frac{9}{2}}\right] = \frac{F}{BW^{\frac{1}{2}}} f_1\left(\frac{a}{w}\right) \tag{6.64}$$

where the fracture load force (F) is obtained from the 3PB test, B is the width of specimen, W is the thickness of specimen and L is the fixture span.

The J-integral method is used to characterize the fracture mechanics of material, and it is defined as

$$J = \int_C \left[wdy - T\left(\frac{\partial u}{\partial x}\right)\right] ds \tag{6.65}$$

where

$$w = \int_0^{\varepsilon} \sigma d\varepsilon \tag{6.66}$$

For the linear elastic material, the critical value of J is equal to the critical strain energy release rate

$$J_c = G_c \tag{6.67}$$

The value of J can be determined by the experiment with a standard specimen

$$J = \frac{2U}{B(W-a)} \tag{6.68}$$

where U is the strain energy. B is the width of specimen, W is the thickness of specimen and a is the crack length.

The aim of fracture mechanics is to find the material fracture toughness. However, the FOWLP is not a homogeneous object. Silicon die and EMC are the main components of FOWLP. The geometry and dimension of FOWLP decide that the FOWLP cannot fulfill the requirement of standard fracture toughness test. Therefore, the task of evaluating FOWLP fracture toughness is impossible.

6.2.2 PROPOSED THEORETICAL MODEL OF FOWLP FATIGUE CRACK GROWTH

The fatigue test is used to evaluate the material reliability under a periodic loading condition. The periodic loading force could be the bending force, compression force and tension force. The range of periodic loading force can be from zero to the predetermined value. The machine repeats the work of loading and unloading till the pre-determined number of cycles or the specimen failure.

The fatigue test is useful and meaningful to the FOWLP reliability. It is because the FOWLP at work often withstands the external force. The FOWLP is always used to volume sensitive electronics devices because of its thin and small features. The thin FOWLP has the low body strength and the low body strength may lead to the crack issue. For example, one of the FOWLP applications is the fingerprint sensor. The fingerprint sensor needs to be pressed, and it may get the chance to crack after multiple times usage. This situation is similar to the fatigue test under the periodic loading force.

The material fatigue crack growth model is also known as Paris law [189]

$$\frac{da}{dN} = C(\Delta K)^m \quad (6.69)$$

where C and m are material constants. ΔK is the range of stress intensity factor. In other words, ΔK is the loading force range of material and it is defined as

$$\Delta K = K_{max} - K_{min} \quad (6.70)$$

The crack may grow up in two conditions in a FOWLP. The first condition is the external force. This phenomenon has been described by Paris law. The second condition is the internal force. The FOWLP is made up of various materials, and various materials have the different CTEs. The mismatched CTE leads to differences in the expansion and shrinkage of different materials. The outcome is the wafer warpage or package warpage. The difference of FOWLP standby temperature and working temperature leads to the package deformation. The microdeformation generates the internal force to accelerate the crack propagation.

There are two famous reliability tests – temperature cycling test and high temperature storage test. Both tests provide a challenging environment of temperature to test the specimen reliability. The specimen functional failure after both tests should have the relationship with their physical failure more or less. The reason is the changing temperature leads to the specimen deformation.

Therefore, the external force does not affect the fatigue growth lonely for the FOWLP especially a working FOWLP. We should add the thermal effect factor to Paris law for the FOWLP fatigue crack growth model. A binomial fatigue crack growth model should be more accurate and more suitable to the FOWLP. The proposed FOWLP fatigue crack growth model is

$$\frac{da}{dN} = \left(\frac{da}{dN}\right)_{fatigue} + \left(\frac{da}{dN}\right)_{thermal} = C(\Delta K)^m + D(\Delta K)^n \Gamma \qquad (6.71)$$

The first component is the normal fatigue crack growth model, which is caused by the external loading force. C and m are material constants. ΔK is the range of stress intensity factor. The second component is the fatigue crack growth rate, which is caused by the thermal effect. D and n are material constants. Γ is the thermal factor, and it represents the degree of thermal effect.

The second component in the proposed fatigue crack growth model represents the thermal effect on the crack growth. There are two uncertain variables. D is a constant, and it can be assumed as [190, 191]

$$D = 10^{a_1 + b_1 T} \qquad (6.72)$$

where a_1 and b_1 are constants from the linear fit function. T is the absolute temperature.

Γ is the thermal factor, and it also can be treated as a probability function with the range from 0 to 1. Γ can be expressed as [192-194]

$$\Gamma = exp\left(-\frac{Q}{kT}\right) \qquad (6.73)$$

where Q is the activation energy [195, 196], k is the Boltzmann constant and T is the absolute temperature. Therefore, the thermal effect component of FOWLP fatigue crack growth model is

$$\left(\frac{da}{dN}\right)_{thermal} = 10^{a_1 + b_1 T} (\Delta K)^n exp\left(-\frac{Q}{kT}\right) \qquad (6.74)$$

Moreover, the final proposed FOWLP fatigue crack growth model is

$$\frac{da}{dN} = \left(\frac{da}{dN}\right)_{fatigue} + \left(\frac{da}{dN}\right)_{thermal} = C(\Delta K)^m + 10^{a_1 + b_1 T}(\Delta K)^n exp\left(-\frac{Q}{kT}\right) \tag{6.75}$$

6.3 SUMMARY

Two new theoretical models of FOWLP strength are proposed. These models are based on the location of initial fracture point. According to the fracture analysis results, the initial fracture point of FOWLP always appears on the silicon die surface or silicon die edge. There are three typical FOWLP structures, and their differences are the silicon die backside. The silicon die backside could be protected by the EMC and BSP tape, and it also could be exposed. However, the silicon die periphery is always encapsulated by the EMC and thus the initial fracture points of FOWLP only can appear on the package interior or package surface. Therefore, two theoretical models of FOWLP strength are proposed.

The comparison of FOWLP strength models with experiment results and simulation results shows that the differences between specimen experiment results and simulation results are small. However, all the FOWLP strength models underestimate their corresponding specimen flexure strength in the lower region of failure probability. The underestimated phenomenon often occurs in the two-

parameter Weibull distribution model, and this is the shortcoming of the two-parameter Weibull distribution. The proposed FOWLP strength models are derived from the two-parameter Weibull distribution and thus they also show the underestimated phenomenon more or less. One of the specimen strength models underestimates both experiment and simulation results in the lower region of failure probability too much. The reason may be the experiment errors. There is a data point far away from the major stream of data point too much. This data point should be an experiment error. The simulation results somewhat overestimate the experiment results in the lower region of failure probability. The reason may be the assembly process effect is not taken into account in the simulation model.

A new theoretical model of FOWLP fatigue crack growth is proposed. The new model adds the effect of thermal factor on the fatigue crack growth compared with the normal fatigue model, and it is based on Paris law. The crack may grow up in two conditions in a FOWLP. The first condition is the external force. This phenomenon has been described by Paris law. The second condition is the internal force. The mismatched CTE leads to the package deformation in the thermal condition, and the package deformation generates the internal force to accelerate the crack propagation. Therefore, we should add the thermal effect factor to Paris law for the FOWLP fatigue crack growth model. A binomial fatigue crack growth model should be more accurate and more suitable to the FOWLP. However, there is not any experiment to verify this model.

CHAPTER 7 CONCLUSIONS AND FUTURE WORK

7.1 CONCLUSIONS

The fan-out wafer level packaging technology has the superiority of ultrathin size. However, the low body strength of thin FOWLP may lead to crack issues. Therefore, it is significant to study the behavior of FOWLP strength. The behavior of FOWLP strength is evaluated by the experimental method and numerical method. We confirm three significant characteristics of FOWLP strength from the experimental work. Firstly, the wafer grinding process still affects the FOWLP strength. The FOWLP backside condition is critical to the FOWLP strength. The FOWLP with smooth backside surface gains the high flexure strength. Secondly, the FOWLP with small silicon die gains the high flexure strength. The reason is the shifting of neutral surface. The tension stress on the lower surface of silicon reduces and the FOWLP strength increases. Thirdly, the thermal factor affects the FOWLP strength significantly. The reason is the change in the material property of EMC. The glass transition and flexure modulus of EMC increases after the thermal processes. In summary, we find the over-molded structure FOWLP is better than the other two structure FOWLPs at the aspect of stability, reliability and cost. The numerical work creates the simulation models of 3PB test. The simulation results prove that the flexure strength of over-molded structure FOWLP is always higher than the flexure strength of other structure FOWLPs with the same thickness. According to the

fracture analysis of FOWLP, the initial fracture point of FOWLP may appear on the silicon die surface or the silicon die edge. Therefore, we propose two theoretical models of FOWLP strength. The usage of these two models is based on the location of initial fracture point. The comparison of FOWLP strength model with experimental results and simulation results shows that they are identical. A new theoretical model of FOWLP fatigue crack growth is proposed. The new model additionally considers the effect of thermal factor on the fatigue crack growth compared with the normal fatigue model, and it is based on Paris law.

7.1.1 CONCLUSIONS OF EVALUATION OF FOWLP STRENGTH BY 3PB TEST METHOD

The 3PB test is conducted by Instron universal tester 5566. The static load cell of Instron 2530-427 is used, and its maximum capacity is ±100 N. The 3PB fixture is customized with a fabrication tolerance ±0.05 mm. The whole experiment is conducted in the biological lab, School of Mechanical and Aerospace Engineering, Nanyang Technological University. The environment temperature is 25°C. There is not any pre-conditioning or heating device attached to the machine to process the specimens before or during the experiment. The default speed of loading force is 0.6 mm/min (0.01 mm/s). The specimens are built by the conventional fan-out wafer level packaging assembly process, and they are considered and designed carefully to fulfill the research objective. The dummy silicon die size of specimen is 5.11 mm × 5.11 mm, and the package size is 8.09 mm × 8.09 mm.

The FOWLPs have three kinds of typical structure, and they are the over-molded structure, die-exposed structure and BSP tape protected structure. The 3PB test results show that the flexure strength of over-molded structure FOWLP is much higher than the flexure strength of other two kinds of structure FOWLP. However, the flexure strength distribution of these three kinds of structure FOWLP shows the different trend. The flexure strength distribution of over-molded structure FOWLP is much tight. The flexure strength distribution of die-exposed structure FOWLP is the widest. The flexure strength distribution of BSP tape protected structure FOWLP is tighter than the flexure strength distribution of die-exposed structure FOWLP even they have the same average flexure strength. The reason is the condition of FOWLP backside. The BSP tape covers the backside defects and forms a smooth surface on top of the wafer backside. Although the BSP tape has a minor contribution to the FOWLP strength, it reduces the effect of wafer grinding process on the flexure strength distribution significantly. Therefore, the over-molded structure and BSP tape protected structure FOWLP is recommended. For the aspect of FOWLP fracture analysis, all the specimens break into two parts after the 3PB test. The initial fracture point only appears on the silicon die surface or silicon die edge regardless the specimen structure.

The PSV layers are lithographed on the three kinds of typical structure FOWLP. The 3PB test results show two trends. The flexure strength of over-molded structure FOWLP increases significantly after lithographing the PSV layers. The thickness of PSV layer is 10 μm. Hence the PSV layer should not affect the FOWLP strength seriously. The reason should be the PSV lithographing process. The PSV lithographing process requires the wafer to store in a high temperature oven for curing. The oven temperature is 225℃, and the storage duration is two hours. The

EMC takes the principal place in the FOWLP and thus the increase in the FOWLP strength should be due to the increase in the EMC strength after the PSV curing process. The flexure strength of die-exposed and BSP tape protected structure FOWLP almost remains the same. The reason is the PSV layer is lithographed on the specimen front side, and the surface condition of specimen backside never changes. Therefore, the over-molded structure FOWLP is recommended.

The PSV curing process is only a short-term thermal process. The temperature cycling test and high temperature storage test are used to evaluate the long-term thermal test effect on the FOWLP strength. The cycling rate in this work is two cycles per hour. The durations of TC test are 500 cycles and 1000 cycles. The temperature of high temperature storage test is 150°C. The durations of HTS test are 500 hours and 1000 hours. The 3PB test results show two trends. The flexure strength of over-molded structure FOWLP increases slightly after both TC test and HTS test. The EMC physical property especially the strength should be affected by the thermal test. The flexure strength of die-exposed and BSP tape protected structure FOWLP increases at the middle point of test and drops at the end of test.

The flexure strength of over-molded structure FOWLP always increases significantly after the thermal process. We hypothesize that the increase in the FOWLP strength comes from the increase in the EMC strength and the EMC strength must be affected by the thermal process seriously. We collect four kinds of EMC specimen. The 3PB test and Vickers hardness test is used to evaluate the strength and hardness of EMC specimen. The Instron universal tester 5569 and a maximum capacity of ±1kN load cell are used to conduct the 3PB test. The FUTURE-TECH microhardness tester FM-300e is used to conduct the Vickers hardness test. The experiment results show that the flexure strength and hardness of EMC specimens

increase rapidly after the one time PSV curing process. However, the growth trends of flexure strength and hardness of EMC specimens become stable after the three times PSV curing process. The reason is the thermal process temperature is higher than the EMC glass transition. The increasing of EMC glass transition and EMC flexural modulus is due to the thermal process. However, the EMC flexure strength still increases significantly after the 500 hours HTS test, and this phenomenon proves that the EMC flexure strength does not become stable after the three times PSV curing process. The strengths of EMC specimens drop after the 1000 hours HTS test except for EMC-2. All the FOWLP specimens use EMC-2 in this research and thus the previous phenomenon of flexure strength up and down is not related to the EMC material. For the relationship between the strength and hardness, it has been proved that there is not any relationship between the strength and hardness. The strength and hardness are two independent material properties.

In order to get a reliable FOWLP, the over-molded structure FOWLP is recommended. The thin over-molded structure FOWLP can fulfill the requirement of volume sensitive device. There are some matters needed attention when we build the over-molded structure FOWLP. The FOWLP with small silicon die and thin PCB bar gains high strength. The reason is the shifting of bending neutral surface. The changing of material volume and material Young's modulus leads to the shifting of neutral surface. The wafer grinding process still affects the FOWLP strength. The FOWLP with the finest molding surface has the highest flexure strength.

7.1.2 CONCLUSIONS OF NUMERICAL STUDY OF FOWLP STRENGTH

ANSYS software is used to implement the numerical study of FOWLP strength. The ANSYS static structural toolbox is used to create the simulation models and explore solutions. There are two different mesh methods applied. The 3PB fixture rollers are meshed with the edge sizing method. The specimen body surface is meshed with the body sizing method. The movement of 3PB roller is controlled by the displacement method. The maximum principal stress of simulation model is processed by the two-parameter Weibull distribution and plotted by Minitab.

The comparison between experiment results and simulation results shows that the experiment curves and simulation curves match each other in the upper region of failure probability closely. However, the simulation curves sometimes overestimate the FOWLP failure probability in the lower region of failure probability compared with the experiment curves. However, the outcome of applying ANSYS simulation software to evaluate the FOWLP strength is ideal and satisfactory. The current simulation models have the potential to replace the experimental method to implement the evaluation work of FOWLP strength. The simulation method has the advantages of stability, minimal environment effect and saving workforce and time. The simulation model also can be further developed to implement the more complicated evaluation work of FOWLP strength.

We propose a new FOWLP and this FOWLP has the over-molded structure. We only use the simulation method to evaluate the strength of this new FOWLP specimen. The proposed FOWLP size is 8.09 mm × 8.09 mm and its die size is 5.11

mm × 5.11 mm. The thicknesses of silicon die and package are 150 μm and 210 μm respectively. Hence the thickness of over-molded layer is 50 μm.

The simulation result shows that the flexure strength of proposed FOWLP is higher than the flexure strength of other FOWLP specimens with the same thickness. The reason is the shifting of bending neutral surface. The proposed FOWLP has the minimum distance between the neutral surface and the lower surface of silicon die compared with other specimens. Therefore, the lower surface of silicon die of proposed FOWLP suffers the minimum tension stress in the 3PB test and thus the flexure strength of proposed specimen is high. The assembly process of proposed specimen only has a minor modification to the current process, and there are not any special or new processes added. However, the assembly process of proposed specimen needs attention to the silicon wafer grinding process. The grinding process quality is critical because the silicon die of new specimen is very tiny. There is an issue when we apply displacement method to evaluate new simulation models. The effective displacement range is uncertain. This problem should be considered in the future work.

7.1.3 CONCLUSIONS OF DEVELOPMENT OF THEORETICAL MODEL OF FOWLP STRENGTH

Two new theoretical models of FOWLP strength are proposed. These models are based on the location of initial fracture point. According to the fracture analysis results, the initial fracture point of FOWLP always appears on the silicon die surface or silicon die edge. There are three typical FOWLP structures, and their differences

are the silicon die backside. The silicon die backside could be protected by the EMC and BSP tape, and it also could be exposed. However, the silicon die periphery is always encapsulated by the EMC and thus the initial fracture points of FOWLP only can appear on the package interior or package surface. Therefore, two theoretical models of FOWLP strength are proposed.

The comparison of FOWLP strength models with experiment results and simulation results shows that the differences between specimen experiment results and simulation results are small. However, all the FOWLP strength models underestimate their corresponding specimen flexure strength in the lower region of failure probability. The underestimated phenomenon often occurs in the two-parameter Weibull distribution model, and this is the shortcoming of the two-parameter Weibull distribution. The proposed FOWLP strength models are derived from the two-parameter Weibull distribution and thus they also show the underestimated phenomenon more or less. One of the specimen strength models underestimates both experiment and simulation results in the lower region of failure probability too much. The reason may be the experiment errors. There is a data point far away from the major stream of data point too much. This data point should be an experiment error. The simulation results somewhat overestimate the experiment results in the lower region of failure probability. The reason may be the assembly process effect is not taken into account in the simulation model.

A new theoretical model of FOWLP fatigue crack growth is proposed. The new model adds the effect of thermal factor on the fatigue crack growth compared with the normal fatigue model, and it is based on Paris law. The crack may grow up in two conditions in a FOWLP. The first condition is the external force. This phenomenon has been described by Paris law. The second condition is the internal

force. The FOWLP is made up of various materials, and various materials have the different CTEs. The mismatched CTE leads to differences in the expansion and shrinkage of different materials. The outcome is the wafer warpage or package warpage. The difference of FOWLP standby temperature and working temperature leads to the package deformation. The microdeformation generates the internal force to accelerate the crack propagation. Therefore, the external force does not affect the fatigue growth lonely for the FOWLP. We should add the thermal effect factor to Paris law for the FOWLP fatigue crack growth model. A binomial fatigue crack growth model should be more accurate and more suitable to the FOWLP. However, there is not any experiment to verify this model.

7.2 MAJOR CONTRIBUTIONS

The major contributions of these studies include:

- Implementing the detailed evaluation of FOWLP strength by the three-point bending test method.
- Explaining the effect of FOWLP structure and passivation on the FOWLP strength.
- Performing fracture analysis of FOWLP after the three-point bending test.
- Investigating the effect of thermal process and thermal reliability test on the FOWLP strength.

- Evaluating the effect of epoxy molding compound on the FOWLP strength by the three-point bending test method and Vickers hardness test method.
- Investigating the effect of package dimension, geometry and PCB bar on the FOWLP strength.
- Confirming the effect of wafer grinding process on the FOWLP strength.
- Applying finite element method to simulate the evaluation work of FOWLP strength.
- Exploring the effect of mesh element size on simulation results.
- Proposing over-molded structure FOWLP to enhance the package strength and minimize the number of wafer grinding process.
- Proposing and validating FOWLP strength models. These models are based on the location of initial fracture points.
- Proposing the FOWLP fatigue crack growth model. This model additionally considers the effect of thermal factor on the FOWLP fatigue crack growth.

7.3 FUTURE WORK

There is much detailed research about the silicon strength over the years. However, the research about the package level strength especially the FOWLP strength is little and limited. The FOWLP becomes more and more popular, and it is widely used to the volume sensitive electronic devices. Therefore, the FOWLP

strength is meaningful and valuable to be studied. The recommended future studies of FOWLP strength include:

1. Evaluating the effect of redistribution layers on the FOWLP strength.

The redistribution layer is a critical component of FOWLP. The redistribution layer is used to expand the circuits of core silicon die. The redistribution layers are lithographed with passivation layers alternately, and there are two redistribution layers and three passivation layers typically. The layout of redistribution layer depends on the package design, and there is not any universal design of redistribution layer. The material of redistribution layer is copper. Copper is a ductile material, while the silicon die and epoxy molding compound are brittle materials. Therefore, the effect of redistribution layer on the FOWLP strength is interesting and worth to be studied.

2. Optimizing and expanding the current simulation work.

The application of finite element method could save much time and workforce compared with experiment method. However, the simulation work still has the space to be improved. The effect of package assembly process should be considered in the future simulation work. The assembly processes such as the backside protection tape lamination process and passivation layer lithographing process need to cure the wafer by the high temperature. The curing process should affect the FOWLP strength. The thermal factor should be counted while optimizing the simulation model. The simulation model also can be further developed. One proposed plan is to add the long-term reliability test (temperature cycling test or high temperature storage test) to the specimen before starting the three-point bending test.

3. Validating the proposed FOWLP fatigue crack growth model.

The crack may grow up in two conditions in a FOWLP. The first condition is the external force. This phenomenon has been described by Paris law. The second condition is the internal force. The FOWLP is made up of various materials, and various materials have the different CTEs. The mismatched CTE leads to differences in the expansion and shrinkage of different materials. The outcome is the wafer warpage or package warpage. The difference of FOWLP standby temperature and working temperature leads to the package deformation. The microdeformation generates the internal force to accelerate the crack propagation. Therefore, the external force does not affect the fatigue growth lonely for the FOWLP especially a working FOWLP. A binomial fatigue crack growth model should be more accurate and more suitable to the FOWLP.

REFERENCES

[1] A. Chen, and R. Lo, *Semiconductor packaging : materials interaction and reliability*: Boca Raton, FL : CRC Press, 2012, 2012.

[2] M. Datta, T. Ōsaka, and J. W. Schultze, *Microelectronic packaging*: Boca Raton, FL : CRC Press, c2005, 2005.

[3] J. H. Lau, *Thermal stress and strain in microelectronics packaging*: New York : Van Nostrand Reinhold, c1993, 1993.

[4] R. K. Ulrich, and W. D. Brown, *Advanced electronic packaging*: Hoboken, NJ : Wiley ; Piscataway, NJ : IEEE, c2006, 2006.

[5] M. Brunnbauer, E. Furgut, G. Beer, and T. Meyer, “Embedded wafer level ball grid array (eWLB),” in 2006 8th Electronics Packaging Technology Conference, 2006, pp. 1-5.

[6] S. Qu, and Y. Liu, *Wafer-level chip-scale packaging : analog and power semiconductor applications*: New York : Springer, 2015.

[7] Z. Chen, T. Gongyue, L. B. Long, D. M. Zhi, E. W. L. Ching, and C. T. Chong, “Thermo-mechanical design of fan-out wafer level package for power converter module,” in 2017 IEEE 19th Electronics Packaging Technology Conference (EPTC), 2017, pp. 1-6.

[8] U. Rahangdale, B. Conjeevaram, A. Doiphode, P. Rajmane, A. Misrak, A. R. Sakib, D. Agonafer, L. T. Nguyen, A. Lohia, and S. Kummerl, “Solder ball reliability assessment of WLCSP - Power cycling versus thermal cycling,” in 2017 16th IEEE Intersociety Conference on Thermal and Thermomechanical Phenomena in Electronic Systems (ITherm), 2017, pp. 1361-1368.

[9] S. W. Yoon, L. Yaojian, S. Gaurav, J. Yonggang, V. P. Ganesh, T. Meyer, P. C. Marimuthu, X. Baraton, and A. Bahr, “Mechanical characterization of next generation eWLB (embedded wafer level BGA) packaging,” in 2011 IEEE

61st Electronic Components and Technology Conference (ECTC), 2011, pp. 441-446.

[10] T. Meyer, G. Ofner, S. Bradl, M. Brunnbauer, and R. Hagen, "Embedded Wafer Level Ball Grid Array (eWLB)," in 2008 10th Electronics Packaging Technology Conference, 2008, pp. 994-998.

[11] M. Brunnbauer, T. Meyer, G. Ofner, K. Mueller, and R. Hagen, "Embedded Wafer Level Ball Grid Array (eWLB)," in 2008 33rd IEEE/CPMT International Electronic Manufacturing Technology Symposium (IEMT), 2008, pp. 1-6.

[12] J. Yonggang, X. Baraton, S. W. Yoon, L. Yaojian, P. C. Marimuthu, V. P. Ganesh, T. Meyer, and A. Bahr, "Next generation eWLB (embedded wafer level BGA) packaging," in 2010 12th Electronics Packaging Technology Conference (EPTC), 2010, pp. 520-526.

[13] Y. Seung Wook, L. Yaojian, and P. C. Marimuthu, "Development and characterization of 300mm large panel eWLB (embedded wafer level BGA)," in 2011 18th European Microelectronics and Packaging Conference (EMPC), 2011, pp. 1-5.

[14] M. Prashant, Y. Seung Wook, L. Yaojian, and P. C. Marimuthu, "Cost effective 300mm large scale eWLB (embedded Wafer Level BGA) technology," in 2011 IEEE 13th Electronics Packaging Technology Conference (EPTC), 2011, pp. 117-121.

[15] J. H. Lau, *3D IC integration and packaging*: New York : McGraw-Hill Education, 2016.

[16] K. Pressel, G. Beer, T. Meyer, M. Wojnowski, M. Fink, and G. Ofner, "Embedded wafer level ball grid array (eWLB) technology for system integration," in 2010 IEEE CPMT Symposium Japan, 2010, pp. 1-4.

[17] J. Yonggang, J. Teysseyrex, X. Baraton, S. W. Yoon, L. Yaojian, and P. C. Marimuthu, "Advanced packaging solutions of next generation eWLB

technology," in 2011 IEEE 13th Electronics Packaging Technology Conference (EPTC), 2011, pp. 739-743.

[18] M. Wojnowski, and K. Pressel, "Embedded wafer level ball grid array (eWLB) technology for high-frequency system-in-package applications," in 2013 IEEE MTT-S International Microwave Symposium Digest (IMS), 2013, pp. 1-4.

[19] L. S. H. Lee, L. I. S. Kang, Y. T. Kwon, T. H. Kim, J. H. Kim, E. J. Lee, and J. K. Lee, "FOWLP technology as wafer level system in packaging (SiP) solution," in 2017 International Conference on Electronics Packaging (ICEP), 2017, pp. 491-493.

[20] B. Q. Qi, and C. Hanna, "A design-of-experiment (DOE) to optimize a SiP design for connectivity applications," in 2016 IEEE 18th Electronics Packaging Technology Conference (EPTC), 2016, pp. 85-88.

[21] Y. Seung Wook, J. A. Caparas, L. Yaojian, and P. C. Marimuthu, "Advanced low profile PoP solution with embedded wafer level PoP (eWLB-PoP) technology," in 2012 IEEE 62nd Electronic Components and Technology Conference (ECTC), 2012, pp. 1250-1254.

[22] J. Yonggang, J. Teysseyre, X. Baraton, S. W. Yoon, L. Yaojian, and P. C. Marimuthu, "Development and characterization of next generation eWLB (embedded Wafer Level BGA) packaging," in 2012 IEEE 62nd Electronic Components and Technology Conference (ECTC), 2012, pp. 1388-1393.

[23] Y. Seung Wook, P. Tang, R. Emigh, L. Yaojian, P. C. Marimuthu, and R. Pendse, "Fanout flipchip eWLB (embedded Wafer Level Ball Grid Array) technology as 2.5D packaging solutions," in 2013 IEEE 63rd Electronic Components and Technology Conference (ECTC), 2013, pp. 1855-1860.

[24] C. C. Liu, S. M. Chen, F. W. Kuo, H. N. Chen, E. H. Yeh, C. C. Hsieh, L. H. Huang, M. Y. Chiu, J. Yeh, T. S. Lin, T. J. Yeh, S. Y. Hou, J. P. Hung, J. C. Lin, C. P. Jou, C. T. Wang, S. P. Jeng, and D. C. H. Yu, "High-performance integrated fan-out wafer level packaging (InFO-WLP): Technology and

system integration," in 2012 IEEE International Electron Devices Meeting (IEDM), 2012, pp. 323-326.

[25] *Fan-out and embedded die: technologies and market trends*, Yole Developpement, 2015.

[26] T. Braun, S. Raatz, S. Voges, R. Kahle, V. Bader, J. Bauer, K. F. Becker, T. Thomas, R. Aschenbrenner, and K. D. Lang, "Large area compression molding for Fan-out Panel Level Packing," in 2015 IEEE 65th Electronic Components and Technology Conference (ECTC), 2015, pp. 1077-1083.

[27] T. Braun, K. F. Becker, M. Wöhrmann, M. Töpper, L. Böttcher, R. Aschenbrenner, and K. D. Lang, "Trends in Fan-out wafer and panel level packaging," in 2017 International Conference on Electronics Packaging (ICEP), 2017, pp. 325-327.

[28] J. Lau, M. Li, N. Fan, E. Kuah, Z. Li, K. H. Tan, T. Chen, I. Xu, M. Li, Y. M. Cheung, W. Kai, J. Hao, R. Beica, T. Taylor, C. Ko, H. Yang, Y. Chen, S. P. Lim, N. Lee, J. Ran, K. S. Wee, Q. Yong, C. Xi, M. Tao, J. Lo, and R. Lee, "Fan-Out Wafer-Level Packaging (FOWLP) of Large Chip with Multiple Redistribution-Layers (RDLs)," in International Symposium on Microelectronics, 2017, pp. 576-583.

[29] T. Enomoto, S. Abe, D. Matsukawa, T. Nakamura, N. Yamazaki, N. Saito, M. Ohe, and T. Motobe, "Recent progress in low temperature curable photosensitive dielectrics," in 2017 International Conference on Electronics Packaging (ICEP), 2017, pp. 498-501.

[30] M. Z. Ding, S. C. Chong, D. S. W. Ho, and S. P. S. Lim, "Molding process development for high density I/Os Fan-Out Wafer Level Package (FOWLP) with fine pitch RDL," in 2016 IEEE 18th Electronics Packaging Technology Conference (EPTC), 2016, pp. 13-18.

[31] K. Honda, N. Suzuki, T. Nonaka, H. Noma, and Y. Ozaki, "Expanding Film and Process for High Efficiency 5 Sides Protection and FO-WLP Fabrication,"

in 2017 IEEE 67th Electronic Components and Technology Conference (ECTC), 2017, pp. 331-336.

[32] I. Watanabe, M. Kouda, K. Makihara, and H. Shinozaki, "Latest material technologies for Fan-Out Wafer Level Package," in 2017 China Semiconductor Technology International Conference (CSTIC), 2017, pp. 1-3.

[33] V. Carias, J. Thompson, P. D. Myers, P. Kumar, L. M. Racz, R. Toomey, and J. Wang, "Development of Mold Compounds With Ultralow Coefficient of Thermal Expansion and High Glass Transition Temperature for Fan-Out Wafer-Level Packaging," *IEEE Transactions on Components, Packaging and Manufacturing Technology,* vol. 5, no. 7, pp. 921-929, 2015.

[34] E. J. R. Phua, M. Liu, B. Cho, Q. Liu, S. Amini, X. Hu, and C. L. Gan, "Novel high temperature polymeric encapsulation material for extreme environment electronics packaging," *Materials & Design,* vol. 141, pp. 202-209, 2018.

[35] K. Byung-Seon, L. Sang-Sun, L. Da Eun, C. Hyung Ouk, and K. Hyun Woo, "Electrostatic discharge failure control of IC package by epoxy molding compound modification," in 2017 China Semiconductor Technology International Conference (CSTIC), 2017, pp. 1-3.

[36] H. S. Ling, B. Lin, C. S. Choong, S. D. Velez, C. T. Chong, and X. Zhang, "Comprehensive Study on the Interactions of Multiple Die Shift Mechanisms During Wafer Level Molding of Multichip-Embedded Wafer Level Packages," *IEEE Transactions on Components, Packaging and Manufacturing Technology,* vol. 4, no. 6, pp. 1090-1098, 2014.

[37] L. Bu, S. Ho, S. D. Velez, T. Chai, and X. Zhang, "Investigation on Die Shift Issues in the 12-in Wafer-Level Compression Molding Process," *IEEE Transactions on Components, Packaging and Manufacturing Technology,* vol. 3, no. 10, pp. 1647-1653, 2013.

[38] G. Sharma, A. Kumar, V. S. Rao, S. W. Ho, and V. Kripesh, "Solutions Strategies for Die Shift Problem in Wafer Level Compression Molding,"

IEEE Transactions on Components, Packaging and Manufacturing Technology, vol. 1, no. 4, pp. 502-509, 2011.

[39] J. Li, B. Zhang, P. Zhu, G. Li, R. Sun, and C. Wong, “Liquid epoxy molding compound with high glass transition temperature and high thermal conductivity,” in 2017 18th International Conference on Electronic Packaging Technology (ICEPT), 2017, pp. 1107-1112.

[40] T. Fujiwara, Y. Shoji, Y. Masuda, K. Hashimoto, Y. Koyama, K. Isobe, H. Araki, R. Okuda, and M. Tomikawa, “Higher reliability for low-temperature curable positive-tone photo-definable dielectric materials,” in 2017 IEEE 19th Electronics Packaging Technology Conference (EPTC), 2017, pp. 1-4.

[41] H. Y. Li, A. Chen, S. Peng, G. Pan, and S. Chen, “Warpage Tuning Study for Multi-chip Last Fan Out Wafer Level Package,” in 2017 IEEE 67th Electronic Components and Technology Conference (ECTC), 2017, pp. 1384-1391.

[42] K. Kwon, Y. Lee, J. Kim, J. Y. Chung, K. Jung, Y. Y. Park, D. Lee, and S. K. Kim, “Compression Molding Encapsulants for Wafer-Level Embedded Active Devices: Wafer Warpage Control by Epoxy Molding Compounds,” in 2017 IEEE 67th Electronic Components and Technology Conference (ECTC), 2017, pp. 319-323.

[43] J. H. Lau, M. Li, D. Tian, N. Fan, E. Kuah, W. Kai, M. Li, J. Hao, Y. M. Cheung, Z. Li, K. H. Tan, R. Beica, T. Taylor, C. T. Ko, H. Yang, Y. H. Chen, S. P. Lim, N. C. Lee, J. Ran, C. Xi, K. S. Wee, and Q. Yong, “Warpage and Thermal Characterization of Fan-Out Wafer-Level Packaging,” *IEEE Transactions on Components, Packaging and Manufacturing Technology,* vol. 7, no. 10, pp. 1729-1738, 2017.

[44] F. Hou, T. Lin, L. Cao, F. Liu, J. Li, X. Fan, and G. Q. Zhang, “Experimental Verification and Optimization Analysis of Warpage for Panel-Level Fan-Out Package,” *IEEE Transactions on Components, Packaging and Manufacturing Technology,* vol. 7, no. 10, pp. 1721-1728, 2017.

[45] R. Farrugia, I. Grech, O. Casha, J. Micallef, E. Gatt, I. Ellul, R. Duca, and I. Borg, "Investigation of warpage in wafer-level Molding: Measurements and FE analysis," in 2015 Symposium on Design, Test, Integration and Packaging of MEMS/MOEMS (DTIP), 2015, pp. 1-6.

[46] C. H. Liu, L. Y. Chen, C. L. Lu, H. C. Chen, C. Y. Chen, and S. C. Chang, "Wafer Form Warpage Characterization Based on Composite Factors Including Passivation Films, Re-Distribution Layers, Epoxy Molding Compound Utilized in Innovative Fan-Out Package," in 2017 IEEE 67th Electronic Components and Technology Conference (ECTC), 2017, pp. 847-852.

[47] C. Zhu, H. Li, G. Xu, and L. Luo, "A novel mechanical diced trench structure for warpage reduction in wafer level packaging process," *Microelectronics Reliability,* vol. 55, no. 2, pp. 418-423, 2015.

[48] Z. Huang, P. P. Conway, E. Jung, R. C. Thomson, C. Liu, T. Loeher, and M. Minkus, "Reliability issues in Pb-free solder joint miniaturization," *Journal of Electronic Materials,* vol. 35, no. 9, pp. 1761-1772, 2006.

[49] C.-C. Chiu, C.-J. Wu, C.-T. Peng, K.-N. Chiang, T. Ku, and K. Cheng, "Failure Life Prediction and Factorial Design of Lead-Free Flip Chip Package," *Journal of the Chinese Institute of Engineers,* vol. 30, no. 3, pp. 481-490, 2007.

[50] B. Salam, N. N. Ekere, and D. Rajkumar, "Study of the interface microstructure of Sn-Ag-Cu lead-free solders and the effect of solder volume on intermetallic layer formation," in Proceedings 51st ECTC 2001, 2001, pp. 471.

[51] B. Salam, N. N. Ekere, and R. Durairaj, "A Study of Inter-Metallic Compounds (IMC) Formation and Growth in Ultra-Fine Pitch Sn-Ag-Cu Lead-Free Solder Joints," in 2006 Electronic Systemintegration Technology Conference, 2006, pp. 988-994.

[52] Y. Tian, X. Liu, J. Chow, Y. P. Wu, and S. K. Sitaraman, "Comparison of IMC Growth in Flip-Chip Assemblies with 100- and 200-μm-Pitch SAC305 Solder Joints," in 2013 IEEE 63rd Electronic Components and Technology Conference (ECTC), 2013, pp. 1005-1009.

[53] Y. Tian, X. Liu, J. Chow, Y. P. Wu, and S. K. Sitaraman, "Experimental evaluation of SnAgCu solder joint reliability in 100-μm pitch flip-chip assemblies," *Microelectronics Reliability,* vol. 54, no. 5, pp. 939-944, 2014.

[54] T. Y. Lee, W. J. Choi, K. N. Tu, J. W. Jang, S. M. Kuo, and J. K. Lin, "Morphology, kinetics, and thermodynamics of solid-state aging of eutectic SnPb and Pb-free solders on Cu," *Journal of Materials Research,* vol. 17, no. 2, pp. 291-301, 2002.

[55] K. S. Kim, S. H. Huh, and K. Suganuma, "Effects of Intermetallic Compounds on Properties of Sn-Ag-Cu Lead-Free Soldered Joints," *Journal of Alloys and Compounds,* vol. 352, no. 1-2, pp. 226-236, 2003.

[56] C. W. Chang, S. C. Yang, C.-T. Tu, and C. R. Kao, "Cross-Interaction Between Ni and Cu Across Sn Layers with Different Thickness," *Journal of Electronic Materials,* vol. 36, no. 11, pp. 1455-1461, 2007.

[57] N. Wade, K. Wu, J. JKunil, and S. Yamada, "Effect of Cu, Ag and Sb on the Creep-Rupture Strength of Lead-Free Solder Alloys," *Journal of Electronic Materials,* vol. 30, no. 9, pp. 1228-1231, 2001.

[58] X. Ma, F. Wang, Y. Qian, and F. Yoshida, "Development of Cu-Sn Intermetallic Compound at Pb-Free Solder/Cu Joint Interface," *Materials Letters,* vol. 57, no. 22-23, pp. 3361-3365, 2003.

[59] G. Y. Li, X. B. Jiang, B. Li, P. Chen, and R. Liao, "Influence of Dopant on IMC Growth and Mechanical Properties of Sn-3.5Ag-0.7Cu Solder Joints," in 2007 International Symposium on High Density packaging and Microsystem Integration, Shanghai, 2007, pp. 1-4.

[60] X. Ma, Y. Qian, and F. Yoshida, "Effect of La on the Cu–Sn intermetallic compound (IMC) growth and solder joint reliability," *Journal of Alloys and Compounds,* vol. 334, no. 1–2, pp. 224-227, 2002.

[61] B. Sabuncuoglu, F. Vanhee, G. Willems, B. Vandevelde, and D. Vandepitte, "Evaluation of Fatigue Behavior of Lead-Free Solder Joints in Four-Point Bending Test by Finite-Element Modeling," *IEEE Transactions on Components, Packaging and Manufacturing Technology,* vol. 7, no. 12, pp. 1957-1964, 2017.

[62] M.-L. Wu, and J.-S. Lan, "Investigation and prediction of solder joint failure analysis for ball grid array package subject to mechanical bending environment," *Soldering & Surface Mount Technology,* vol. 29, no. 2, pp. 75-84, 2017.

[63] P. L. Tu, Y. C. Chan, and J. K. L. Lai, "Effect of intermetallic compounds on the thermal fatigue of surface mount solder joints," *IEEE Transactions on Components, Packaging, and Manufacturing Technology: Part B,* vol. 20, no. 1, pp. 87-93, 1997.

[64] Y. Tian, J. Chow, X. Liu, Y. P. Wu, and S. K. Sitaraman, "Study of Intermetallic Growth and Kinetics in Fine-Pitch Lead-Free Solder Bumps for Next-Generation Flip-Chip Assemblies," *Journal of Electronic Materials,* vol. 42, no. 2, pp. 230-239, 2013.

[65] C.-T. Peng, C.-M. Liu, J.-C. Lin, H.-C. Cheng, IEEE Member, and K.-N. Chiang, "Reliability Analysis and Design for the Fine-Pitch Flip Chip BGA Packaging," *IEEE Transactions on Components and Packaging Technologies,* vol. 27, no. 4, pp. 684-693, 2004.

[66] Y. Tian, X. Liu, J. Chow, Y. P. Wu, and S. K. Sitaraman, "Comparison of Sn-Ag-Cu Solder Alloy Intermetallic Compound Growth under Different Thermal Excursions for Fine-Pitch Flip-Chip Assemblies," *Journal of Electronic Materials,* vol. 42, no. 8, pp. 2724-2731, 2013.

[67] Y.-M. Jen, Y.-C. Chiou, and C.-L. Yu, "Fracture mechanics study on the intermetallic compound cracks for the solder joints of electronic packages," *Engineering Failure Analysis,* vol. 18, no. 2, pp. 797-810, 2011.

[68] K. N. Tu, "Reliability challenges in 3D IC packaging technology," *Microelectronics Reliability,* vol. 51, no. 3, pp. 517-523, 2011.

[69] W.-H. Chen, C.-F. Yu, H.-C. Cheng, Y.-m. Tsai, and S.-T. Lu, "IMC growth reaction and its effects on solder joint thermal cycling reliability of 3D chip stacking packaging," *Microelectronics Reliability,* vol. 53, no. 1, pp. 30-40, 2013.

[70] W. Huang, J. M. Loman, and B. Sener, "Study of the effect of reflow time and temperature on Cu-Sn intermetallic compound layer reliability," *Microelectronics Reliability,* vol. 42, no. 8, pp. 1229-1234, 2002.

[71] M. Y. Tsai, H. Y. Liu, C. M. Liu, H. L. Chen, and C. Y. Huang, "Bending Strength Evaluation of Si Interposers by PoEF Test Associated With Acoustic Emission Method," *IEEE Transactions on Device and Materials Reliability,* vol. 17, no. 2, pp. 364-370, 2017.

[72] M. Demant, T. Welschehold, M. Oswald, S. Bartsch, T. Brox, S. Schoenfelder, and S. Rein, "Microcracks in Silicon Wafers I: Inline Detection and Implications of Crack Morphology on Wafer Strength," *IEEE Journal of Photovoltaics,* vol. 6, no. 1, pp. 126-135, 2016.

[73] O. Borrero-López, T. Vodenitcharova, M. Z. Quadir, and M. Hoffman, "Scratch Fracture of Polycrystalline Silicon Wafers," *Journal of the American Ceramic Society,* vol. 98, no. 8, pp. 2587-2594, 2015.

[74] W. Fong, K. L. Koay, and I. A. Azid, "Experimental evaluation on the silicon mechanical performance of electronic packaging," *Journal of Mechanical Engineering & Science,* vol. 11, no. 1, pp. 2456, 2017.

[75] N. Marsi, B. Y. Majlis, A. A. Hamzah, and F. Mohd-Yasin, "The Mechanical Characterization of Bending Test for MEMS Capacitive Pressure Sensor

based 3C-SiC in High Temperature," *Applied Mechanics & Materials,* vol. 754-755, pp. 602, 2015.

[76] J. H. Kim, T. I. Lee, J. W. Shin, T. S. Kim, and K. W. Paik, "Bending Properties of Anisotropic Conductive Films Assembled Chip-in-Flex Packages for Wearable Electronics Applications," *IEEE Transactions on Components, Packaging and Manufacturing Technology,* vol. 6, no. 2, pp. 208-215, 2016.

[77] T. W. Kim, T. I. Lee, Y. Pan, W. Kim, S. Zhang, T. S. Kim, and K. W. Paik, "Effect of Nanofiber Orientation on Nanofiber Solder Anisotropic Conductive Films Joint Properties and Bending Reliability of Flex-on-Flex Assembly," *IEEE Transactions on Components, Packaging and Manufacturing Technology,* vol. 6, no. 9, pp. 1317-1329, 2016.

[78] J. H. Kim, T. I. Lee, T. S. Kim, and K. W. Paik, "The Effect of Anisotropic Conductive Films Adhesion on the Bending Reliability of Chip-in-Flex Packages for Wearable Electronics Applications," *IEEE Transactions on Components, Packaging and Manufacturing Technology,* vol. 7, no. 10, pp. 1583-1591, 2017.

[79] M. Li, J. Tudor, R. Torah, and S. Beeby, "Stress Analysis and Optimization of a Flip Chip on Flex Electronic Packaging Method for Functional Electronic Textiles," *IEEE Transactions on Components, Packaging and Manufacturing Technology,* vol. 8, no. 2, pp. 186-194, 2018.

[80] V. Subramanian, K. Yazzie, T. Alazar, B. Penmecha, P. Liu, Y. Bai, and P. Malatkar, "Characterization of Bulk and Thin Film Fracture in Electronic Packaging," *Journal of Electronic Packaging,* vol. 139, no. 2, pp. 020912-1-020912-7, 2017.

[81] Y. C. Chao, P. S. Huang, H. T. Keng, M. Y. Tsai, and P. C. Lin, "Mechanical strength of thin Cu-TSV memory dies used in 3D IC packaging," in 2015 10th International Microsystems, Packaging, Assembly and Circuits Technology Conference (IMPACT), 2015, pp. 107-110.

[82] K. Miyama, and Y. Katoh, “Effects of external bending stress on device-embedded substrate,” in 2017 International Conference on Electronics Packaging (ICEP), 2017, pp. 86-89.

[83] J. Brueckner, A. Dehé, E. Auerswald, R. Dudek, D. Vogel, B. Michel, and S. Rzepka, “Investigating fracture strength of poly-silicon membranes using microscopic loading tests and numerical simulation,” *Microsystem Technologies,* vol. 22, no. 3, pp. 569-575, 2016.

[84] D. K. Shetty, A. R. Rosenfield, P. McGuire, G. K. Bansai, and W. H. Duckworth, “Biaxial flexure test for ceramics,” *America Ceram Soc Bull,* vol. 59, no. 12, pp. 1193, 1980.

[85] G. D. With, and H. H. M. Wagemans, “Ball-on-Ring Test Revisited,” *Journal of American Ceramic Society,* vol. 72, no. 8, pp. 1538-1541, 1989.

[86] G. Hawkins, H. Berg, M. Mahalingam, G. Lewis, and L. Lofgran, “Measurement of silicon strength as affected by Wafer Back processing,” in 25th annual reliability physics symposium, 1987, pp. 216-223.

[87] M. Y. Tsai, and C. H. Chen, “Evaluation of Test Methods for Silicon Die Strength,” *Microelectronics Reliability,* vol. 48, no. 6, pp. 933-941, 2008.

[88] M. Y. Tsai, and C. S. Lin, “Determination of Silicon Die Strength,” in 55th Electronic Components and Technology Conference Proceedings, 2005, pp. 1155-1162.

[89] M.-Y. Tsai, and C. S. Lin, “Testing and Evaluation of Silicon Die Strength,” *IEEE Transactions on Electronics Packaging Manufacturing,* vol. 30, no. 2, pp. 106-114, 2007.

[90] "Plastics – Determination of flexural properties," DIN EN ISO 178, April 2011.

[91] "Standard Test Methods for Flexural Properties of Unreinforced and Reinforced Plastics and Electrical Insulating Materials," ASTM D790-03, March 2003.

[92] "Standard Test Method for Flexural Properties of Unreinforced and Reinforced Plastics and Electrical Insulating Materials by Four-Point Bending," ASTM D6272 – 00, July 2000.

[93] B. Yeung, and T.-Y. T. Lee, "An Overview of Experimental Methodologies and Their Applications for Die Strength Measurement," *IEEE Transactions on Components and Packaging Technologies,* vol. 26, no. 2, pp. 423-428, 2003.

[94] J. D. Wu, C. Y. Huang, and C. C. Liao, "Fracture Strength Characterization and Failure Analysis of Silicon Dies," *Microelectronics Reliability,* vol. 43, no. 2, pp. 269-277, 2003.

[95] E. Wu, I. G. Shih, Y. N. Chen, S. C. Chen, C. Z. Tsai, and C. A. Shao, "Influence of grinding process on semiconductor chip strength," in 52nd Electronic Components and Technology Conference, 2002, pp. 1617-1621.

[96] X. Bie, F. Qin, L. Zhou, J. Sun, P. Chen, and Z. Wang, "Impacts of back-grinding process parameters on the strength of thinned silicon wafer," in 2016 17th International Conference on Electronic Packaging Technology (ICEPT), 2016, pp. 1197-1200.

[97] P. Zhou, Y. Yan, N. Huang, Z. Wang, R. Kang, and D. Guo, "Residual Stress Distribution in Silicon Wafers Machined by Rotational Grinding," *Journal of Manufacturing Science and Engineering,* vol. 139, no. 8, pp. 081012-1-081012-7, 2017.

[98] J. Sun, F. Qin, P. Chen, and T. An, "A predictive model of grinding force in silicon wafer self-rotating grinding," *International Journal of Machine Tools and Manufacture,* vol. 109, pp. 74-86, 2016.

[99] S. Gao, Z. Dong, R. Kang, B. Zhang, and D. Guo, "Warping of silicon wafers subjected to back-grinding process," *Precision Engineering,* vol. 40, pp. 87-93, 2015.

[100] J. Sun, P. Chen, F. Qin, T. An, H. Yu, and B. He, "Modelling and experimental study of roughness in silicon wafer self-rotating grinding," *Precision Engineering,* vol. 51, pp. 625-637, 2018.

[101] S. Gao, H. Huang, X. Zhu, and R. Kang, "Surface integrity and removal mechanism of silicon wafers in chemo-mechanical grinding using a newly developed soft abrasive grinding wheel," *Materials Science in Semiconductor Processing,* vol. 63, pp. 97-106, 2017.

[102] H. Zhou, M. Guo, and X. Wang, "Ultraprecision grinding of silicon wafers using a newly developed diamond wheel," *Materials Science in Semiconductor Processing,* vol. 68, pp. 238-244, 2017.

[103] J. Sun, F. Qin, P. Chen, and T. An, "Residual stress distribution in wafers ground by different grinding parameters," in 2017 18th International Conference on Electronic Packaging Technology (ICEPT), 2017, pp. 327-331.

[104] L. Zhou, F. Qin, J. Sun, P. Chen, H. Yu, Z. Wang, and L. Tang, "Fracture strength of silicon wafer after different wafer treatment methods," in 16th International Conference on Electronic Packaging Technology (ICEPT), 2015, pp. 871-874.

[105] H. H. Jiun, I. Ahmad, A. Jalar, and G. Omar, "Effects of wafer thinning methods towards fracture strength and topography of silicon die," *Microelectronics Reliability,* vol. 46, pp. 836-845, 2006.

[106] J.-H. Zhao, J. Tellkamp, V. Gupta, and D. R. Edwards, "Experimental Evaluation of the Strength of Silicon Die by 3-Point-Bend Versus Ball-on-Ring Tests," *IEEE Transactions on Electronics Packaging Manufacturing,* vol. 23, no. 4, pp. 248-255, 2009.

[107] J. P. Gambino, "Thin silicon wafer processing and strength characterization," in 20th IEEE International Symposium on the Physical and Failure Analysis of Integrated Circuits (IPFA), 2013, pp. 199-207.

[108] S. Barnat, H. Fremont, A. Gracia, and E. Cadalen, "Evaluation by Three-Point-Bend and Ball-on-Ring Tests of Thinning Process on Silicon Die

Strength," *Microelectronics Reliability,* vol. 52, no. 9-10, pp. 2278-2282, 2012.

[109] B. H. Yeung, V. Hause, and T.-Y. T. Lee, "Assessment of Backside Processes Through Die Strength Evaluation," *IEEE Transactions on Advanced Packaging,* vol. 23, no. 3, pp. 582-587, 2000.

[110] L. Arapan, G. Wong, B. Dulmet, T. Baron, J. M. Friedt, V. Placet, and S. Alzuaga, "Stress-sensitivity of wafer-level packaged SAW delay lines," in 2016 European Frequency and Time Forum (EFTF), 2016, pp. 1-5.

[111] T. Liu, P. Ge, W. Bi, and P. Wang, "Fracture strength of silicon wafers sawn by fixed diamond wire saw," *Solar Energy,* vol. 157, pp. 427-433, 2017.

[112] A. S. Azar, B. Holme, and Ø. Nielsen, "Effect of sawing induced micro-crack orientations on fracture properties of silicon wafers," *Engineering Fracture Mechanics,* vol. 154, pp. 262-271, 2016.

[113] M. Domke, B. Egle, S. Stroj, M. Bodea, E. Schwarz, and G. Fasching, "Ultrafast-laser dicing of thin silicon wafers: strategies to improve front- and backside breaking strength," *Applied Physics A: Materials Science & Processing,* vol. 123, no. 12, pp. 746, 2017.

[114] M. R. Marks, Z. Hassan, and K. Y. Cheong, "Effect of Nanosecond Laser Dicing on the Mechanical Strength and Fracture Mechanism of Ultrathin Si Dies With Cu Stabilization Layer," *IEEE Transactions on Components, Packaging and Manufacturing Technology,* vol. 5, no. 12, pp. 1885-1897, 2015.

[115] S. j. Wu, H. C. Hsu, W. F. Lin, and S. L. Fu, "An investigation on ultrathin wafer dicing by ultrafast laser with high density plasma etching," in 2017 International Conference on Electronics Packaging (ICEP), 2017, pp. 139-143.

[116] S. H. Chae, J. H. Zhao, D. R. Edwards, and P. S. Ho, "Effect of Dicing Technique on the Fracture Strength of Si Dies With Emphasis on Multimodal Failure Distribution," *IEEE Transactions on Device and Materials Reliability,* vol. 10, no. 1, pp. 149-156, 2010.

[117] D. I. Cereno, and S. Wickramanayaka, "Stealth Dicing Challenges for MEMS Wafer Applications," in 2017 IEEE 67th Electronic Components and Technology Conference (ECTC), 2017, pp. 358-363.

[118] S. Shuai, L. Dapeng, N. Yuling, and P. Seungbae, "Die stress in stealth dicing for MEMS," in 2016 15th IEEE Intersociety Conference on Thermal and Thermomechanical Phenomena in Electronic Systems (ITherm), 2016, pp. 539-545.

[119] P. Jacob, and W. Rothkirch, "Unusual defects, generated by wafer sawing: Diagnosis, mechanisms and how to distinguish from related failures," *Microelectronics Reliability,* vol. 48, no. 8, pp. 1253-1257, 2008.

[120] W.-S. Lei, A. Kumar, and R. Yalamanchili, "Die singulation technologies for advanced packaging: A critical review," *Journal of Vacuum Science & Technology B, Nanotechnology and Microelectronics: Materials, Processing, Measurement, and Phenomena,* vol. 30, no. 4, 2012.

[121] M. Fuegl, G. Mackh, E. Meissner, and L. Frey, "Analytical stress characterization after different chip separation methods," *Microelectronics Reliability,* vol. 54, no. 9–10, pp. 1735-1740, 2014.

[122] J. Noh, J.-H. Kim, H. Sohn, and J.-H. Lee, "Comparison of bending fracture strength of silicon after ablation with nanosecond and picosecond lasers," *International Journal of Advanced Manufacturing Technology,* vol. 84, no. 9-12, pp. 2029-2036, 2016.

[123] M. R. Marks, Z. Hassan, and K. Y. Cheong, "Ultrathin Wafer Pre-Assembly and Assembly Process Technologies: A Review," *Critical Reviews in Solid State and Materials Sciences,* vol. 40, no. 5, pp. 251-290, 2015.

[124] N. Sudani, K. Venkatakrishnan, and B. Tan, "Laser singulation of thin wafer: Die strength and surface roughness analysis of 80 μm silicon dice," *Optics and Lasers in Engineering,* vol. 47, no. 7–8, pp. 850-854, 2009.

[125] S. Schoenfelder, M. Ebert, C. Landesberger, K. Bock, and J. Bagdahn, "Investigations of the Influence of Dicing Techniques on the Strength

Properties of Thin Silicon," *Microelectronics Reliability,* vol. 47, no. 2-3, pp. 168-178, 2007.

[126] N. McLellan, N. Fan, S. Liu, K. Lau, and J. Wu, "Effect of wafer thinning condition on the roughness, morphology and fracture strength of silicon die," *ASME Journal Electronic Packaging,* vol. 126, pp. 110-114, 2004.

[127] S. H. Chae, J. H. Zhao, D. R. Edwards, and P. S. Ho, "Effect of backside scratch direction on the Si die strength," in 2010 12th IEEE Intersociety Conference on Thermal and Thermomechanical Phenomena in Electronic Systems, 2010, pp. 1-6.

[128] D. Y. R. Chong, W. E. Lee, J. H. L. Pang, T. H. Low, and B. K. Lim, "Mechanical failure strength characterization of silicon dice," in Proceedings of the 5th Electronics Packaging Technology Conference (EPTC 2003), 2003, pp. 600-605.

[129] D. Y. R. Chong, W. E. Lee, B. K. Lim, J. H. L. Pang, and T. H. Low, "Mechanical characterization in failure strength of silicon dice," in The Ninth Intersociety Conference on Thermal and Thermomechanical Phenomena In Electronic Systems, 2004, pp. 203-210.

[130] S. Chen, C. Z. Tsai, E. Wu, I. G. Shih, and Y. N. Chen, "Study on the Effects of Wafer Thinning and Dicing on Chip Strength," *IEEE Transactions on Advanced Packaging,* vol. 29, no. 1, pp. 149-157, 2006.

[131] B. Cotterell, Z. Chen, J. B. Han, and N. X. Tan, "The Strength of the Silicon Die in Flip-Chip Assemblies," *Journal of Electronic Packaging,* vol. 125, no. 1, pp. 114-119, 2003.

[132] W. Weibull, *A Statistical Theory of the Strength of Materials*: Generalstabens litografiska anstalts förlag, 1939.

[133] R. B. Abernethy, *The New Weibull Handbook: Reliability & Statistical Analysis for Predicting Life, Safety, Risk, Support Costs, Failures, and Forecasting Warranty Claims, Substantiation and Accelerated Testing, Using*

Weibull, Log Normal, Crow-AMSAA, Probit, and Kaplan-Meier Models: R.B. Abernethy, 2006.

[134] W. Weibull, "A statistical distribution function of wide applicability," *Journal Applied Mechanics,* vol. 18, pp. 293-297, 1951.

[135] E. S. Lindquist, "Strength of materials and the Weibull distribution," *Probabilistic Engineering Mechanics,* vol. 9, no. 3, pp. 191-194, 1994.

[136] S. L. Fok, B. C. Mitchell, J. Smart, and B. J. Marsden, "A numerical study on the application of the Weibull theory to brittle materials," *Engineering Fracture Mechanics,* vol. 68, no. 10, pp. 1171-1179, 2001.

[137] C. Zweben, and B. W. Rosen, "A statistical theory of material strength with application to composite materials," *Journal of the Mechanics and Physics of Solids,* vol. 18, no. 3, pp. 189-206, 1970.

[138] S. Shimizu, "Weibull Distribution Function Application to Static Strength and Fatigue Life of Materials," *Tribology Transactions,* vol. 55, no. 3, pp. 267-277, 2012.

[139] G. Srinivasa Rao, M. Aslam, and O. H. Arif, "Estimation of reliability in multicomponent stress–strength based on two parameter exponentiated Weibull Distribution," *Communications in Statistics - Theory and Methods,* vol. 46, no. 15, pp. 7495-7502, 2017.

[140] J. H. Zhao, "A probabilistic mechanics approach to die cracking prediction in flip-chip ball grid array package," in The Ninth Intersociety Conference on Thermal and Thermomechanical Phenomena In Electronic Systems (IEEE Cat. No.04CH37543), 2004, pp. 177-183.

[141] J. H. Zhao, "A Three-Parameter Weibull-Like Fitting Function for Flip-Chip Die Strength Data," *Microelectronics Reliability,* vol. 44, no. 3, pp. 459-470, 2004.

[142] J. H. Zhao, "A probabilistic mechanics approach to die cracking prediction in flip-chip ball grid array package," *IEEE Transactions on Components and Packaging Technologies,* vol. 28, no. 3, pp. 390-396, 2005.

[143] D. Wu, J. Zhou, and Y. Li, "Methods for estimating Weibull parameters for brittle materials," *Journal of Materials Science,* vol. 41, no. 17, pp. 5630-5638, 2006.

[144] C. Bohm, T. Hauck, A. Juritza, and W. H. Muller, "Weibull statistics of silicon die fracture," in Proceedings of 6th Electronics Packaging Technology Conference (EPTC 2004), 2004, pp. 782-786.

[145] C. Bohm, T. Hauck, W. H. Muller, and A. Juritza, "Probability of silicon fracture in molded packages [ICs]," in EuroSimE 2004. Proceedings of 5th International Conference on Thermal and Mechanical Simulation and Experiments in Microelectronics and Microsystems, 2004, pp. 75-81.

[146] T. Hauck, C. Bohm, and W. H. Muller, "Weibull statistics for multiple flaw distributions and its application in silicon fracture prediction," in EuroSimE 2005. Proceedings of the 6th International Conference on Thermal, Mechanial and Multi-Physics Simulation and Experiments in Micro-Electronics and Micro-Systems, 2005, pp. 242-247.

[147] A. Nasr, S. Gasmi, and F. Ben Hmida, "Parameter estimation of the flexible Weibull distribution for type I censored samples," *Journal of Applied Statistics,* vol. 44, no. 14, pp. 2499-2512, 2017.

[148] I. J. Myung, "Tutorial on maximum likelihood estimation," *Journal of Mathematical Psychology,* vol. 47, no. 1, pp. 90-100, 2003.

[149] U. Genschel, and W. Q. Meeker, "A Comparison of Maximum Likelihood and Median-Rank Regression for Weibull Estimation," *Quality Engineering,* vol. 22, no. 4, pp. 236-255, 2010.

[150] N. Balakrishnan, and M. Kateri, "On the maximum likelihood estimation of parameters of Weibull distribution based on complete and censored data," *Statistics & Probability Letters,* vol. 78, no. 17, pp. 2971-2975, 2008.

[151] I. Paul, B. Majeed, K. M. Razeeb, and J. Barton, “Statistical Fracture Modelling of Silicon with Varying Thickness,” *Acta Materialia,* vol. 54, no. 15, pp. 3991-4000, 2006.

[152] M. Z. Raqab, S. A. Al-Awadhi, and D. Kundu, “Discriminating among Weibull, log-normal, and log-logistic distributions,” *Communications in Statistics - Simulation and Computation*, pp. 1-23, 2017.

[153] "Temperature Cycling," JESD22-A104D, March 2009.

[154] F. X. Che, “Study on board level solder joint reliability for extreme large fan-out WLP under temperature cycling,” in 2016 IEEE 18th Electronics Packaging Technology Conference (EPTC), 2016, pp. 207-212.

[155] K. C. Wu, S. Y. Lin, T. Y. Hung, and K. N. Chiang, “Reliability Assessment of Packaging Solder Joints Under Different Thermal Cycle Loading Rates,” *IEEE Transactions on Device and Materials Reliability,* vol. 15, no. 3, pp. 437-442, 2015.

[156] B. I. Noh, J. W. Yoon, and S. B. Jung, “Effects of Underfill Materials and Thermal Cycling on Mechanical Reliability of Chip Scale Package,” *IEEE Transactions on Components and Packaging Technologies,* vol. 32, no. 3, pp. 633-638, 2009.

[157] Y. Hyungseok, and J. Insu, “Verification of Faulty Mechanism for Fan-Out Wafer Level Package Using Numerical Analysis,” *Applied Mechanics & Materials,* vol. 789-790, pp. 609, 2015.

[158] D. Yap, K. S. Wong, L. Petit, R. Antonicelli, and S. W. Yoon, “Reliability of eWLB (Embedded Wafer Level BGA) for Automotive Radar Applications,” in 2017 IEEE 67th Electronic Components and Technology Conference (ECTC), 2017, pp. 1473-1479.

[159] C. C. Lee, “Effect of wafer level underfill on the microbump reliability of ultrathin-chip stacking type 3D-IC assembly during thermal cycling tests,” *Materials,* vol. 10, no. 10, 2017.

[160] "High Temperature Storage Life," JESD22-A103C, November 2004.

[161] B. Zhang, M. Johlitz, A. Lion, L. Ernst, K. M. B. Jansen, D. K. Vu, and L. Weiss, “Aging of epoxy moulding compound - Thermomechanical properties during high temperature storage,” in 2016 17th International Conference on Thermal, Mechanical and Multi-Physics Simulation and Experiments in Microelectronics and Microsystems (EuroSimE), 2016, pp. 1-6.

[162] T. Braun, K. F. Becker, M. Koch, V. Bader, R. Aschenbrenner, and H. Reichl, “High-temperature reliability of Flip Chip assemblies,” *Microelectronics Reliability,* vol. 46, no. 1, pp. 144-154, 2006.

[163] J. Park, H. J. Cha, B. S. Kim, Y. B. Jo, J. K. Park, S. Y. Kim, S. C. Shin, M. Y. Shin, K. I. Ouh, and H. Jeon, “Interfacial Degradation Mechanism of Au/Al and Alloy/Al Bonds Under High Temperature Storage Test: Contamination, Epoxy Molding Compound, Wire and Bonding Strength,” *IEEE Transactions on Components and Packaging Technologies,* vol. 30, no. 4, pp. 731-744, 2007.

[164] J. Gomes, and M. Mayer, “Effect of Bond Geometry on Shear Strength and HTS Reliability for Au Ball Bond on Al Pad,” *IEEE Transactions on Components, Packaging and Manufacturing Technology,* vol. 6, no. 2, pp. 306-313, 2016.

[165] A. Mavinkurve, L. Goumans, G. M. O’Halloran, R. T. H. Rongen, and M. L. Farrugia, “Copper wire interconnect reliability evaluation using in-situ High Temperature Storage Life (HTSL) tests,” *Microelectronics Reliability,* vol. 54, no. 9–10, pp. 1661-1665, 2014.

[166] M. Mayer, D. E. Xu, and K. Ratcliffe, “The Electrical Reliability of Silver Wire Bonds under High Temperature Storage,” in 2016 IEEE 66th Electronic Components and Technology Conference (ECTC), 2016, pp. 654-659.

[167] R. Pelzer, M. Nelhiebel, R. Zink, S. Wöhlert, A. Lassnig, and G. Khatibi, “High temperature storage reliability investigation of the Al–Cu wire bond

interface," *Microelectronics Reliability,* vol. 52, no. 9–10, pp. 1966-1970, 2012.

[168] M. Han, M. Wang, L. Zhang, B. Yan, J. Li, M. Song, and V. Mathew, "Copper wire bond pad/IMC interfacial layer crack study during HTSL (high temperature storage life) test," in 2016 IEEE 18th Electronics Packaging Technology Conference (EPTC), 2016, pp. 797-800.

[169] A. Schubert, R. Dudek, H. Walter, E. Jung, A. Gollhardt, B. Michel, and H. Reichl, "Reliability assessment of flip-chip assemblies with lead-free solder joints," in 52nd Electronic Components and Technology Conference 2002, 2002, pp. 1246-1255.

[170] Z. Y. Oh, F. J. Foo, and W. Qiu, "Detailed package failure analysis on short failures after high temperature storage," in Proceedings of the 21th International Symposium on the Physical and Failure Analysis of Integrated Circuits (IPFA), 2014, pp. 278-282.

[171] W. Sabbah, F. Arabi, O. Avino-Salvado, C. Buttay, L. Théolier, and H. Morel, "Lifetime of power electronics interconnections in accelerated test conditions: High temperature storage and thermal cycling," *Microelectronics Reliability,* vol. 76-77, pp. 444-449, 2017.

[172] A. Fischer, T. Grabolla, H. Richter, G. Obermeier, P. Krottenthaler, and R. Wahlich, "Mechanical strength of 300 mm diameter silicon wafers at high temperatures: modeling and simulation," *Microelectronic Engineering,* vol. 45, no. 2–3, pp. 209-223, 1999.

[173] T. Jiang, C. Wu, P. Su, P. Chia, L. Li, H. Y. Son, M. S. Suh, N. S. Kim, J. Im, R. Huang, and P. S. Ho, "Effect of high temperature storage on the stress and reliability of 3D stacked chip," in 2014 IEEE 64th Electronic Components and Technology Conference (ECTC), 2014, pp. 1122-1127.

[174] R. Rongen, R. Roucou, P. J. vd Wel, F. Voogt, F. Swartjes, and K. Weide-Zaage, "Reliability of Wafer Level Chip Scale Packages," *Microelectronics Reliability,* vol. 54, no. 9–10, pp. 1988-1994, 2014.

[175] P. H. Hochstenbach, W. D. van Driel, D. G. Yang, J. J. M. Zaal, and E. Bagerman, “Designing for reliability using a new Wafer Level Package structure,” *Microelectronics Reliability,* vol. 50, no. 4, pp. 528-535, 2010.

[176] "Accelerated Moisture Resistance - Unbiased HAST," JESD22-A118, June 2008.

[177] P. Lall, S. Deshpande, L. Nguyen, and M. Murtuza, “Microstructural Indicators for Prognostication of Copper-Aluminum Wire Bond Reliability Under High-Temperature Storage and Temperature Humidity,” *IEEE Transactions on Components, Packaging and Manufacturing Technology,* vol. 6, no. 4, pp. 569-585, 2016.

[178] A. A. O. Tay, and T. Y. Lin, “Influence of temperature, humidity, and defect location on delamination in plastic IC packages,” *IEEE Transactions on Components and Packaging Technologies,* vol. 22, no. 4, pp. 512-518, 1999.

[179] D. K. Singh, *Strength of materials*: New Delhi : Ane Books ; Boca Raton : CRC Press, Third edition, 2014.

[180] C. Suryanarayana, *Experimental techniques in materials and mechanics*: Boca Raton : CRC Press, c2011, 2011.

[181] T.-C. Chiu, H.-W. Huang, and Y.-S. Lai, “Warpage evolution of overmolded ball grid array package during post-mold curing thermal process,” *Microelectronics Reliability,* vol. 51, no. 12, pp. 2263-2273, 2011.

[182] M. Mengel, J. Mahler, and W. Schober, “Effect of Post-mold Curing on Package Reliability,” *Journal of Reinforced Plastics and Composites,* vol. 23, no. 16, pp. 1755-1765, 2004.

[183] J. d. Vreugd, K. M. B. Jansen, L. J. Ernst, C. Bohm, and R. Pufall, “High temperature storage influence on molding compound properties,” in 2010 11th International Thermal, Mechanical & Multi-Physics Simulation, and Experiments in Microelectronics and Microsystems (EuroSimE), 2010, pp. 1-6.

[184] S. Liu, and Y. Liu, *Modeling and Simulation for Microelectronic Packaging Assembly : Manufacturing, Reliability and Testing*, Hoboken, N.J.: Wiley, 2011.

[185] G. E. Totten, and H. Liang, *Mechanical tribology : materials, characterization, and applications*: New York : Marcel Dekker, 2004.

[186] H. Behnken, M. Apel, and D. Franke, "Simulation of mechanical stress during bending tests for crystalline wafers," in 3rd World conference on photovoltaic energy conversion, 2003.

[187] J. R. Turner, "Contact on a transversely isotropic half-space, or between two transversely isotropic bodies," *International Journal of Solids and Structures,* vol. 16, pp. 409-419, 1966.

[188] N. Carbajal, and F. Mujika, "Determination of compressive strength of unidirectional composites by three-point bending tests," *Polymer Testing,* vol. 28, no. 2, pp. 150-156, 2009.

[189] P. P. Benham, R. J. Crawford, and C. G. Armstrong, *Mechanics of engineering materials*: Harlow, Essex : Longman 2nd ed., 1996.

[190] H. Liu, R. Bao, J. Zhang, and B. Fei, "A creep–fatigue crack growth model containing temperature and interactive effects," *International Journal of Fatigue,* vol. 59, pp. 34-42, 2014.

[191] R. P. Wei, and Z. Huang, "Influence of dwell time on fatigue crack growth in nickel-base superalloys," *Materials Science and Engineering: A,* vol. 336, no. 1–2, pp. 209-214, 2002.

[192] T. Yokobori, and T. Aizawa, "The influence of temperature and stress intensity factor upon the striation spacing and fatigue crack propagation rate of aluminum alloy," *International Journal of Fracture,* vol. 9, no. 4, pp. 489-491, 1973.

[193] T. Yokobori, A. T. Yokobori, and A. Kamei, "Dislocation dynamics theory for fatigue crack growth," *International Journal of Fracture,* vol. 11, no. 5, pp. 781-788, 1975.

[194] T. Kawasaki, S. Nakanishi, Y. Sawaki, K. Hatanaka, and T. Yokobori, "Fracture toughness and fatigue crack propagation in high strength steel from room temperature to −180°c," *Engineering Fracture Mechanics,* vol. 7, no. 3, pp. 465-472, 1975.

[195] K. Makhlouf, and J. W. Jones, "Effects of temperature and frequency on fatigue crack growth in 18% Cr ferritic stainless steel," *International Journal of Fatigue,* vol. 15, no. 3, pp. 163-171, 1993.

[196] R. P. Wei, "Fatigue-crack propagation in a high-strength aluminum alloy," *International Journal of Fracture Mechanics,* vol. 4, no. 2, pp. 159-168, 1968.